

**Guises of Gouy:  
The phase anomaly in  
optical wavefields**



VRIJE UNIVERSITEIT

**Guises of Gouy:  
The phase anomaly in optical wavefields**

ACADEMISCH PROEFSCHRIFT

ter verkrijging van de graad van Doctor  
aan de Vrije Universiteit Amsterdam,  
op gezag van de Rector Magnificus  
Prof. Dr. F.A. van der Duyn Schouten,  
in het openbaar te verdedigen  
ten overstaan van de promotiecommissie  
van de faculteit der Exact Wetenschappen  
op dinsdag 5 november 2013 om 13.45 uur  
in het auditorium van de universiteit,  
De Boelelaan 1105

door

**Xiaoyan PANG**

geboren te Yanshi, China.

Dit proefschrift is goedgekeurd door de promotor:  
Prof. Dr. T. D. Visser

Samenstelling leescommissie:

Prof. Dr. W. M. G. Ubachs,	Vrije Universiteit Amsterdam
Prof. Dr. G. J. Gbur,	University of North Carolina at Charlotte, USA
Dr. B. J. Hoenders,	Universiteit Groningen
Dr. H. F. Schouten,	Vrije Universiteit Amsterdam

This work is financially supported by the China Scholarship Council.



# Contents

<b>Contents</b>	<b>7</b>
<b>1 Introduction</b>	<b>9</b>
1.1 Geometrical optics and physical optics . . . . .	9
1.2 The Gouy phase . . . . .	10
1.3 Singular optics . . . . .	13
1.4 Coherence theory . . . . .	14
1.5 Outline of this thesis . . . . .	17
<b>2 Phase anomaly and phase singularities of the field in the focal region of high-numerical aperture systems</b>	<b>19</b>
2.1 Introduction . . . . .	20
2.2 Focusing systems with a high angular aperture . . . . .	20
2.3 Phase singularities . . . . .	22
2.4 The Gouy phase anomaly . . . . .	26
2.5 Conclusions . . . . .	33
<b>3 The Gouy phase of Airy beams</b>	<b>35</b>
3.1 Introduction . . . . .	36
3.2 The Schrödinger equation and the paraxial wave equation . . . . .	37
3.3 Green's function and Hankel function . . . . .	39
3.4 The Gouy phase of Airy beams . . . . .	40
<b>4 A generalized Gouy phase for focused, partially coherent wavefields and its implications for optical metrology</b>	<b>47</b>
4.1 Introduction . . . . .	49

---

4.2	Fully coherent focused fields . . . . .	49
4.3	Partially coherent focused fields . . . . .	52
4.4	A generalized Gouy phase . . . . .	54
4.5	The origin of the generalized Gouy phase . . . . .	58
4.6	Implications for interferometry . . . . .	63
4.7	Conclusions . . . . .	68
<b>5</b>	<b>Manifestation of the Gouy phase in strongly focused, radially polarized beams</b>	<b>69</b>
5.1	Introduction . . . . .	70
5.2	Focused, radially polarized fields . . . . .	71
5.3	Two Gouy phases . . . . .	73
5.4	The Gouy phase and the state of polarization . . . . .	76
5.5	Conclusions . . . . .	85
<b>6</b>	<b>Wavefront spacing and the Gouy phase in the presence of primary spherical aberration</b>	<b>87</b>
6.1	Introduction . . . . .	88
6.2	A focused field with spherical aberration . . . . .	89
6.3	The Gouy phase . . . . .	91
6.4	Conclusions . . . . .	97
	<b>Bibliography</b>	<b>101</b>
	<b>List of publications</b>	<b>113</b>
	<b>Samenvatting</b>	<b>115</b>
	<b>Biography</b>	<b>117</b>
	<b>Acknowledgments</b>	<b>119</b>

# Chapter 1

## Introduction

### 1.1 Geometrical optics and physical optics

Optics is the field of science concerned with the behavior and properties of light. Traditionally, optics is divided into two main branches: *geometrical optics* and *physical optics*. Geometrical optics describes light as rectilinear rays. These rays can be reflected and refracted at the interface between two media. Geometrical optics is governed by the eikonal equation. Physical optics describes light as a wave phenomenon. These waves can interfere with each other, and they can be diffracted by obstacles. The central formula in this approach is the wave equation. These two theories are not unrelated, in fact, geometrical optics can be regarded as an asymptotic limit of physical optics as the wavenumber  $k = 2\pi/\lambda$  ( $\lambda$  denoting the wavelength) tends to infinity [BORN AND WOLF, 1999, Sec. 3.1]. Physical optics can be further subdivided into two branches. In the vector theory, which is based on Maxwell's equations, the full electromagnetic field is analyzed. In the scalar theory a much more simplified picture is used, and field properties such as polarization are ignored.

In this thesis the methods of physical optics are used to analyze the *phase behavior* of wave fields under different circumstances.

## 1.2 The Gouy phase

More than 120 years ago, L.G. Gouy (see Fig. 1.1) discovered an anomalous phase behavior in a converging, diffracted spherical wave as it passes through its focus [GOUY, 1890; GOUY, 1891]. He wrote (translated from French):

*“If one considers a converging wave that has passed through a focus and has then become divergent, a simple calculation shows that the vibration of that wave has advanced half a period compared to what it should be according to the distance travelled and the speed of light.”*



Figure 1.1: Louis Georges Gouy (1854-1926), around the time of his discovery of the phase anomaly that now bears his name.

Gouy confirmed his theoretical analysis by an interferometric experiment. Letting the light from a point source impinge onto two mirrors,

one concave, the other plane, two beams were generated. The mirrors were positioned so that the beams were nearly parallel to each other. In any transverse plane of observation their superposition yielded a circular interference pattern, with ring-shaped fringes. The central disk was found to change from dark to bright, or vice versa, when the observation plane was moved through the focus of the converging beam. This transition confirmed the predicted  $180^\circ$  phase change. Since Gouy's original work many additional observations have been reported [FARNELL, 1958; MERTZ, 1959; RUFFIN *et al.*, 1999; MCGOWAN *et al.*, 2000; FEURER *et al.*, 2002; CHOW *et al.*, 2004; KLAASSEN *et al.*, 2004; LAMOUCHE *et al.*, 2004; LINDNER *et al.*, 2004; STEUERNAGEL *et al.*, 2005; ZHU *et al.*, 2007; KANDPAL *et al.*, 2007; ROLLAND *et al.*, 2010].

However, the origin of the phase anomaly continues to be a matter of debate, with different authors attributing it to widely differing causes. One of the earliest treatments of the Gouy phase was given by Walker [WALKER, 1904], who used the principle of stationary phase to demonstrate that when a ray associated with an astigmatic wavefront passes through the two centers of curvature, there is a phase discontinuity of an amount of  $\pi/2$  at each of them, in agreement with Gouy's prediction. The first three-dimensional analysis of the phase behavior in the focal region is due to Linfoot and Wolf [LINFOOT AND WOLF, 1956] who examined the phase anomaly along different rays through the geometrical focus.

Boyd [BOYD, 1980] has attributed the Gouy phase to the diffraction properties of Gaussian beams. But the phase anomaly has also been associated with Berry's phase, which is an additional geometric (or topological) phase acquired by a system after a cyclic adiabatic evolution in parameter space [SIMON AND MUKUNDA, 1993; SUBBARAO, 1995]. There is also an explanation based on Heisenberg's uncertainty relations [HARIHARAN AND ROBINSON, 1996; FENG AND WINFUL, 2001], in which the lateral confinement of the field near the focus is accompanied by an increase in momentum in the longitudinal direction. The tilted wave interpretation is yet another way to explain the Gouy phase shift [ZHAN, 2004a; CHEN *et al.*, 2007]. There it is related to the averaged phase retardation of the tilted plane-wave components of a Gaussian beam.

A recent paper showed that the phase anomaly can be considered as

a degenerate case of a rapid  $\pi/2$  phase change that occurs at each focal line of an astigmatic pencil of rays [VISSER AND WOLF, 2010]. In this paper, it was pointed out that the phase anomaly near focus can be understood by considering a wave of a more general form, namely a converging wave exhibiting astigmatism. As is well-known, a geometrical optics analysis of this situation shows that the wavefront of such a field has, at each point, two principal radii of curvature and two, mutually orthogonal, focal lines [BORN AND WOLF, 1999, Sec. 4.6]. Geometrical optics may be regarded as the asymptotic limit of physical optics as the wavenumber  $k = 2\pi/\lambda$  tends to infinity. With the help of the method of stationary phase it can be shown that in this limit the field exhibits a phase discontinuity of an amount  $\pi/2$  at each focal line [VAN KAMPEN, 1949; STAMNES, 1986]. Geometrical optics is governed by the eikonal equation, the actual wave field however, satisfies the Helmholtz equation. The solutions of the latter are well known to be continuous. Hence, according to physical optics, the two phase discontinuities have to be “smoothed out”, and become continuous but rapid phase changes. When the astigmatic wave aberration decreases to zero, i.e., when the field in the aperture becomes a converging spherical wave, the two foci coincide and the sharp phase change in the focal region is the Gouy phase change of an amount  $\pi$ . In this way, the phase anomaly can be understood from elementary properties of rays and from the relation between geometrical optics and physical optics.

In higher-order laser modes the Gouy phase has a more complicated behavior than in the converging spherical waves discussed so far. For a Hermite-Gaussian mode with indices  $(m, n)$  it has the value  $(m + n + 1)\pi$ , and for a Laguerre-Gaussian mode with indices  $(p, l)$  it takes on the value  $(2p + l + 1)\pi$  [SIEGMAN, 1986].

The Gouy phase is of great importance because it plays a role in so many physical systems and applications. In curved-mirror laser cavities, it determines the resonance frequencies of different transverse modes [SIEGMAN, 1986]. For such modes, the Gouy phase also can supply quantitative information about the optical aberrations in cavities [KLAASSEN *et al.*, 2004]. Utilizing the Gouy phase, one can transform a Hermite-Gaussian mode into a Laguerre-Gaussian mode and vice versa [ALLEN *et al.*, 1992; BEIJERSBERGEN *et al.*, 1993]. In nonlinear optics, the Gouy phase influences

the efficiency of higher-order harmonics generation [BOYD, 1992; LINDNER *et al.*, 2003]. It has also been used in the creation of so-called bottle beams [ARLT AND PADGETT, 2000] and in optical coherence tomography [LAMOUCHE *et al.*, 2004]. In singular optics, the Gouy phase affects the propagation of optical vortices [HAMAZAKI *et al.*, 2006; BAUMANN *et al.*, 2009]. In addition, the Gouy phase can be used in the interferometry of a single nanoparticle [HWANG AND MOERNER, 2007] and in the application of Terahertz time-domain spectroscopy [FEDERICI *et al.*, 2006]. In chemical reactions, the Gouy phase can be used to control the branching ratio for products formed at different total energies [BARGE *et al.*, 2006; GORDON AND BARGE, 2007; BARGE *et al.*, 2008]. The Gouy phase is not limited to electromagnetic waves but has also been found in acoustic fields [HOLME *et al.*, 2003; KOLOMENSKII *et al.*, 2005]. Very recently, it has even been observed in matter waves [GUZZINATI *et al.*, 2013].

Although the term Gouy phase is traditionally reserved for *focused* wave fields, recently its meaning has been extended to apply to beam-like fields as well. In [MARTELLI *et al.*, 2010] it is used to characterize the phase of a non-diffracting Bessel beam by comparing it to that of a plane wave with the same frequency.

In the next two sections we briefly review some concepts that will be used throughout this thesis.

### 1.3 Singular optics

Singular optics [NYE AND BERRY, 1974; NYE, 1999; SOSKIN AND VASNETSOV, 2001; KARMAN *et al.*, 1997; BERRY, 1998; NYE, 1998; SCHOUTEN *et al.*, 2003; SCHOONOVER AND VISSER, 2006; DENNIS *et al.*, 2009] is a branch of wave analysis concerned with the presence of singular structures in a wavefield and the topology of the wavefield around those structures. The most common singular structure is a *phase singularity*. Consider a complex monochromatic scalar field  $U(\mathbf{r}, t)$  of frequency  $\omega$  which can be written as

$$U(\mathbf{r}, t) = A(\mathbf{r})e^{i\psi(\mathbf{r})}e^{i\omega t}, \quad (1.1)$$

Here  $\mathbf{r}$  denotes a position, and  $t$  a moment in time. A phase singularity occurs at points where the amplitude  $A(\mathbf{r})$  vanishes and the phase  $\psi(\mathbf{r})$  therefore is undefined or *singular*. The two key concepts of singular optics

are the *topological charge* and the *topological index* of the features. The topological charge  $s$  of a phase singularity is defined as

$$s \equiv \frac{1}{2\pi} \oint_C \nabla\psi(\mathbf{r}) \cdot d\mathbf{r}, \quad (1.2)$$

where the path  $C$  encloses the phase singularity and is traversed in a counter-clockwise direction. The topological index is defined as the topological charge of the vector field  $\nabla\psi(\mathbf{r})$ . In this field the “phase” is the orientation angle of  $\nabla\psi(\mathbf{r})$ .

In a monochromatic electromagnetic beam, the field is completely polarized at each point in space [BORN AND WOLF, 1999, Sec. 1.4]. The polarization ellipse is characterized by three parameters describing its eccentricity, orientation and handedness, respectively. A *polarization singularity* [BERRY AND DENNIS, 2001] occurs at a point at which the polarization ellipse is degenerate. Points where the polarization is purely circular, and hence the orientation of the ellipse is undefined, are called  $C$ -points. At  $L$ -lines, where the polarization is linear, the handedness is undefined.

If the field is partially coherent, its statistical properties in the space-frequency domain are described by the *spectral degree of coherence* [MANDEL AND WOLF, 1995, Sec. 4.3], see also Sec. 1.4 in this Chapter. This is a complex-valued function of two spatial variables  $\mathbf{r}_1$  and  $\mathbf{r}_2$ , so at pairs of points where the spectral degree of coherence vanishes, its phase is undefined and a *coherence singularity* [GBUR AND VISSER, 2003] occurs. In contrast to the classical singularities that are found in two or three dimensions, coherence singularities occur in a six-dimensional space.

## 1.4 Coherence theory

In optics, coherence theory is the study of the statistical properties of light. It describes optical fields in terms of correlation functions, which can be measured through interference experiments.

Consider a random, wide-sense stationary scalar wave field  $V(\mathbf{r}, t)$ , which is a member of an ensemble of realizations  $\{V(\mathbf{r}, t)\}$ . The correlation properties of the field can be described by the *mutual coherence function*, which is defined as ([MANDEL AND WOLF, 1995], Sec.4.3.1)

$$\Gamma(\mathbf{r}_1, \mathbf{r}_2, \tau) = \langle V^*(\mathbf{r}_1, t)V(\mathbf{r}_2, t + \tau) \rangle, \quad (1.3)$$

where  $\tau$  is the time difference, the asterisk indicates the complex conjugate and the angular brackets denote an ensemble average. It is convenient to normalize the mutual coherence function by defining the *complex degree of coherence* as

$$\gamma(\mathbf{r}_1, \mathbf{r}_2, \tau) = \frac{\Gamma(\mathbf{r}_1, \mathbf{r}_2, \tau)}{\sqrt{I(\mathbf{r}_1)I(\mathbf{r}_2)}}, \quad (1.4)$$

where

$$I(\mathbf{r}) = \Gamma(\mathbf{r}, \mathbf{r}, 0), \quad (1.5)$$

is the averaged intensity at position  $\mathbf{r}$ . In Young's interference experiment, the value of  $|\gamma(\mathbf{r}_1, \mathbf{r}_2, \tau)|$  equals the visibility of fringes that are produced when two pinholes (located at position  $\mathbf{r}_1$  and  $\mathbf{r}_2$ ) are illuminated with equal intensity. When  $|\gamma(\mathbf{r}_1, \mathbf{r}_2, \tau)| = 1$  the light at the two pinholes is called fully coherent, resulting in a fringe pattern with maximal sharpness. When  $|\gamma(\mathbf{r}_1, \mathbf{r}_2, \tau)| = 0$  the light at the two pinholes is completely incoherent and there is no visible interference pattern. For intermediate values of  $|\gamma(\mathbf{r}_1, \mathbf{r}_2, \tau)|$  the light is called partially coherent.

For many applications it is advantageous to work in the space-frequency domain, where the basic quantity is the *cross-spectral density function*  $W(\mathbf{r}_1, \mathbf{r}_2, \omega)$ , which is the temporal Fourier transform of the mutual coherence function, i.e.

$$W(\mathbf{r}_1, \mathbf{r}_2, \omega) = \frac{1}{2\pi} \int_{-\infty}^{\infty} \Gamma(\mathbf{r}_1, \mathbf{r}_2, \tau) e^{i\omega\tau} d\tau. \quad (1.6)$$

It can be shown that, like the mutual coherence function, the cross-spectral density function  $W(\mathbf{r}_1, \mathbf{r}_2, \omega)$  is also a correlation function ([MANDEL AND WOLF, 1995], Sec.4.7.2), that is

$$W(\mathbf{r}_1, \mathbf{r}_2, \omega) = \langle U^*(\mathbf{r}_1, \omega)U(\mathbf{r}_2, \omega) \rangle_{\omega}, \quad (1.7)$$

where  $U(\mathbf{r}, \omega)$  is a member of an ensemble of monochromatic realizations of the field. The suffix  $\omega$  on the angular brackets is to stress that the average is taken over an ensemble of space-frequency realizations. Often it is useful to consider a normalized version of  $W$ , the *spectral degree of coherence*, which is given by the expression

$$\mu(\mathbf{r}_1, \mathbf{r}_2, \omega) = \frac{W(\mathbf{r}_1, \mathbf{r}_2, \omega)}{\sqrt{S(\mathbf{r}_1, \omega)S(\mathbf{r}_2, \omega)}}, \quad (1.8)$$

where

$$S(\mathbf{r}, \omega) = W(\mathbf{r}, \mathbf{r}, \omega), \quad (1.9)$$

is the *spectral density* at position  $\mathbf{r}$ . Just like the complex degree of coherence, the spectral degree of coherence can also be determined by Young's interference experiment but now with filters in front of the pin-holes [WOLF, 1983]. It can be shown that spectral degree of coherence is bounded ([MANDEL AND WOLF, 1995], Sec.4.3.2 ) by

$$0 \leq |\mu(\mathbf{r}_1, \mathbf{r}_2, \omega)| \leq 1, \quad (1.10)$$

where 0 represents complete spatial incoherence, and 1 represents full spatial coherence.

Each of these two correlation functions obeys two precise propagation laws. The mutual coherence function in free space satisfies the two wave equations [WOLF, 1955]

$$\begin{aligned} (\nabla_1^2 - \frac{1}{c^2} \frac{\partial^2}{\partial \tau^2}) \Gamma(\mathbf{r}_1, \mathbf{r}_2, \tau) &= 0, \\ (\nabla_2^2 - \frac{1}{c^2} \frac{\partial^2}{\partial \tau^2}) \Gamma(\mathbf{r}_1, \mathbf{r}_2, \tau) &= 0, \end{aligned} \quad (1.11)$$

where  $\nabla_1^2$  and  $\nabla_2^2$  denote the Laplace operator acting on  $\mathbf{r}_1$  and  $\mathbf{r}_2$ , respectively and  $c$  is the speed of light. The cross-spectral density satisfies two Helmholtz equations, namely

$$\begin{aligned} (\nabla_1^2 + k^2) W(\mathbf{r}_1, \mathbf{r}_2, \omega) &= 0, \\ (\nabla_2^2 + k^2) W(\mathbf{r}_1, \mathbf{r}_2, \omega) &= 0, \end{aligned} \quad (1.12)$$

where  $k = \omega/c$  is the wave number corresponding to frequency  $\omega$ . The two pairs of equations above imply that these two correlation functions both have a wave-like character.

Thus far we have considered scalar fields, but the concept of correlation functions can be generalized to electromagnetic beams and forms the basis of the *unified theory of coherence and polarization* [WOLF, 2003a; WOLF, 2003b]. Coherence describes the correlation between fluctuations at two or more points in space. Polarization, on the other hand, is a manifestation of the correlation between fluctuating components of the electric field vector at a single point. The basic quantity of the unified theory of coherence

and polarization is the *electric cross-spectral density matrix*  $\mathbf{W}(\mathbf{r}_1, \mathbf{r}_2, \omega)$ , which is defined as

$$\mathbf{W}(\mathbf{r}_1, \mathbf{r}_2, \omega) = \begin{bmatrix} W_{xx}(\mathbf{r}_1, \mathbf{r}_2, \omega) & W_{xy}(\mathbf{r}_1, \mathbf{r}_2, \omega) \\ W_{yx}(\mathbf{r}_1, \mathbf{r}_2, \omega) & W_{yy}(\mathbf{r}_1, \mathbf{r}_2, \omega) \end{bmatrix}, \quad (1.13)$$

where

$$W_{ij}(\mathbf{r}_1, \mathbf{r}_2, \omega) = \langle E_i^*(\mathbf{r}_1, \omega) E_j(\mathbf{r}_2, \omega) \rangle, \quad (i, j = x, y). \quad (1.14)$$

Here  $E_i(\mathbf{r}, \omega)$  is a Cartesian component of the electric field at a point specified by a position vector  $\mathbf{r}$  at frequency  $\omega$ , of a typical realization of the statistical ensemble representing the beam.

The coherence properties of a beam are described only by the diagonal elements of the electric cross-spectral density matrix whereas the state of polarization depends also on the off-diagonal elements. An overview is given by Wolf [WOLF, 2007]. Recently, the role of the off-diagonal matrix elements in characterizing the state of coherence has been emphasized [SETÄLA *et al.*, 2006].

## 1.5 Outline of this thesis

Nearly all the literature dealing with the Gouy phase uses the scalar theory. In a high-aperture optical system, however, the vector nature of the field can no longer be ignored. In Chapter 2, the Gouy phases of the three Cartesian components of the electric field are examined. We show that these components exhibit different phase anomalies. It is also found that the phase of the electric field exhibits singularities in all three components.

As one kind of the recently discovered non-diffracting beams, Airy beams have attracted considerable attention. Such beams have unique properties, like their “accelerating” behavior and their capacity for “self-healing”. The latter means that they are remarkably insensitive to perturbations. In Chapter 3 the Gouy phase for idealized infinite-energy Airy beams is defined, and analytical expressions for its behavior are derived. It is shown numerically that these expressions are excellent approximations for the Gouy phase of realistic finite-energy Airy beams generated under typical conditions.

Under many practical circumstances, light is not monochromatic, but is partially coherent, and its phase is a random quantity. When such a field is focused, the Gouy phase is therefore undefined. However, the correlation functions that characterize partially coherent fields *do* have a well-defined phase. In Chapter 4, partially coherent fields are examined and it is demonstrated that their correlation functions exhibit a generalized Gouy phase. In the coherent limit this generalized Gouy phase reduces to the classical Gouy phase. It is also shown that this generalized Gouy phase affects the interference of focused fields, altering the fringe spacing in a non-trivial manner.

In Chapter 5 we examine the focusing of radially polarized fields. If one follows the state of polarization along an oblique ray through the focus, it is seen to vary rapidly. We show that is a manifestation of the different Gouy phases that the two electric field components undergo.

Every lens suffers from some form of wave front aberrations. In Chapter 6 we analyze the influence of primary spherical aberration on the Gouy phase. We find that the phase anomaly in front of the diffraction focus and right behind it are quite different. This coincides with a wavefront spacing that is larger than the effective wavelength on one side, and smaller than the effective wavelength on the other side. This has consequences for optical metrology in which one strives for accuracy levels of  $10^{-10}$ .

## Chapter 2

# Phase anomaly and phase singularities of the field in the focal region of high-numerical aperture systems

This Chapter is based on

- X. Pang, T.D. Visser and E. Wolf,  
“Phase anomaly and phase singularities of the field in the focal region of high-numerical aperture systems,”  
*Optics Communications*, vol. 284, pp. 5517-5522 (2011).

### **Abstract**

The phase characteristics of the three Cartesian components of the electric field in the focal region of a high-numerical aperture system are studied. The Gouy phase anomaly and the phase singularities are examined in detail. It is found that the three components exhibit different behaviors.

## 2.1 Introduction

With a few notable exceptions [DIEHL AND VISSER, 2004; FOLEY AND WOLF, 2005; ZHAN, 2004a; CHEN *et al.*, 2007], most papers published on the Gouy phase are limited to scalar fields. When a beam of light is focused by a high-aperture optical system, the phase behavior near focus becomes more complicated since the scalar description becomes inaccurate.

Using the scalar approximation, it was found by Linfoot and Wolf [LINFOOT AND WOLF, 1956] that the on-axis wavefront spacing is larger than  $\lambda$ , the wavelength of a plane wave. In particular they found that near the focus the wavefronts are separated by a distance  $\lambda/(1 - a^2/4f^2)$ , where  $a$  and  $f$  denote the aperture radius and focal length of the lens, respectively. But using a vectorial description, one finds that in high-aperture systems, the wavefront spacing is highly irregular. This holds both for incident fields that are linearly polarized [FOLEY AND WOLF, 2005] and fields that are radially polarized [VISSER AND FOLEY, 2005].

In addition, the vectorial character of the field can no longer be neglected in a high-aperture system. For example, for an incident linearly polarized plane wave, the field components near focus are non-zero in the two directions perpendicular to the polarization of the incident field. Wolf *et al.* [RICHARDS AND WOLF, 1956; WOLF, 1959; RICHARDS AND WOLF, 1959; BOIVIN AND WOLF, 1965; BOIVIN *et al.*, 1967] derived expressions for the electric and magnetic field vectors in the focal region of such a system. In the present chapter we use this formalism to analyze the phase behavior, in particular the occurrence of phase singularities and the Gouy phase anomaly. Restricting ourselves to the electric field, three phases—one for each Cartesian component—rather than a single phase have to be considered. As we will demonstrate, all the three phases exhibit singularities, and their associated phase anomalies are markedly different.

## 2.2 Focusing systems with a high angular aperture

Let us consider an aplanatic focusing system  $L$  of focal length  $f$  and with a semi-aperture angle  $\alpha$  (see Fig. 2.1). We take the origin  $O$  of a right-handed Cartesian coordinate system at the geometrical focus. A

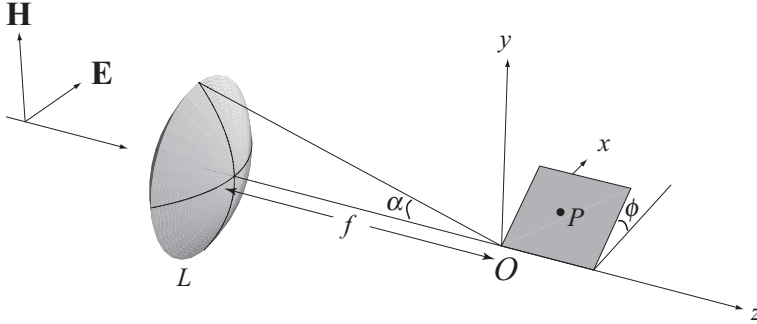


Figure 2.1: A high-numerical-aperture focusing system.

monochromatic plane wave of angular frequency  $\omega$  is incident upon the system, with the electric field polarized along the  $x$ -direction. The position of an observation point  $P$  is indicated by the dimensionless Lommel variables  $u$  and  $v$ , together with the azimuthal angle  $\phi$ , defined as

$$u = kz \sin^2 \alpha, \quad (2.1)$$

$$v = k(x^2 + y^2)^{1/2} \sin \alpha. \quad (2.2)$$

Here the wavenumber  $k = \omega/c$ , with  $c$  denoting the speed of light. The electric and magnetic fields are of the form

$$\mathbf{E}(u, v, \phi, t) = \text{Re} [\mathbf{e}(u, v, \phi) \exp(-i\omega t)], \quad (2.3)$$

$$\mathbf{H}(u, v, \phi, t) = \text{Re} [\mathbf{h}(u, v, \phi) \exp(-i\omega t)], \quad (2.4)$$

respectively, where  $\text{Re}$  denotes the real part and  $t$  the time. The time-independent parts,  $\mathbf{e}$  and  $\mathbf{h}$ , of the electric and magnetic fields at a point  $P(u, v, \phi)$  have been shown to be given by the expressions [RICHARDS AND WOLF, 1959]:

$$e_x(u, v, \phi) = -iA[I_0(u, v) + I_2(u, v) \cos 2\phi], \quad (2.5a)$$

$$e_y(u, v, \phi) = -iAI_2(u, v) \sin 2\phi, \quad (2.5b)$$

$$e_z(u, v, \phi) = -2AI_1(u, v) \cos \phi, \quad (2.5c)$$

$$h_x(u, v, \phi) = -iAI_2(u, v) \sin 2\phi, \quad (2.6a)$$

$$h_y(u, v, \phi) = -iA[I_0(u, v) - I_2(u, v) \cos 2\phi], \quad (2.6b)$$

$$h_z(u, v, \phi) = -2AI_1(u, v) \sin \phi. \quad (2.6c)$$

where

$$I_0(u, v) = \int_0^\alpha \cos^{1/2} \theta \sin \theta (1 + \cos \theta) J_0 \left( \frac{v \sin \theta}{\sin \alpha} \right) \exp \left( \frac{iu \cos \theta}{\sin^2 \alpha} \right) d\theta, \quad (2.7)$$

$$I_1(u, v) = \int_0^\alpha \cos^{1/2} \theta \sin^2 \theta J_1 \left( \frac{v \sin \theta}{\sin \alpha} \right) \exp \left( \frac{iu \cos \theta}{\sin^2 \alpha} \right) d\theta, \quad (2.8)$$

$$I_2(u, v) = \int_0^\alpha \cos^{1/2} \theta \sin \theta (1 - \cos \theta) J_2 \left( \frac{v \sin \theta}{\sin \alpha} \right) \exp \left( \frac{iu \cos \theta}{\sin^2 \alpha} \right) d\theta. \quad (2.9)$$

In these integrals  $J_n(x)$  denotes the Bessel function of the first kind and of order  $n$ . The amplitude  $A$  will be taken to be unity from now on. It is to be noted that all the functions in Eqs. (2.5)–(2.9) depend on the semi-aperture angle  $\alpha$  (not explicitly shown).

The following symmetry relations follow immediately from Eqs. (2.5) and (2.7)–(2.9):

$$e_x(-u, v, \phi) = -e_x^*(u, v, \phi), \quad (2.10a)$$

$$e_y(-u, v, \phi) = -e_y^*(u, v, \phi), \quad (2.10b)$$

$$e_z(-u, v, \phi) = e_z^*(u, v, \phi). \quad (2.10c)$$

By comparing Eqs. (2.5) and (2.6) it is clear that the behavior of the magnetic field components is similar to that of the electric field components. In particular, the magnetic field component  $h_x$  is identical to the electric field component  $e_y$ ;  $h_y$  in a meridional plane  $\phi = \text{constant}$  is identical to  $e_x$  in the plane  $\phi \rightarrow \phi + \pi/2$ ; and  $h_z$  in the meridional plane  $\phi$  is identical to  $e_z$  in the plane  $\phi \rightarrow \phi + \pi/2$ . In view of these relations we will restrict our analysis to the electric field only.

### 2.3 Phase singularities

According to Eq. (2.5a) the electric field component  $e_x$  in the focal plane ( $u = 0$ ) is purely imaginary. As noted by Richards and Wolf [RICHARDS

AND WOLF, 1959], the focal plane contains ring-shaped phase singularities of  $e_x$ , centered on the  $u$ -axis, at which  $\text{Im}[e_x]$  changes sign. They also showed that in the low-aperture limit ( $\alpha \rightarrow 0$ ),  $e_x$  is the only non-vanishing component of the electric field, and these singularities form the well-known Airy rings of classical scalar diffraction theory. An example is shown in Fig. 2.2. The color blue corresponds to a phase of  $-\pi/2$ , whereas the color red indicates a phase of  $\pi/2$ . The white lines between the two different colors are the phase singularities of  $e_x$ .

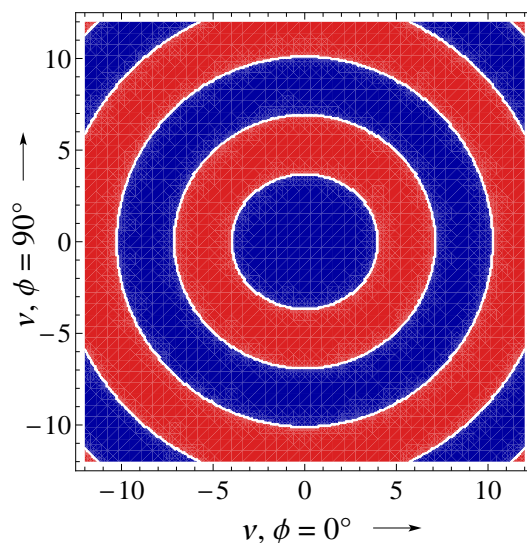


Figure 2.2: The phase behavior of  $e_x$  in the focal plane. Blue indicates a phase of  $-\pi/2$ , whereas red indicates a phase of  $\pi/2$ . The white circular lines are the phase singularities. In this example the semi-aperture angle  $\alpha = 45^\circ$

From Eq. (2.5b), it is seen that  $e_y$  is also purely imaginary in the focal plane. Its phase behavior is displayed in Fig. 2.3. Again blue denotes a phase of  $-\pi/2$ , red a phase of  $\pi/2$  and white lines represent the phase singularities. Furthermore Eq. (2.5b) indicates that  $e_y = 0$  when  $\phi = 0, \pi/2, \pi, \text{ or } 3\pi/2$ . This explains the two (white) line singularities across the focal plane.

The phase behavior of  $e_z$  in the focal plane can be calculated from Eq. (2.5c). Unlike  $e_x$  and  $e_y$ ,  $e_z$  is strictly real-valued. The only two phase values of  $e_z$  are therefore 0 and  $\pi$ . In Fig. 2.4 blue indicates a phase of 0, whereas red indicates a phase of  $\pi$ . White lines are the phase singularities. From Eq. (2.5c) it is seen that  $e_z = 0$  when  $\phi = \pi/2$  or  $3\pi/2$ . This explains the vertical line singularity in the focal plane. It is to be noted that the approximately circular singularities of  $e_x$ ,  $e_y$  and  $e_z$  do not coincide.

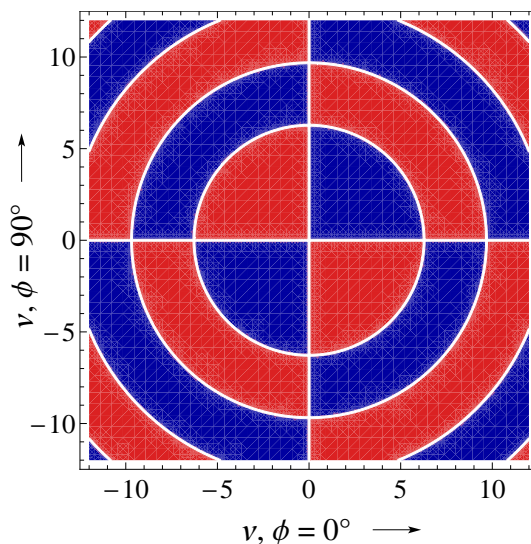


Figure 2.3: The phase behavior of  $e_y$  in the focal plane. Blue indicates a phase of  $-\pi/2$ , whereas red indicates a phase of  $\pi/2$ . White lines are the phase singularities. In this example the semi-aperture angle  $\alpha = 45^\circ$

In the  $u, v$ -plane, excluding the points discussed above, no phase singularities of  $e_x$  were found. However, for the other two field components,  $e_y$  and  $e_z$ , they were observed. The phase behavior of  $e_y$  is illustrated in Fig. 2.5. In this figure the phase is color-coded, with phase singularities

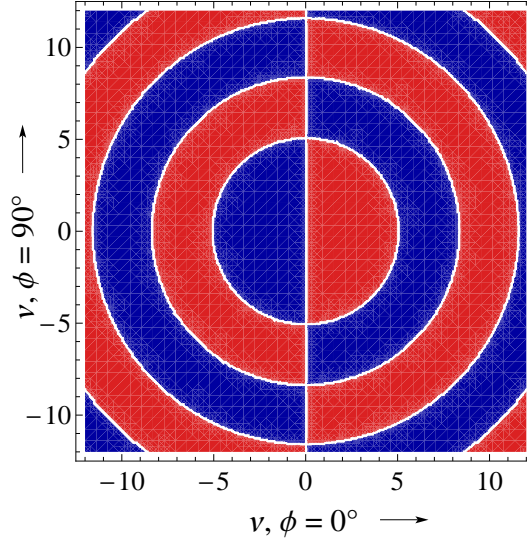


Figure 2.4: The phase behavior of  $e_z$  in the focal plane. Here blue indicates a phase of 0, whereas red indicates a phase of  $\pi$ . White lines are the phase singularities. In this example the semi-aperture angle  $\alpha = 45^\circ$

indicated by the intersections of contour lines. A pair of singularities of opposite topological charge can be seen along the line  $u = 23$ . It follows from Eq. (2.5b) that the phase singularities of  $e_y$  form rings centered on the  $z$ -axis.

The phase of the longitudinal field component  $e_z$  is shown in Figure. 2.6. Again, several ring-shaped phase singularities can be observed. As shown in [DIEHL AND VISSER, 2004], a pair of these singularities merges with two phase saddle points when the semi-aperture angle  $\alpha$  is changed. In such an annihilation process both the topological charge and the topological index are conserved.

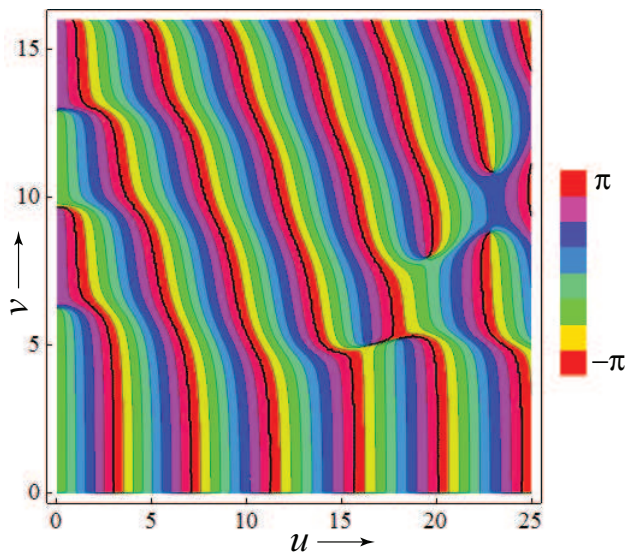


Figure 2.5: Contours of the phase of the transverse electric field component  $e_y(u, v, \phi)$  in the  $u, v$ -plane. Intersections of different contours (e.g. at  $u = 20, v = 8$ ) indicate phase singularities. The semi-aperture angle  $\alpha$  of the focusing system was taken to be  $45^\circ$ .

## 2.4 The Gouy phase anomaly

The only component of the electric field which does not vanish along the optical axis ( $v = 0$ ) is  $e_x$ . The wavefront spacing of that component is highly irregular (see for example [LINFOOT AND WOLF, 1956; FOLEY AND WOLF, 2005] and the references therein). This behavior is seen from a plot of the real and the imaginary part,  $\text{Re}[e_x(u, v, \phi)]$  and  $\text{Im}[e_x(u, v, \phi)]$ , with the longitudinal Lommel variable  $u$  as the parameter. An example is presented in Fig. 2.7.

Alternatively, one can compare the phase  $\psi[e_x(u, v, \phi)]$  of  $e_x$ , with that of a converging, non-diffracted spherical wave in the half-space  $z < 0$ , namely  $-kR$ , and with that of a diverging spherical wave in the half-space  $z \geq 0$ , namely  $+kR$ , where  $kR = k(x^2 + y^2 + z^2)^{1/2} = (v^2 + u^2/\sin^2 \alpha)^{1/2}/\sin \alpha$ . The Gouy phase anomaly for the  $x$ -component of the

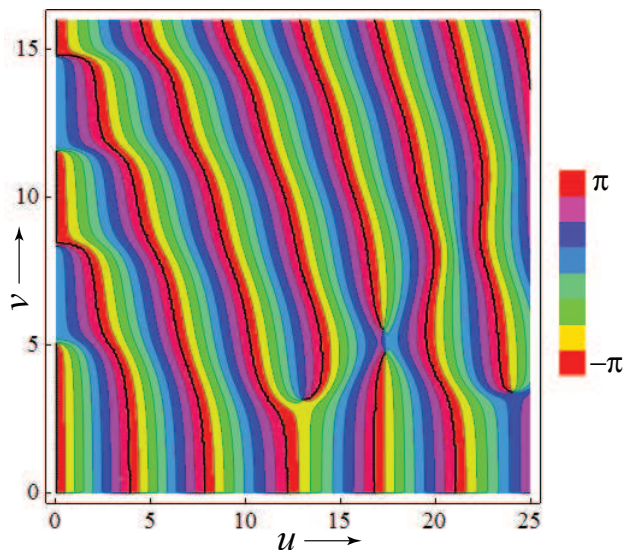


Figure 2.6: Contours of the phase of the longitudinal electric field component  $e_z(u, v, \phi)$  in the  $u, v$ -plane. Intersections of different contours (e.g. at  $u = 13, v = 3$ ) indicate phase singularities. The semi-aperture angle  $\alpha$  was taken to be  $45^\circ$ .

electric field,  $\delta_x(u, v, \phi)$ , is then defined as (see [BORN AND WOLF, 1999, Sec. 8.8.4] or [STAMNES, 1986, Ch. 8]):

$$\delta_x(u, v, \phi) = \begin{cases} \psi[e_x(u, v, \phi)] + kR & \text{when } z < 0, \\ \psi[e_x(u, v, \phi)] - kR & \text{when } z \geq 0. \end{cases} \quad (2.11)$$

From Eqs. (2.5a) and (2.11) one immediately finds that the phase anomaly at two points that are symmetrically located with respect to the geometrical focus, satisfies the relation

$$\delta_x(u, v, \phi) + \delta_x(-u, v, \phi + \pi) = -\pi. \quad (2.12)$$

At the focus ( $u = v = 0$ ) one has, according to Eq. (2.5a),

$$\delta_x(0, 0) = \psi[e_x(0, 0)] = -\pi/2. \quad (2.13)$$

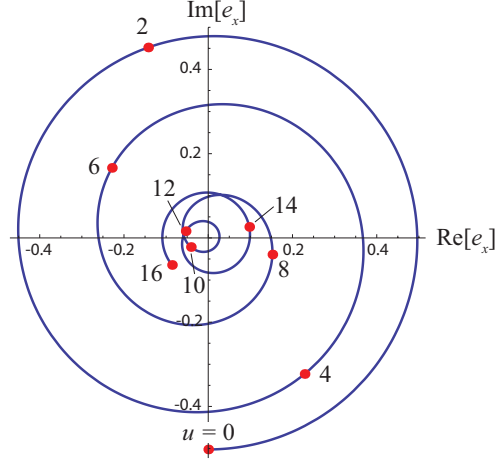


Figure 2.7: Parametric plot of  $\text{Re}[e_x]$  and  $\text{Im}[e_x]$  along the optical axis. The dots correspond with the values  $u = 0, 2, \dots, 16$ . The semi-aperture angle  $\alpha$  was taken to be  $45^\circ$ .

The on-axis phase anomaly  $\delta_x(u, v = 0)$  is shown in Fig. 2.8 for selected values of the semi-aperture angle  $\alpha$  of the focusing system. When  $\alpha$  increases, the change in phase near focus is seen to become more gradual and to decrease. Scalar theory [BORN AND WOLF, 1999, Sec. 8.8.4] predicts a linear behavior of the phase anomaly, with a discontinuity of  $\pi$  at each phase singularity (panel a). It is seen that for smaller values of the semi-aperture angle the phase behavior tends to that given by scalar theory. In connection with Fig. 2.8 it is important to bear in mind that the longitudinal coordinate  $u$  is, by virtue of Eq. (2.1), dependent on the value of the semi-aperture angle  $\alpha$ .

In Fig. 2.9 the behavior of the phase anomaly of  $e_x$  is shown along several rays through the geometrical focus  $O$ . As an oblique ray passes through focus, the angle  $\phi$  that defines the meridional plane in which the ray lies, changes by  $\pi$ . It is seen that when the angle of inclination  $\theta$  of the ray (with  $\theta = \tan^{-1}[v \sin \alpha / |u|]$ ) increases, the change in  $\delta_x(u, v, \phi)$  near focus decreases.

According to Eq. (2.5b) the  $y$ -component of the electric field vanishes

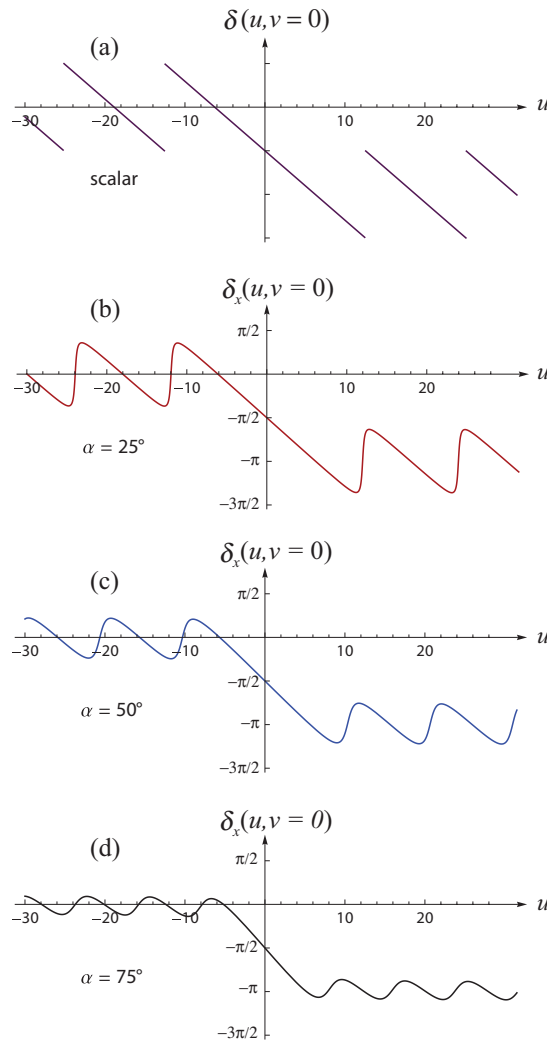


Figure 2.8: The phase anomaly along the optical axis according to scalar theory (a), and the phase anomaly  $\delta_x(u, v = 0)$  of the electric field component  $e_x$  for selected values of the semi-aperture angle  $\alpha$ , (b)  $\alpha = 25^\circ$ , (c)  $\alpha = 50^\circ$ , and (d)  $\alpha = 75^\circ$ .

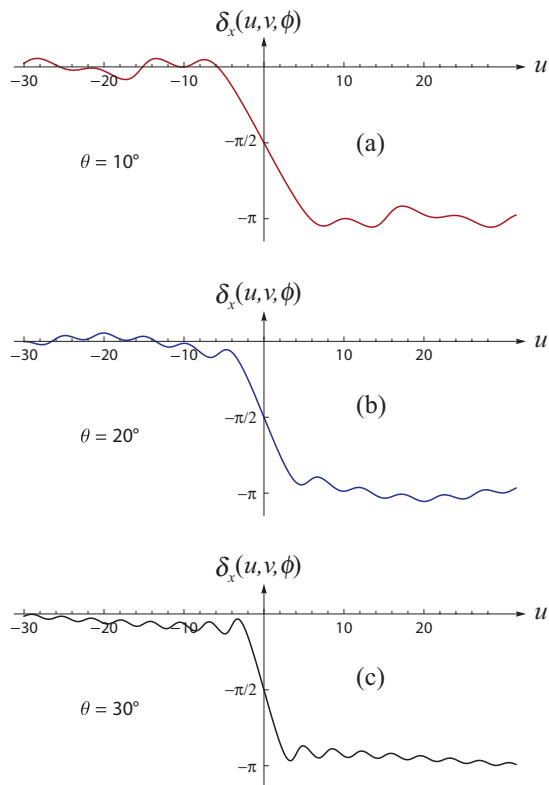


Figure 2.9: The phase anomaly  $\delta_x(u, v, \phi)$  of the electric field component  $e_x$  along several rays in the meridional plane  $\phi = 0^\circ$  through the geometric focus. The angle of inclination of each ray is denoted by  $\theta$ , with (a)  $\theta = 10^\circ$ , (b)  $\theta = 20^\circ$ , and (c)  $\theta = 30^\circ$ . In this example the semi-aperture angle  $\alpha$  was taken to be  $45^\circ$ .

along the optical axis, and hence its phase  $\psi[e_y(u, v)]$  is singular there. Along oblique rays through the geometric focus, however, this phase is defined. In analogy with Eqs. (2.11) we define the phase anomaly  $\delta_y(u, v, \phi)$  of  $e_y$  as

$$\delta_y(u, v, \phi) = \begin{cases} \psi[e_y(u, v, \phi)] + kR & \text{when } z < 0, \\ \psi[e_y(u, v, \phi)] - kR & \text{when } z > 0. \end{cases} \quad (2.14)$$

From Eqs. (2.5b) and (2.14) we find that the phase anomaly at two points that are symmetrically located with respect to the geometrical focus, satisfies the relation

$$\delta_y(u, v, \phi) + \delta_y(-u, v, \phi + \pi) = -\pi. \quad (2.15)$$

A ray with  $v \propto |u|$  runs through the geometrical focus. On using the fact that for small arguments  $J_n(x) \sim x^n$ , we find from Eq. (2.5b) that along such a ray  $e_y \sim -iu^2 \sin 2\phi$ . Hence

$$\lim_{u \downarrow 0} \delta_y(u, v, \phi + \pi) = \lim_{u \uparrow 0} \delta_y(u, v, \phi) = -\frac{\pi}{2} \times \text{sign}[\sin 2\phi]. \quad (2.16)$$

Here the subscripts  $u \downarrow 0$  and  $u \uparrow 0$  indicate that the quantity  $u$  approaches the limiting value 0 from above and from below, respectively. Further,  $\text{sign}(x)$  denotes the sign function

$$\text{sign}(x) = \begin{cases} -1 & \text{if } x < 0, \\ 1 & \text{if } x > 0. \end{cases} \quad (2.17)$$

Although both limits in Eq. (2.16) are equal, the phase anomaly  $\delta_y(u, v, \phi)$  is undefined at the geometric focus because  $e_y$  vanishes there. An example of this behavior is shown in Fig. 2.10. The two discontinuities near  $u = 1$  and  $u = 3$  are a consequence of the fact that the phase is defined up to an integral number of  $2\pi$ .

Next we define, again in analogy with Eqs. (2.11), the phase anomaly  $\delta_z(u, v, \phi)$  of the longitudinal component of the electric field as

$$\delta_z(u, v, \phi) = \begin{cases} \psi[e_z(u, v, \phi)] + kR & \text{when } z < 0, \\ \psi[e_z(u, v, \phi)] - kR & \text{when } z > 0. \end{cases} \quad (2.18)$$

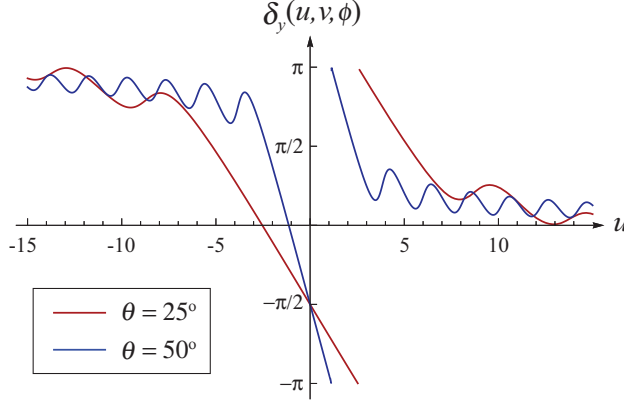


Figure 2.10: The phase anomaly  $\delta_y(u, v, \phi)$  of the electric field component  $e_y$  along two rays in the meridional plane  $\phi = 45^\circ$  through the geometrical focus. The angle of inclination of each ray is denoted by  $\theta$ . In this example the semi-aperture angle  $\alpha = 50^\circ$ .

It is seen from Eqs. (2.10) that the phase behavior of the longitudinal component  $e_z$  of the electric field in the focal region differs from that of the two transverse components. From Eqs. (2.5c) and (2.18) it follows that the phase anomaly at two points that are symmetrically located with respect to the geometrical focus, satisfies the relation

$$\delta_z(u, v, \phi) + \delta_z(-u, v, \phi + \pi) = \pi. \quad (2.19)$$

Just as the  $y$ -component, the longitudinal component  $e_z$  equals zero along the optical axis. On using the small argument approximation for the Bessel function in Eq. (2.5c), one finds that along an oblique ray through the geometrical focus  $e_z \sim -|u| \cos \phi$ , and hence

$$\lim_{u \uparrow 0} \delta_z(u, v, \phi) = \pi \times \Theta[\cos \phi], \quad (2.20a)$$

$$\lim_{u \downarrow 0} \delta_z(u, v, \phi + \pi) = \pi \times \Theta[-\cos \phi]. \quad (2.20b)$$

with  $\Theta(x)$  being the Heaviside stepfunction

$$\Theta(x) = \begin{cases} 0 & \text{if } x < 0, \\ 1 & \text{if } x > 0. \end{cases} \quad (2.21)$$

The  $\pi$  phase discontinuity in  $e_z$  as the ray passes through focus is related to the fact that the angle  $\phi$ , which defines the orientation of the meridional plane that contains the ray, has a discontinuity there of an amount  $\pi$ . (It is to be noted that the  $\phi$ -dependence of  $e_x$  and  $e_y$  is such that this jump does not affect these two field components.) Examples of the phase anomaly of the longitudinal electric field are shown in Fig. 2.11. It is seen that when the angle that the ray makes with the axis becomes larger, the oscillations of the phase anomaly become more damped. A comparison of Eqs. (2.12), (2.15) and (2.19) shows that the phases of the three Cartesian components of the electric field satisfy different symmetry relations. Furthermore, Eqs. (2.13), (2.16) and (2.20) show that their behavior at the geometrical focus is also different.

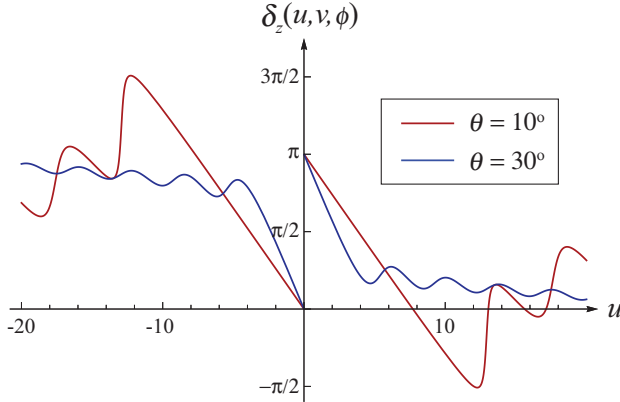


Figure 2.11: The phase anomaly  $\delta_z(u, v, \phi)$  of the electric field component  $e_z$  along two rays through the geometric focus in the meridional plane  $\phi = 180^\circ$ . The angle of inclination of each ray is denoted by  $\theta$ . In this example the semi-aperture angle  $\alpha = 45^\circ$ .

## 2.5 Conclusions

We have examined the phase behavior of the electric field in the vicinity of the geometric focus of an aplanatic, high-numerical aperture system.

All three Cartesian components were found to possess phase singularities. We also showed that the phase anomalies associated with each of the phases are markedly different. The  $x$ -component, along the direction of polarization of the incident field, shows the classical Gouy phase behavior expressed by Eqs. (2.12) and (2.13). Its precise behavior depends on the semi-aperture angle  $\alpha$  of the focusing system. In contrast to the  $x$ -component of the electric field, the other transverse component,  $e_y$ , is singular at the geometric focus. Equation (2.16) shows that its phase anomaly at the focus depends on the orientation of the meridional plane (i.e., on the angle  $\phi$ ), but behaves in a similar manner. The phase anomaly of the longitudinal component  $e_z$  is the only one which does not tend to  $\pm\pi/2$  at the focus. Instead this phase undergoes a phase discontinuity there, by an amount  $\pi$ .

## Chapter 3

# The Gouy phase of Airy beams

This Chapter is based on

- X. Pang, G. Gbur and T.D. Visser,  
“The Gouy phase of Airy beams,”  
*Optics Letters*, vol. 36, pp. 2492-2494 (2011).

### **Abstract**

The phase behavior of Airy beams is studied, and their Gouy phase is defined. Analytic expressions for the idealized, infinite-energy type beam are derived. They are shown to be excellent approximations for finite-energy beams generated under typical experimental conditions.

## 3.1 Introduction

Beams that do not spread on propagation, so-called non-diffracting beams, have attracted considerable attention since they were discovered by Durnin *et al.* [DURNIN, 1987; DURNIN *et al.*, 1987; TURUNEN AND FRIBERG, 2010]. A special type of such beams are the so-called Airy beams described by Berry and Balazs in the context of quantum mechanics [BERRY AND BALAZS, 1979]. These beams have the remarkable property that they “accelerate” away from the original direction of propagation. Airy beams are idealizations, because they carry an infinite amount of energy. Siviloglou and Christodoulides discussed how an exponentially modulated Airy function source would produce a finite-energy beam, which would retain its non-diffracting and accelerating behavior over an appreciable propagation distance [SIVILOGLOU AND CHRISTODOULIDES, 2007]. After the experimental realization of such a beam [SIVILOGLOU *et al.*, 2007], several studies have been devoted to their properties [BANDRES, 2008; MORRIS *et al.*, 2009; S. VO *et al.*, 2010; KAGANOVSKY AND HEYMAN, 2010], and a number of applications are being pursued. For instance, the “self-healing” capacity of Airy beams [BROKY *et al.*, 2008] makes them excellent candidates for optical communication through turbulent media [GU AND GBUR, 2010]. Other intriguing applications are the generation of curved plasma channels [POLYNKIN *et al.*, 2009], and the manipulation of particles along bends in labs-on-a-chip [HANNAPPEL *et al.*, 2009].

Traditionally, the term Gouy phase describes how the phase of a monochromatic, focused field differs from that of a plane wave with the same frequency (see [VISSER AND WOLF, 2010] and the references therein). Recently, however, it has also been used to describe the phase of a non-diffracting Bessel beam [MARTELLI *et al.*, 2010]. In this chapter we study the phase behavior of both finite-energy and infinite-energy Airy beams. By comparing their phase to that of a suitable reference field, their Gouy phase can be defined. A good understanding of the phase properties of Airy beams is of great importance in interferometric or remote sensing applications employing them.

## 3.2 The Schrödinger equation and the paraxial wave equation

The one-dimensional potential-free Schrödinger equation for a particle with mass  $m$  reads

$$-\frac{\hbar}{2m} \frac{\partial^2 \psi(x, t)}{\partial x^2} = i\hbar \frac{\partial \psi(x, t)}{\partial t}. \quad (3.1)$$

A possible solution [BERRY AND BALAZS, 1979] can be expressed as

$$\psi(x, t) = \text{Ai} \left[ \frac{B}{\hbar^{2/3}} \left( x - \frac{B^3 t^2}{4m^2} \right) \right] \exp \left[ i \frac{B^3 t}{2m\hbar} \left( x - \frac{B^3 t^2}{6m^2} \right) \right]. \quad (3.2)$$

Here Ai denotes the Airy function and  $B$  is an arbitrary constant. In this solution, the probability density  $|\psi|^2$  propagates without distortion and with constant acceleration. The correctness of Eq. (3.2) can be verified by direct substitution, while making use of the differential property of the Airy function [ABRAMOWITZ AND STEGUN, 1965]

$$\frac{d^2 \text{Ai}(z)}{dz^2} = z \text{Ai}(z). \quad (3.3)$$

The one-dimensional paraxial wave equation reads [MANDEL AND WOLF, 1995, Sec. 5.6.1]

$$\frac{\partial^2 \phi}{\partial x^2} + 2ik \frac{\partial \phi}{\partial z} = 0, \quad (3.4)$$

where  $k = 2\pi/\lambda$  is the wavenumber and  $(x, z)$  are the transverse and longitudinal coordinates, respectively. Comparing Eqs. (3.4) and (3.1) we find that the two equations are of the same mathematical form. We therefore try a solution for the paraxial wave equation of the type

$$\phi(x, z) = \text{Ai}(\chi x - \epsilon z^2) \exp[i(\gamma x z - \eta z^3)], \quad (3.5)$$

with  $\chi$  an arbitrary constant, and  $\epsilon, \gamma, \eta$  to be determined. Differentiation with respect to  $x$  yields

$$\frac{\partial \phi}{\partial x} = (\chi \text{Ai}' + i\gamma z \text{Ai}) \exp[i(\gamma x z - \eta z^3)], \quad (3.6)$$

and

$$\frac{\partial^2 \phi}{\partial x^2} = (\chi^2 \text{Ai}'' + i2\chi\gamma z \text{Ai}' - \gamma^2 z^2 \text{Ai}) \exp[i(\gamma x z - \eta z^3)]. \quad (3.7)$$

Using the differential property of the Airy function [Eq. (3.3)], we find that the previous equation can be re-written as

$$\frac{\partial^2 \phi}{\partial x^2} = [i2\chi\gamma z \text{Ai}' + (\chi^3 x - \gamma^2 z^2 - \epsilon \chi^2 z^2) \text{Ai}] \exp[i(\gamma x z - \eta z^3)]. \quad (3.8)$$

Differentiation with respect to  $z$  of Eq. (3.5) gives

$$-i2k \frac{\partial \phi}{\partial z} = [i4\epsilon k z \text{Ai}' + (2\gamma k x - 6\eta k z^2) \text{Ai}] \exp[i(\gamma x z - \eta z^3)]. \quad (3.9)$$

The terms in  $\text{Ai}$  and  $\text{Ai}'$  in Eq. (3.8) and Eq. (3.9) must be identical, and thus we obtain the relations

$$2\gamma k x - 6\eta k z^2 = \chi^3 x - (\gamma^2 + \epsilon \chi^2) z^2, \quad (3.10)$$

$$4\epsilon k = 2\chi\gamma. \quad (3.11)$$

Since the same kind of terms in  $x$  and  $z$  must have the same coefficients, we find the following relationships

$$\gamma = \chi^3 / (2k) = 1 / (2k x_0^3), \quad (3.12)$$

$$\epsilon = \chi^4 / (4k^2) = 1 / (4k^2 x_0^4), \quad (3.13)$$

$$\eta = \chi^6 / (12k^3) = 1 / (12k^3 x_0^6), \quad (3.14)$$

where we have defined  $\chi = 1/x_0$ . So a solution of the paraxial wave equation in terms of an Airy function can be expressed as

$$\phi(x, z) = \text{Ai} \left[ \frac{x}{x_0} - \left( \frac{z}{2k x_0^2} \right)^2 \right] \exp \left[ i \frac{xz}{2k x_0^3} - i \frac{1}{12} \left( \frac{z}{k x_0^2} \right)^3 \right]. \quad (3.15)$$

Next we define  $s \equiv x/x_0$ , which represents a dimensionless transverse coordinate, and  $\xi \equiv z/(k x_0^2)$ , a normalized propagation distance. The field envelope  $\phi$  can then be rewritten as [SIVILOGLOU AND CHRISTODOULIDES, 2007]

$$\phi(s, \xi) = \text{Ai} \left[ s - \left( \frac{\xi}{2} \right)^2 \right] \exp(i s \xi / 2 - i \xi^3 / 12). \quad (3.16)$$

This expression for the envelope of an infinite-energy Airy beam will be analyzed in the succeeding sections.

### 3.3 Green's function and Hankel function

The Helmholtz equation for scalar fields reads

$$\nabla^2 U(\mathbf{r}, \omega) + k^2 U(\mathbf{r}, \omega) = -4\pi\kappa(\mathbf{r}, \omega), \quad (3.17)$$

where  $\kappa$  is the source density.

A differential equation such as Eq. (3.17) defines a local relationship between the field at given point and the source term. A Green's function is an integral kernel that can be used to solve such an equation with certain boundary conditions. For the Helmholtz equation, the Green's function is defined as:

$$\nabla^2 G(\mathbf{r}, \mathbf{r}', \omega) + k^2 G(\mathbf{r}, \mathbf{r}', \omega) = -4\pi\delta(\mathbf{r} - \mathbf{r}'). \quad (3.18)$$

The Green's function of Eq. (3.18) can be used to construct the solution

$$U(\mathbf{r}, \omega) = \int_V d^3r' G(\mathbf{r}, \mathbf{r}', \omega)\kappa(\mathbf{r}', \omega), \quad (3.19)$$

in which a homogeneous solution of Eq. (3.17) is omitted and the  $V$  is the support of  $\kappa$ . In three-dimensional space the Green function is of the form

$$G(\mathbf{r}, \mathbf{r}', \omega) = \frac{e^{ik|\mathbf{r}-\mathbf{r}'|}}{|\mathbf{r} - \mathbf{r}'|}. \quad (3.20)$$

In two-dimensional space the Green's function is given by the formula

$$G(\boldsymbol{\rho}, \boldsymbol{\rho}', \omega) = -\frac{i}{4}H_0^{(1)}(k|\boldsymbol{\rho} - \boldsymbol{\rho}'|), \quad (3.21)$$

where  $H_0^{(1)}$  is the Hankel function of the first kind and zero order. The Hankel functions of order  $\alpha$ , which are also known as Bessel functions of the third kind, are defined by the relations

$$H_\alpha^{(1)}(x) = J_\alpha(x) + iY_\alpha(x), \quad (3.22a)$$

$$H_\alpha^{(2)}(x) = J_\alpha(x) - iY_\alpha(x), \quad (3.22b)$$

where  $J_\alpha(x)$  and  $Y_\alpha(x)$  are Bessel functions of first and second kind, respectively. We will make use of Eq. (3.21) in the next section.

### 3.4 The Gouy phase of Airy beams

Consider a monochromatic, one-dimensional beam-like wave field  $U(x, z, \omega)$  that propagates in the positive  $z$ -direction, and can be written as

$$U(x, z, \omega) = \phi(x, z)e^{i(kz - \omega t)}, \quad (3.23)$$

with the envelope  $\phi(x, z)$  a solution of the paraxial wave equation

$$\frac{\partial^2 \phi}{\partial x^2} + 2ik \frac{\partial \phi}{\partial z} = 0. \quad (3.24)$$

Here  $k = \omega/c$  is the wavenumber associated with frequency  $\omega$ ,  $c$  denotes the speed of light, and  $t$  the time. As discussed in Section 3.2, a possible solution to Eq. (3.24) is the so-called Airy beam, given by the expression [BERRY AND BALAZS, 1979]

$$\phi(s, \xi) = \text{Ai} \left[ s - \left( \frac{\xi^2}{4} \right) \right] \exp \left[ i \left( \frac{s\xi}{2} - \frac{\xi^3}{12} \right) \right], \quad (3.25)$$

with  $\text{Ai}$  the Airy function,  $s = x/x_0$  a dimensionless transverse coordinate, and  $\xi = z/kx_0^2$  a normalized propagation distance. In the remainder the constant  $x_0$  is taken to be positive, and the time-dependent part of the wave field is suppressed. An example of the intensity distribution of an Airy beam is shown in Fig. 3.1, from which both the diffraction-free propagation and the transverse acceleration can be seen.

Because of its curved trajectory, we define the Gouy phase  $\delta$  of an Airy beam as the difference between its phase  $\psi$  and that of an ideal (non-diffracted) diverging cylindrical wave  $U_{\text{cyl}}(x, z, \omega)$  centered on the  $y$ -axis and propagating into the half-space  $z > 0$ , i.e.

$$\delta(x, z, \omega) = \psi[U(x, z, \omega)] - \psi[U_{\text{cyl}}(x, z, \omega)], \quad (3.26)$$

with

$$U_{\text{cyl}}(x, z, \omega) = \frac{iC}{4} H_0^{(1)}(k\rho). \quad (3.27)$$

Here  $C$  is a complex-valued constant,  $H_0^{(1)}$  denotes a Hankel function of the first kind of order zero, and  $\rho = (x^2 + z^2)^{1/2}$ . The asymptotic

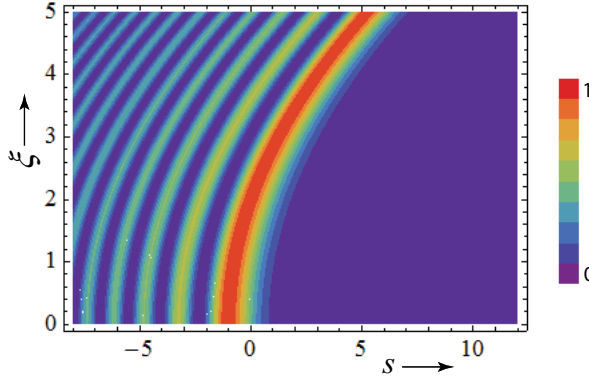


Figure 3.1: Normalized intensity distribution of an Airy beam propagating in the positive  $\xi$ -direction.

behavior of the cylindrical wave field is given by the expression [ARFKEN AND WEBER, 1995]

$$U_{\text{cyl}}(x, z, \omega) \sim C \sqrt{\frac{2}{\pi k \rho}} e^{i(k\rho - \pi/4)}, \quad (k\rho \gg 1/4). \quad (3.28)$$

We choose the constant  $C$  in Eq. (3.27) such that  $\psi[U_{\text{cyl}}(x, z, \omega)] = k\rho$ . For  $z \gg x$  this may be written as

$$k\rho \approx kz \left[ 1 + \frac{1}{2} \left( \frac{x}{z} \right)^2 \right] = kz + \frac{1}{2} \frac{s^2}{\xi}. \quad (3.29)$$

Thus we have from Eqs. (3.23), (3.25) and (3.29) that

$$\delta(s, \xi, \omega) = \frac{s\xi}{2} - \frac{\xi^3}{12} - \frac{s^2}{2\xi} + \psi_{\text{Ai}}, \quad (3.30)$$

where  $\psi_{\text{Ai}}$  is the phase of the Airy function of Eq. (3.25). For real values of its argument the Airy function is real, and hence  $\psi_{\text{Ai}}$  equals 0 or  $\pi$ . The first zero of  $\text{Ai}(x)$  (i.e. the zero with the largest value of  $x$ ), occurs near  $x = -2.34$ . On making use of this in Eq. (3.25), we find that  $\psi_{\text{Ai}} = 0$  when  $\xi < 2(s + 2.34)^{1/2}$ . We first restrict our attention to this region of  $s\xi$ -space.

It is seen from Eq. (3.25) that the maximum beam intensity,  $|\phi(s, \xi)|^2$ , occurs on a quadratic trajectory. We therefore study the behavior of the Gouy phase on curves of the type  $s = \alpha\xi^2$ , with  $\alpha$  a positive constant. On substituting this form into Eq. (3.30), it immediately follows that the Gouy phase vanishes identically along two curves, viz.

$$\delta(s, \xi, \omega) = 0, \quad \text{if } s = (3 \pm 3^{1/2})\xi^2/6. \quad (3.31)$$

Similarly, it is seen that the maximum Gouy phase occurs along the curve  $s = \xi^2/2$ , namely

$$\delta(s, \xi, \omega) = \frac{\xi^3}{24}, \quad \text{if } s = \xi^2/2. \quad (3.32)$$

The quadratic trajectory along which the intensity equals  $\text{Ai}^2(0)$ , (next to the maximum intensity, see Fig. 3.1) is given by the expression  $s = \xi^2/4$ . On substituting this form into Eq. (3.30) we find that

$$\delta(s, \xi, \omega) = \frac{\xi^3}{96}, \quad \text{if } s = \xi^2/4. \quad (3.33)$$

We notice in passing that along the  $\xi$ -axis (i.e., the  $z$ -direction) the Gouy phase takes on negative values, i.e.

$$\delta(0, \xi, \omega) = -\frac{\xi^3}{12}. \quad (3.34)$$

Contours of the Gouy phase are shown in Fig. 3.2. Superposed are several quadratic curves. It is seen that the two dashed curves given by Eq. (3.31) indeed coincide with the zero contours. The curve along which the Gouy phase reaches its maximum [see Eq. (3.32)] is displayed as a solid line. The dotted curve is given by Eq. (3.33).

We next turn our attention to the region  $\xi > 2(s + 2.34)^{1/2}$ . Here the Airy function can take on the value zero. At such points its phase  $\psi_{\text{Ai}}$  is singular, as is the Gouy phase. Both phases display a discontinuity of an amount  $\pi$  at these singularities. An example of this behavior is shown in Fig. 3.3. The diagonal line that runs from the left-hand bottom to the right-hand top indicates the fifth zero of the Airy function, i.e.  $\text{Ai}(s - \xi^2/4 = -7.94) = 0$ . It is seen from the color-coding that the Gouy phase exhibits a  $\pi$ -discontinuity across this line.

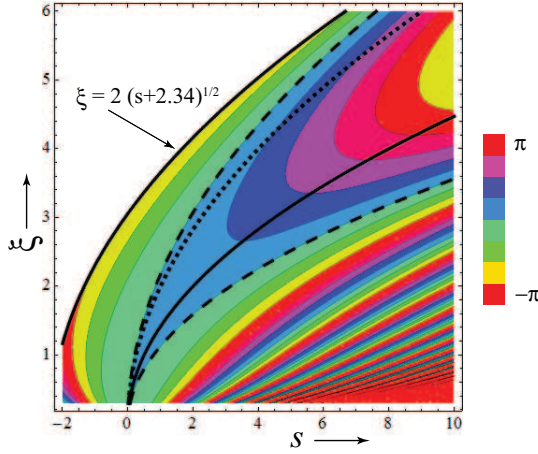


Figure 3.2: Color-coded plot of the Gouy phase of an Airy beam. Only the  $s\xi$ -region in which the Airy function has no zeros is shown. Along the two dashed curves, given by Eq. (3.31), the Gouy phase equals zero. Along the solid curve, given by Eq. (3.32), the Gouy phase reaches its maximum. The dotted curve is given by Eq. (3.33).

The beams we discussed so far are idealizations because the Airy function is not square integrable, i.e. a beam described by Eq. (3.25) carries an infinite amount of energy. Siviloglou and Christodoulides [SIVILOGLOU AND CHRISTODOULIDES, 2007] considered an Airy beam source with an exponential envelope, i.e.

$$\phi^{(fe)}(s, 0) = \text{Ai}(s) e^{as}, \quad (3.35)$$

with the decay parameter  $a > 0$  as to ensure a finite energy contribution, called ( $fe$ ), from the tail of the Airy function. They showed that such a beam propagates as

$$\begin{aligned} \phi^{(fe)}(s, \xi) &= \text{Ai}(s - \xi^2/4 + ia\xi) e^{as - a\xi^2/2} \\ &\times e^{i[-\xi^3/12 + a^2\xi/2 + s\xi/2]}. \end{aligned} \quad (3.36)$$

Such a finite-energy beam still shows the characteristic acceleration and is, at least to some extent, diffraction-free. A beam of this type has

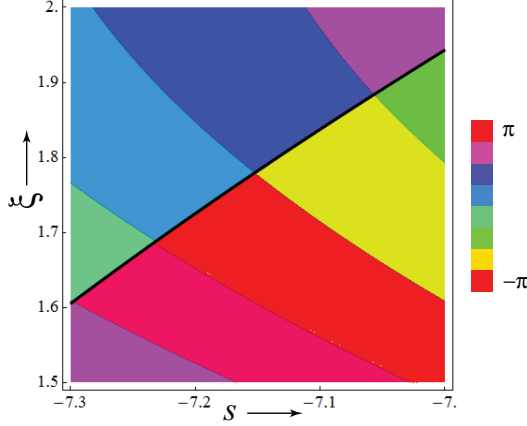


Figure 3.3: Color-coded plot of the Gouy phase of an Airy beam. A portion of the region in which the function  $\text{Ai}(x)$  has zeros is shown. The solid black line indicates the fifth zero of the Airy function. The Gouy phase jumps by an amount  $\pi$  across this line.

been realized using a Gaussian beam incident on a spatial light modulator [SIVILOGLOU *et al.*, 2007]. It follows from Eqs. (3.26) and (3.4) that the Gouy phase for such beams is given by the expression

$$\delta^{(fe)}(s, \xi, \omega) = \frac{s\xi}{2} - \frac{\xi^3}{12} - \frac{s^2}{2\xi} + \frac{a^2\xi}{2} + \psi_{\text{Ai}}. \quad (3.37)$$

It is to be noted that  $\psi_{\text{Ai}}$  now pertains to the Airy function of Eq. (3.4), and is no longer restricted to the values 0 and  $\pi$ . In the experiment reported in [SIVILOGLOU *et al.*, 2007] the parameter values were  $x_0 = 53 \mu\text{m}$ ,  $a = 0.11$  and  $\lambda = 488 \text{ nm}$ . In Fig. 3.4 intensity contours of a finite-energy Airy beam are shown and in Fig. 3.5 selected cross-sections of the corresponding beam intensity are plotted. On propagation the height of the central peak gradually decreases and the beam remains essentially diffraction-free up to  $\xi \approx 5$  (corresponding to a propagation length of 18 cm), after which it rapidly spreads. However, the result expressed in Eq. (3.31), namely that the Gouy phase is zero along two quadratic curves, is still an excellent approximation under these conditions. This is shown in Fig. 3.6 in which the Gouy phase  $\delta^{(fe)}(s, \xi, \omega)$  is plotted along the curves

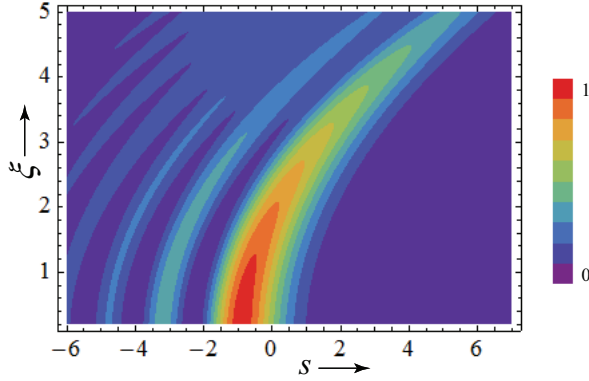


Figure 3.4: Normalized intensity distribution of a finite-energy Airy beam propagating in the positive  $\xi$ -direction. In this example  $x_0 = 53 \mu\text{m}$ ,  $a = 0.11$  and  $\lambda = 488 \text{ nm}$ .

$s = (3 \pm 3^{1/2})\xi^2/6$ . It is seen that the actual value of the phase anomaly is always less than 2. This corresponds to a deviation of less than  $\lambda/3$  from the approximate value zero after a propagation distance of 360,000 wavelengths. Along the curves of Eqs. (3.32) and (3.33) the difference between the analytic expressions pertaining to the infinite-energy beam and a numerical evaluation of Eq. (3.37) is even smaller.

In conclusion, the phase behavior of infinite-energy Airy beams has been analyzed. By comparing this behavior to that of an outgoing cylindrical wave, analytical expressions for their Gouy phase were derived. It was shown numerically that these results are excellent approximations for the Gouy phase of finite-energy Airy beams generated under typical conditions.

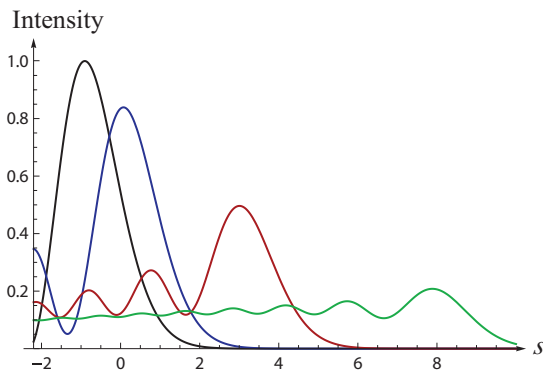


Figure 3.5: Intensity of a finite-energy Airy beam in different cross-sections perpendicular to the  $\xi$ -axis: the source plane  $\xi = 0$  (black),  $\xi = 2$  (blue),  $\xi = 4$  (red), and  $\xi = 6$  (green),

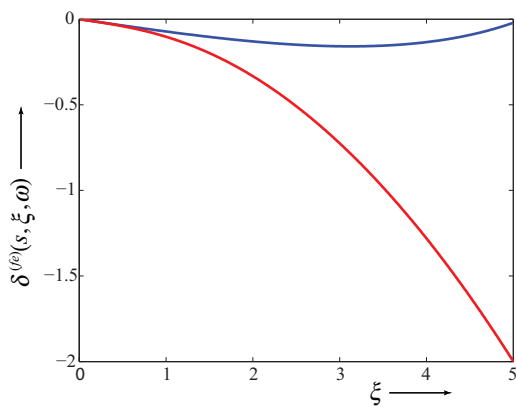


Figure 3.6: Gouy phase of a finite-energy Airy beam along the curves  $s = (3 + 3^{1/2})/6]\xi^2$  (red), and  $s = (3 - 3^{1/2})/6]\xi^2$  (blue).

## Chapter 4

# A generalized Gouy phase for focused, partially coherent wavefields and its implications for optical metrology

This Chapter is based on

- X. Pang, D.G. Fischer and T.D. Visser,  
“Generalized Gouy phase for focused, partially coherent light and its implications for optical metrology,”  
*J. Opt. Soc. Am. A.*, vol. 29, pp. 989-993 (2012).

### **Abstract**

When a monochromatic wavefield is focused, its phase, compared to that of a non-diffracted spherical wave, undergoes a rapid  $\pi$  phase change. This effect bears the name of its discoverer, L.G. Gouy. In a partially coherent wavefield the phase is a random quantity and therefore, when such a field is focused, its Gouy phase is undefined. However, the phase of the correlation functions that characterize partially coherent fields, such as the cross-spectral density and the spectral degree of coherence, *do* have

a well-defined phase. By introducing a generalized Gouy phase that is a function of two positions, we demonstrate that the correlation functions also undergo a rapid  $\pi$  phase change near focus. The dependence of this phenomenon on the state of coherence is examined. It is shown that in the coherent limit this generalized Gouy phase reduces to the classical Gouy phase. The implications for practical applications such as interference microscopy are examined. It is found that the fringe spacing is strongly influenced by the state of coherence.

## 4.1 Introduction

Traditionally, the Gouy phase is defined as the phase difference between a deterministic monochromatic, focused field and a plane wave or a non-diffracted spherical wave with the same frequency (see [VISSER AND WOLF, 2010] and the references therein). In practice, however, the field is often partially coherent, such as light that is produced by a multi-mode laser, or light that has traveled through the atmosphere or biological tissue. In those cases the phase of the wave field is a random quantity, and hence the Gouy phase is undefined in this situation.

In the space-frequency domain, partially coherent wavefields are characterized by correlation functions such as the cross-spectral density and the spectral degree of coherence [MANDEL AND WOLF, 1995]. In contrast to the field, these complex-valued functions typically have a well-defined phase. By introducing a generalized Gouy phase we show that the correlation functions exhibit a phase anomaly near focus that is remarkably similar to the rapid  $\pi$  phase change that occurs in focused, deterministic wavefields and in the coherent limit the generalized Gouy phase reduces to the classical phase anomaly. The phase behavior of the two-point correlation functions plays a central role in interference effects. We find that the fringe spacing that is observed in a Linnik interferometer is influenced by the state of coherence in a non-trivial manner. The focusing of partially coherent light has been examined by several authors and is reviewed in [GBUR AND VISSER, 2010]. Whereas most such studies deal with intensity distributions, in this chapter we will be concerned with the behavior of correlation functions.

## 4.2 Fully coherent focused fields

Let us first consider a converging, monochromatic field of frequency  $\omega$  that emerges from a circular aperture with radius  $a$  (see Fig. 4.1). The origin  $O$  of the coordinate system is taken at the geometrical focus. The amplitude of the field in the aperture is  $U^{(0)}(\mathbf{r}', \omega)$ , with  $\mathbf{r}'$  the position vector of a point  $Q(\mathbf{r}')$ . According to the Huygens-Fresnel principle, the field at a point  $P(\mathbf{r})$  near focus can be expressed as ([BORN AND WOLF, 1999],

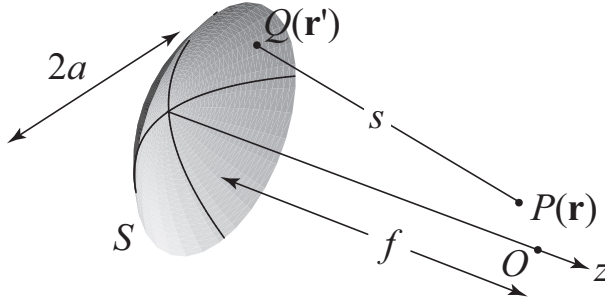


Figure 4.1: Illustrating the notation.

Sec. 8.8)

$$U(\mathbf{r}, \omega) = -\frac{i}{\lambda} \int_S U^{(0)}(\mathbf{r}', \omega) \frac{\exp(iks)}{s} d^2r', \quad (4.1)$$

where the integration extends over the spherical wavefront  $S$  that fills the aperture,  $s = |\mathbf{r} - \mathbf{r}'|$  denotes the distance  $QP$ ,  $\lambda$  is the wavelength and  $k = 2\pi/\lambda$  is the wavenumber associated with frequency  $\omega$ . Using the Debye approximation one can derive for the space-dependent part of the field the expression ([BORN AND WOLF, 1999], Sec. 8.8)

$$U(x, y, z) = -ik \frac{a^2}{f^2} C e^{ikz} \int_0^1 J_0 \left( k \frac{a}{f} \sqrt{x^2 + y^2} \rho \right) e^{-ikz\rho^2 a^2 / 2f^2} \rho d\rho, \quad (4.2)$$

where  $f$  denotes the radius of the wavefront,  $C$  is a positive constant, and  $J_0$  is the Bessel function of the first kind and zero order. For axial points ( $x = y = 0$ ), Eq. (4.2) reduces to

$$U(0, 0, z) = -ik \frac{a^2}{f^2} C e^{ikz} \int_0^1 e^{-ikz\rho^2 a^2 / 2f^2} \rho d\rho, \quad (4.3)$$

$$= -ik \frac{a^2 C}{2f^2} \text{sinc} \left( kz \frac{a^2}{4f^2} \right) e^{ikz(1-a^2/4f^2)}, \quad (4.4)$$

where  $\text{sinc}(x) \equiv \sin(x)/x$ . The argument (or “phase”) of the field is therefore given by the expression

$$\arg[U(0, 0, z)] = \begin{cases} -\frac{\pi}{2} + kz \left(1 - \frac{a^2}{4f^2}\right) \pmod{2\pi}^1, & \text{if } \text{sinc}\left(kz \frac{a^2}{4f^2}\right) > 0, \\ \frac{\pi}{2} + kz \left(1 - \frac{a^2}{4f^2}\right) \pmod{2\pi}, & \text{if } \text{sinc}\left(kz \frac{a^2}{4f^2}\right) < 0. \end{cases} \quad (4.5)$$

Since

$$\text{sinc}\left(kz \frac{a^2}{4f^2}\right) > 0, \quad \text{if } |z| < 2\lambda f^2/a^2, \quad (4.6)$$

the phase of the field in the immediate vicinity of the focus can be written as

$$\arg[U(0, 0, z)] = -\frac{\pi}{2} + kz \left(1 - \frac{a^2}{4f^2}\right). \quad (4.7)$$

It follows from Eq. (4.7) that on the optical axis the phase changes *slower* than that of a plane wave of the same frequency<sup>2</sup>: The effective wavelength near focus equals  $\lambda/(1 - a^2/4f^2)$ .

The Gouy phase  $\delta(z)$  of a focused, monochromatic field at an axial point  $\mathbf{r} = (0, 0, z)$  is defined as the difference between the argument of the field  $U(0, 0, z)$  and that of a plane wave of the same frequency, i.e.

$$\delta(z) \equiv \arg[U(0, 0, z)] - kz \pmod{2\pi}. \quad (4.8)$$

On substituting from Eq. (4.7) into Eq. (4.8) we find that

$$\delta(0) = -\pi/2. \quad (4.9)$$

Furthermore, the Gouy phase has the symmetry property

$$\delta(z) + \delta(-z) = -\pi, \quad (4.10)$$

<sup>1</sup>The symbol  $\text{mod } 2\pi$  denotes that the two sides of the equation are indeterminate to the extent of an additive constant  $2m\pi$  where  $m$  is any integer.

<sup>2</sup>This was first derived in [LINFOOT AND WOLF, 1956], but on page 828 it is erroneously stated that “the equiphase surfaces are spaced *closer* together, by a factor  $1 - a^2/4f^2 \dots$ ”.

and its derivative of near focus is given by the expression

$$\frac{d\delta(z)}{dz} = -k \frac{a^2}{4f^2} \quad [\text{rad/m}]. \quad (4.11)$$

An example of the behavior of the Gouy phase is shown in Fig. 4.2. The discontinuities by an amount of  $\pi$  occur at the zeros (or phase singularities) of the field.

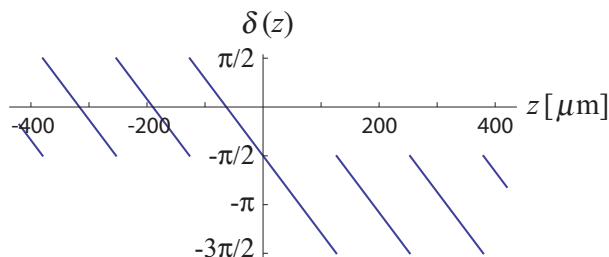


Figure 4.2: The classical Gouy phase  $\delta(z)$  along the optical axis for a deterministic (i.e., fully coherent) focused wave field. In this example  $a = 1$  cm,  $f = 10$  cm and  $\lambda = 0.6328$   $\mu\text{m}$ .

### 4.3 Partially coherent focused fields

For a partially coherent wave field one must consider, instead of the stochastic amplitude  $U^{(0)}(\mathbf{r}', \omega)$ , the cross-spectral density function ([MANDEL AND WOLF, 1995], Sec. 2.4) of the field at two points  $Q_1(\mathbf{r}'_1)$  and  $Q_2(\mathbf{r}'_2)$ , namely,

$$W^{(0)}(\mathbf{r}'_1, \mathbf{r}'_2, \omega) = \langle U^{(0)*}(\mathbf{r}'_1, \omega) U^{(0)}(\mathbf{r}'_2, \omega) \rangle. \quad (4.12)$$

Here the angled brackets denote the average, take over a statistical ensemble of monochromatic realizations  $\{U^{(0)}(\mathbf{r}', \omega) \exp(-i\omega t)\}$  ([MANDEL AND WOLF, 1995], Sec. 4.7) and the asterisk denotes the complex conjugate. The cross-spectral density of the focused field is given by the similar expression

$$W(\mathbf{r}_1, \mathbf{r}_2, \omega) = \langle U^*(\mathbf{r}_1, \omega) U(\mathbf{r}_2, \omega) \rangle. \quad (4.13)$$

On substituting from Eq. (4.1) into Eq. (4.13) we find that

$$W(\mathbf{r}_1, \mathbf{r}_2, \omega) = \frac{1}{\lambda^2} \int_S \int_S W^{(0)}(\mathbf{r}', \mathbf{r}'', \omega) \frac{e^{ik(s_2 - s_1)}}{s_1 s_2} d^2 r' d^2 r'', \quad (4.14)$$

with

$$s_1 = |\mathbf{r}_1 - \mathbf{r}'|, \quad (4.15)$$

$$s_2 = |\mathbf{r}_2 - \mathbf{r}''|. \quad (4.16)$$

From now on we omit the dependence of the various quantities on the frequency  $\omega$ . We assume that the field in the aperture is a Gaussian Schell-model field ([MANDEL AND WOLF, 1995], Sec. 5.4) with uniform intensity  $A^2$ , i.e.,

$$W^{(0)}(\mathbf{r}', \mathbf{r}'') = W^{(0)}(\boldsymbol{\rho}', \boldsymbol{\rho}'') = A^2 e^{-(\boldsymbol{\rho}'' - \boldsymbol{\rho}')^2 / 2\sigma^2}, \quad (4.17)$$

where  $\boldsymbol{\rho} = (x, y)$  is a two-dimensional transverse vector and  $\sigma$  is a positive constant that is a measure of the effective transverse coherence length of the field.

In the following we restrict our attention to observation points on the  $z$ -axis, i.e.  $\mathbf{r}_1 = (0, 0, z_1)$ ,  $\mathbf{r}_2 = (0, 0, z_2)$ . The factors  $s_i$  ( $i = 1, 2$ ) in the denominator of Eq. (4.14) can be approximated by the focal length  $f$  and in the exponent they may be approximated by the expressions

$$s_1 \approx f - \hat{\mathbf{q}}' \cdot \mathbf{r}_1, \quad (4.18)$$

$$s_2 \approx f - \hat{\mathbf{q}}'' \cdot \mathbf{r}_2, \quad (4.19)$$

where  $\hat{\mathbf{q}}'$  and  $\hat{\mathbf{q}}''$  are unit vectors in the directions  $O\mathbf{r}'$  and  $O\mathbf{r}''$ , respectively. In cylindrical coordinates  $\rho$  and  $\phi$  we thus find that

$$\hat{\mathbf{q}}' \cdot \mathbf{r}_1 \approx -z_1(1 - \rho'^2/2f^2), \quad (4.20)$$

$$\hat{\mathbf{q}}'' \cdot \mathbf{r}_2 \approx -z_2(1 - \rho''^2/2f^2). \quad (4.21)$$

On making use of these expressions, Eq. (4.14) becomes

$$W(z_1, z_2) = \left(\frac{A}{\lambda f}\right)^2 \int_0^{2\pi} \int_0^a \int_0^{2\pi} \int_0^a e^{-[\rho'^2 + \rho''^2 - 2\rho'\rho'' \cos(\phi' - \phi'')]/2\sigma^2} \times e^{ik[-z_1(1 - \rho'^2/2f^2) + z_2(1 - \rho''^2/2f^2)]} \rho'\rho'' d\phi' d\rho' d\phi'' d\rho'' \quad (4.22)$$

where we have used the relation  $dx dy = \rho d\rho d\phi$ . Since

$$\int_0^{2\pi} \int_0^{2\pi} e^{\rho' \rho'' \cos(\phi' - \phi'') / \sigma^2} d\phi' d\phi'' = 4\pi^2 I_0 \left( \frac{\rho' \rho''}{\sigma^2} \right), \quad (4.23)$$

with  $I_0$  denoting the modified Bessel function of order zero, we finally obtain for the cross-spectral density the formula [FISCHER AND VISSER, 2004]

$$W(z_1, z_2) = A^2 \frac{k^2}{f^2} \int_0^a \int_0^a e^{-(\rho'' + \rho')^2 / 2\sigma^2} I_0 \left( \frac{\rho' \rho''}{\sigma^2} \right) \times e^{ik[-z_1(1-\rho'^2/2f^2) + z_2(1-\rho''^2/2f^2)]} \rho' \rho'' d\rho' d\rho''. \quad (4.24)$$

The cross-spectral density can be normalized by defining the spectral degree of coherence as

$$\mu(z_1, z_2) \equiv \frac{W(z_1, z_2)}{[S(z_1)S(z_2)]^{1/2}}, \quad (4.25)$$

with the spectral density distribution  $S(z) = W(z, z)$ . Since  $S(z)$  is a positive, real-valued function, the spectral degree of coherence  $\mu(z_1, z_2)$  and the cross-spectral density  $W(z_1, z_2)$  have the same phase.

## 4.4 A generalized Gouy phase

Let us introduce a *generalized Gouy phase* as the difference between the phase of the cross-spectral density  $W(z_1, z_2)$  and the phase of  $e^{ik(z_2 - z_1)}$ , i.e.

$$\delta_\mu(z_1, z_2) = \arg[W(z_1, z_2)] - k(z_2 - z_1) \pmod{2\pi}. \quad (4.26)$$

Here the subscript  $\mu$  indicates that this definition pertains to the phase of the cross-spectral density or, equivalently, the spectral degree of coherence. The reference phases  $kz_1$  and  $kz_2$  are those of a plane wave of frequency  $\omega = kc$ , with  $c$  the speed of light, at positions  $z_1$  and  $z_2$ , respectively. In contrast to the classical Gouy phase, definition (4.26) involves the phase of a two-point correlation function rather than that of a deterministic wave field that only depends on a single spatial variable. In addition, two reference phases are taken into account instead of one.

Let us take the first observation point at origin  $O$ , i.e.,  $z_1 = 0$ . The cross-spectral density of Eq. (4.24) now becomes

$$W(0, z_2) = A^2 \frac{k^2}{f^2} \int_0^a \int_0^a e^{-(\rho'' + \rho')^2 / 2\sigma^2} I_0 \left( \frac{\rho' \rho''}{\sigma^2} \right) e^{ikz_2(1 - \rho''^2 / 2f^2)} \rho' \rho'' d\rho' d\rho'', \quad (4.27)$$

and Eq. (4.26) reduces to

$$\delta_\mu(0, z_2) = \arg \left[ \int_0^a \int_0^a e^{-(\rho'' + \rho')^2 / 2\sigma^2} I_0 \left( \frac{\rho' \rho''}{\sigma^2} \right) e^{-ikz_2 \rho''^2 / 2f^2} \rho' \rho'' d\rho' d\rho'' \right]. \quad (4.28)$$

Examples of the generalized Gouy phase are shown in Fig. 4.3 for different values of the normalized transverse coherence length  $\sigma/a$ . It is seen that  $\delta_\mu(0, z_2)$  exhibits an anomalous phase behavior that is quite similar to that of deterministic fields, with the phase near focus undergoing a rapid phase change of  $\pi$ . In addition, the generalized Gouy phase obeys the following relations:

$$\delta_\mu(0, 0) = 0 \quad (4.29)$$

and

$$\delta_\mu(0, z_2) + \delta_\mu(0, -z_2) = 0, \quad (4.30)$$

which are the statistical analogs of Eqs. (4.9) and (4.10) for the deterministic case. In fact, apart from a  $\pi/2$  offset, which can be traced back to the prefactor  $i$  in Eq. (4.1), they are identical.

On the other hand, there are some striking differences. For instance, the modulation depth of the generalized Gouy phase is dependent on the transverse coherence length of the incident field. It is small for incoherent fields and increases in size as the coherence length is increased. In addition, the generalized Gouy phase has regions of both positive and negative slope, unlike the coherent case for which the slope is always negative. The implications of this for interference experiments will be discussed shortly.

Next we show that the classical phase anomaly is a special case of the generalized Gouy phase. Repeating Eq. (4.13), we have that

$$W(z_1, z_2) = \langle U^*(z_1)U(z_2) \rangle. \quad (4.31)$$

When the field is deterministic, only a single realization exists and the cross-spectral density  $W(z_1, z_2)$  factorizes into the form

$$W(z_1, z_2) = U^*(z_1)U(z_2). \quad (4.32)$$

In that case the Gouy phase expressed by Eq. (4.26) becomes

$$\delta_\mu(z_1, z_2) = \arg[U^*(z_1)] + \arg[U(z_2)] - k(z_2 - z_1) \pmod{2\pi}. \quad (4.33)$$

If we set  $z_1 = 0$ , we get

$$\delta_\mu(0, z_2) = \arg[U(z_2)] - kz_2 + \pi/2 \pmod{2\pi}, \quad (4.34)$$

where we made use of Eq. (4.4). It is seen that in this special case the generalized Gouy phase, apart from an inconsequential constant, reduces to the classical Gouy phase [given by Eq. (4.8)]. Furthermore, in the coherent limit ( $\sigma \rightarrow \infty$ ) Eq. (4.28) can be solved analytically and we obtain the result that near  $z = 0$

$$\delta_\mu(0, z_2) = -kz_2a^2/4f^2, \quad (4.35)$$

which is identical to the Gouy phase behavior of deterministic waves as discussed in connection with Fig. 4.2.

The behavior of the spectral degree of coherence has been studied by [FISCHER AND VISSER, 2004]. An example, calculated from Eq. (4.25) is shown for pairs of axial points  $z_1$  and  $z_2$  in Fig. 4.4. It is seen that  $|\mu(z_1, z_2)|$  is an oscillatory function of the distance  $|z_1 - z_2|$ .

Using Eq. (4.26) the generalized Gouy phase for axial points  $z_1$  and  $z_2$  is computed and displayed in Fig. 4.5. Here the value of the normalized coherence length  $\sigma/a = 0.5$ . In this plot the diagonal line denotes the Gouy phase of the cross-spectral density when  $z_1 = z_2$ . When the coherence length of the field increases, the different contour lines move closer together, as can be seen in Fig. 4.6 and Fig. 4.7.

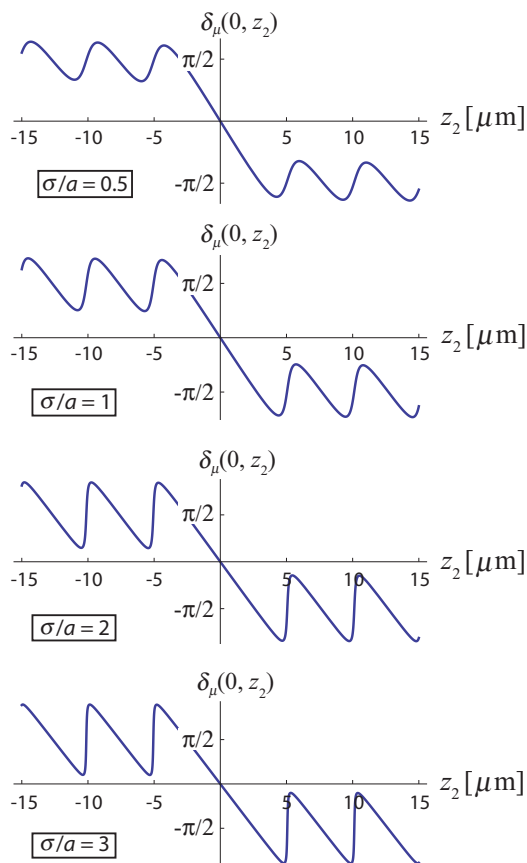


Figure 4.3: The generalized Gouy phase  $\delta_\mu(0, z_2)$  of a focused partially coherent field for different values of the transverse coherence length of the field in the aperture. In these examples  $a = 1$  cm,  $f = 2$  cm, and  $\lambda = 0.6328 \mu\text{m}$ .

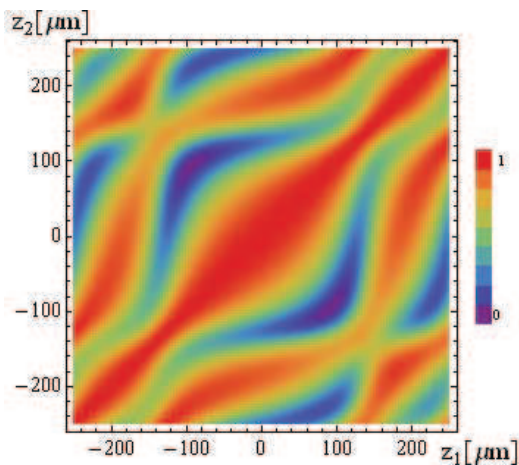


Figure 4.4: Color-coded plot of the modulus of the spectral degree of coherence,  $|\mu(z_1, z_2)|$  when the incident field has a normalized coherence length  $\sigma/a = 0.5$ . In this example  $a = 1$  cm,  $f = 10$  cm, and  $\lambda = 0.6328$   $\mu\text{m}$ .

## 4.5 The origin of the generalized Gouy phase

The physical origin of the classical Gouy phase has been discussed in [VISSER AND WOLF, 2010]. In this section we show that a similar analysis explains the  $\pi$  phase change that the generalized Gouy phase undergoes near focus.

Consider an astigmatic surface  $S'$  with focal lines at  $C_1$  and  $C_2$ . The point  $Q$  represents the intersection of  $S'$  and the  $z$ -axis (see Fig. 4.8), and is taken as the origin of the coordinate system. The two focal lengths are denoted by  $f_1 = QC_1$  and  $f_2 = QC_2$ , respectively.

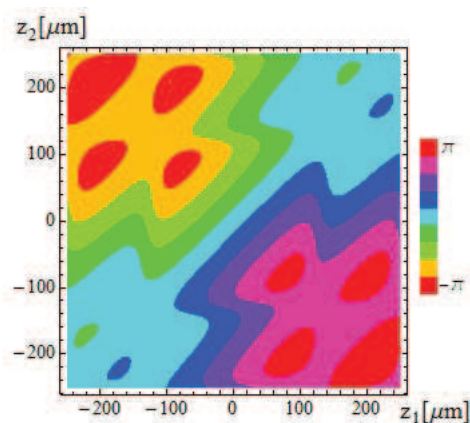


Figure 4.5: The generalized Gouy phase of the cross-spectral density for pairs of axial points  $z_1$  and  $z_2$  when the incident field has a normalized coherence length  $\sigma/a = 0.5$ . In this example  $a = 1$  cm,  $f = 10$  cm, and  $\lambda = 0.6328$   $\mu\text{m}$ .

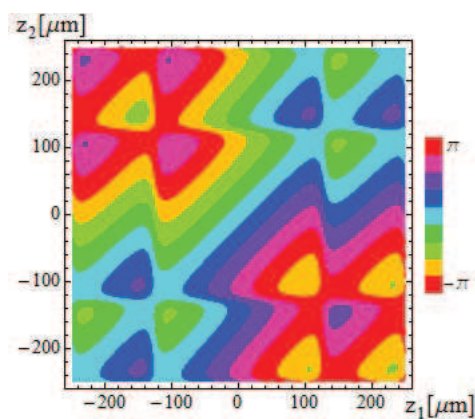


Figure 4.6: The generalized Gouy phase of the cross-spectral density for pairs of axial points  $z_1$  and  $z_2$  when the incident field has a normalized coherence length  $\sigma/a = 1$ . In this example  $a = 1$  cm,  $f = 10$  cm, and  $\lambda = 0.6328$   $\mu\text{m}$ .

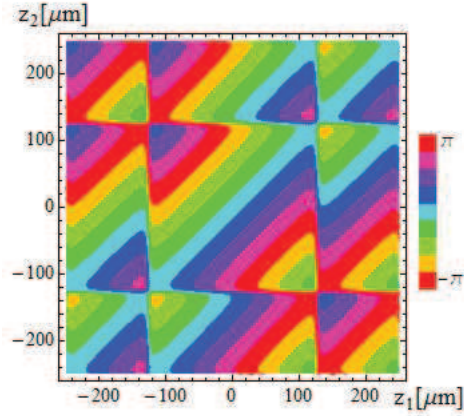


Figure 4.7: The generalized Gouy phase of the cross-spectral density for pairs of axial points  $z_1$  and  $z_2$  when the incident field has a normalized coherence length  $\sigma/a = 2$ . In this example  $a = 1$  cm,  $f = 10$  cm, and  $\lambda = 0.6328$   $\mu\text{m}$ .

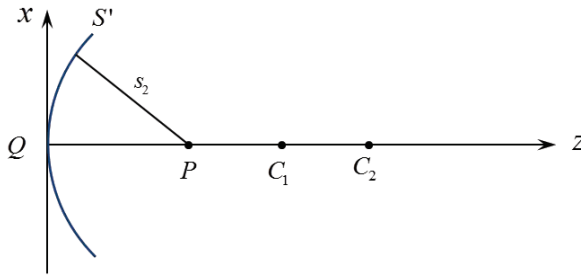


Figure 4.8: An astigmatic surface  $S'$  with focal lines at  $C_1$  and  $C_2$ . The focal lengths  $QC_1 = f_1$  and  $QC_2 = f_2$ . The distance from a point of integration on  $S'$  to the observation point  $P$  is denoted by  $s_2$ .

According to Eq. (4.14) the cross-spectral density can be written as

$$W(\mathbf{r}_1, \mathbf{r}_2) = \frac{1}{\lambda^2} \int_{S'} \int_{S'} W^{(0)}(\mathbf{r}', \mathbf{r}'') \frac{e^{ik(s_2 - s_1)}}{s_1 s_2} d^2 r' d^2 r'', \quad (4.36)$$

with  $s_1, s_2$  given by Eqs. (4.15) and (4.16). If the distance between the two focal lines may be assumed to be small, we have that

$$\frac{1}{s_1} \approx \frac{1}{s_2} \approx \frac{1}{f}, \quad (4.37)$$

where

$$f = \frac{f_1 + f_2}{2}. \quad (4.38)$$

Hence

$$W(\mathbf{r}_1, \mathbf{r}_2) \approx \frac{1}{\lambda^2 f^2} \int_{S'} \int_{S'} W^{(0)}(\mathbf{r}', \mathbf{r}'') e^{ik(s_2 - s_1)} d^2 r' d^2 r''. \quad (4.39)$$

The main contribution to this oscillatory integral comes from those points where  $s_1$  and  $s_2$  are stationary, i.e. in the vicinity of the point  $Q$  in Fig. 4.8. In that region the amplitude function  $W^{(0)}(\mathbf{r}', \mathbf{r}'')$  may be approximated by the value  $W^{(0)}(0, 0)$ . Also, since only the immediate neighborhood around this stationary point contributes significantly to the integral, it is justified to expand the limits of the integration in Eq. (4.39) to minus and plus infinity. Thus we find that

$$W(\mathbf{r}_1, \mathbf{r}_2) \approx C_1 \frac{W^{(0)}(0, 0)}{\lambda^2 f^2} \int_{-\infty}^{\infty} e^{iks_2} d^2 r'' \int_{-\infty}^{\infty} e^{-iks_1} d^2 r', \quad (4.40)$$

with  $C_1$  a constant [STAMNES, 1986].

Next we restrict ourselves to axial points, i.e.  $\mathbf{r}_1 = (0, 0, z_1)$ ,  $\mathbf{r}_2 = (0, 0, z_2)$ . Then Eq. (4.40) can be written as

$$W(z_1, z_2) \approx C_2 \int_{-\infty}^{\infty} e^{iks_2} d^2 r'' \int_{-\infty}^{\infty} e^{-iks_1} d^2 r', \quad (4.41)$$

where  $C_2$  is a constant. Let us first analyze the left-hand integral. Since the equation of the surface  $S'$  is approximately

$$z = \frac{x^2}{2f_1} + \frac{y^2}{2f_2}, \quad (4.42)$$

we have that

$$s_2 = \sqrt{x^2 + y^2 + (z_2 - z)^2}, \quad (4.43)$$

$$\approx z_2 + \alpha_1 x^2 + \alpha_2 y^2, \quad (4.44)$$

where

$$\alpha_1 = \frac{f_1 - z_2}{2f_1z_2}, \quad (4.45)$$

$$\alpha_2 = \frac{f_2 - z_2}{2f_2z_2}. \quad (4.46)$$

This way we find that

$$\int_{-\infty}^{\infty} e^{iks_2} d^2r'' \approx e^{ikz_2} \int_{-\infty}^{\infty} e^{ik(\alpha_1x^2 + \alpha_2y^2)} dx dy. \quad (4.47)$$

Now let us write  $\xi = x\sqrt{k}$ ,  $\mu = y\sqrt{k}$ , then Eq. (4.47) becomes

$$\int_{-\infty}^{\infty} e^{iks_2} d^2r'' \approx e^{ikz_2} \int_{-\infty}^{\infty} e^{i\alpha_1\xi^2} d\xi \int_{-\infty}^{\infty} e^{i\alpha_2\mu^2} d\mu. \quad (4.48)$$

Since

$$\int_{-\infty}^{\infty} e^{\pm it^2} dt = (1 \pm i) \sqrt{\frac{\pi}{2}}, \quad (4.49)$$

we have that

$$\int_{-\infty}^{\infty} e^{i\alpha\xi^2} d\xi = (1 \pm i) \sqrt{\frac{\pi}{2|\alpha|}}, \quad (4.50)$$

according as  $\alpha$  is positive or negative. Three cases can now be distinguished:

- 1) The point  $P$  lies to the left of  $C_1$  and  $C_2$ , i.e.,  $z_2 < f_1 < f_2$ . In this case  $\alpha_1, \alpha_2 > 0$  and

$$\int_{S'} e^{iks_2} d^2r'' \approx i2\pi z_2 e^{ikz_2} \sqrt{\frac{f_1 f_2}{(f_1 - z_2)(f_2 - z_2)}}. \quad (4.51)$$

- 2) The point  $P$  is located between  $C_1$  and  $C_2$ , i.e.,  $f_1 < z_2 < f_2$ . In this case  $\alpha_1$  is negative and  $\alpha_2$  is positive, and

$$\int_{-\infty}^{\infty} e^{iks_2} d^2r'' \approx 2\pi z_2 e^{ikz_2} \sqrt{\frac{-f_1 f_2}{(f_1 - z_2)(f_2 - z_2)}}. \quad (4.52)$$

- 3) The point  $P$  lies to the right of  $C_2$ , i.e.,  $z_2 > f_2 > f_1$ . Then  $\alpha_1, \alpha_2 < 0$ , and

$$\int_{-\infty}^{\infty} e^{iks_2} d^2r'' \approx -i2\pi z_2 e^{ikz_2} \sqrt{\frac{f_1 f_2}{(f_1 - z_2)(f_2 - z_2)}}. \quad (4.53)$$

A comparison of Eqs. (4.51), (4.52) and (4.53) shows that when the point  $P$  moves through the two focal lines at  $C_1$  and  $C_2$ , the phase of the first integral of Eq. (4.41) twice jumps by an amount of  $\pi/2$ . If now we take the limit of the astigmatism going to zero, the surface  $S'$  becomes spherical and  $f_1 = f_2 = f$ . Also, the two successive  $\pi/2$  phase jumps coincide to yield a single  $\pi$  phase jump.

When we set  $z_1 = (f_2 + f_1)/2 = f$  the second integral becomes

$$\int_{-\infty}^{\infty} e^{-iks_1} d^2r' = \int_{-\infty}^{\infty} e^{-ikf} d^2r' = \text{Constant}. \quad (4.54)$$

The value of this integral can be absorbed in a new constant  $C_3$ , and we obtain the expression

$$W(z_1, z_2) = C_3 \int_{-\infty}^{\infty} e^{iks_2} d^2r''. \quad (4.55)$$

According to Eqs. (4.51)–(4.53), for a spherical surface the generalized Gouy phase undergoes a  $\pi$  phase jump, just like its classical counterpart. This discontinuous behavior is the result of the use of the method of stationary phase in which the limit  $k \rightarrow \infty$  is studied. As is well known, this limit yields the results of geometrical optics. The actual field, however, satisfies the Helmholtz equation, the solutions of which are continuous. We can therefore expect the  $\pi$  phase jump to be “smoothed out” into a rapid, but continuous  $\pi$  phase change as is indeed seen in Fig. 4.3.

## 4.6 Implications for interferometry

It is well known that the fringe spacing in interference microscopy is typically irregular, and depends on both the numerical aperture and the apodization [CREATH, 1989; FOLEY AND WOLF, 2005]. It has also recently been established that the spatial coherence of the incident field plays a role, although its treatment has been empirical to date.

To quantitatively investigate the effects of spatial coherence on interference fringe spacing (and, ultimately, on interference metrology) and the role that the generalized Gouy phase plays, we consider the Linnik microscope [KINO AND KORLE, 1996]. Such microscope is a two-beam interferometer which is widely used for studying the structure of reflecting specimens. A sketch is shown in Fig. 4.9. In this figure, two identical microscope objectives are placed in each arm. In one arm a reference object is placed in the focal plane. In the other arm a test object can be scanned through the focus. The superposition of the two reflected beams is recorded as a function of the axial position  $z_2$ . The detected interference pattern is formed by the light emerging from the two axial points,  $P_1 = (0, 0, 0)$ ,  $P_2 = (0, 0, z_2)$ . On making use of Eq. (4.25) we can write the spectral density of this superposition as

$$|U(0) + U(z_2)|^2 = S(0) + S(z_2) + 2\sqrt{S(0)S(z_2)}\text{Re}[\mu(0, z_2)], \quad (4.56)$$

which is commonly known as the *spectral interference law* [MANDEL AND WOLF, 1995, Sec. 4.3].

It is clear from Eq. (4.56) that in an interferogram, in which the spectral density of the superposition is recorded as a function of the distance  $z_2$ , the spacing of the ensuing fringe pattern is determined by  $\mu(0, z_2)$ , the spectral degree of coherence. When the field is fully coherent, the spectral density of the field can be expressed analytically from Eqs. (4.4), (4.32) and (4.56), as

$$\begin{aligned} S(M) = & C^2 \frac{k^2 a^4}{4f^4} + C^2 \frac{4}{z_2^2} \sin^2 \left( kz_2 \frac{a^2}{4f^2} \right) \\ & + 2C^2 \frac{ka^2}{f^2 z_2} \sin \left( kz_2 \frac{a^2}{4f^2} \right) \cos \left[ kz_2 \left( 1 - \frac{a^2}{4f^2} \right) \right]. \end{aligned} \quad (4.57)$$

While for a partially coherent field, such as in our model,  $\mu(0, z_2)$  is characterized by a single parameter, namely the transverse coherence length  $\sigma$  of the field in the aperture. As was seen in Fig. 4.3, this parameter has a significant influence on the phase behavior of the spectral degree of coherence near focus.

For low NA fields,  $S(z_2)$  is a slowly varying function compared to  $\mu(0, z_2)$ , which varies sinusoidally on the scale of the wavelength. For

high NA fields, however,  $S(z_2)$  changes much faster and the maxima of the interference term in Eq. (4.56) are no longer coincident with those of  $\text{Re}[\mu(0, z_2)]$ .

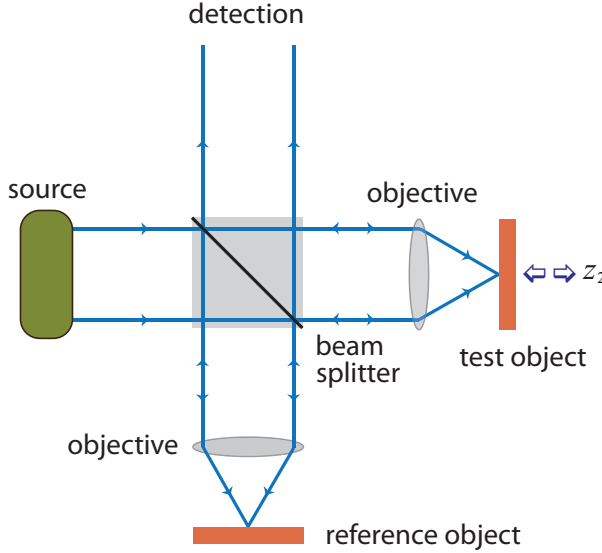


Figure 4.9: Sketch of a Linnik interferometer.

To quantify the effect of the state of coherence of the incident field on the interference process, we have computed the spacing of the fringes for three cases, each with the same (relatively high) numerical aperture and varying degrees of spatial coherence:  $\sigma/a = 0.5$ ,  $\sigma/a = 1$ , and  $\sigma/a = 50$ . The results are listed in Table 4.1 for the first 11 fringes.

As can be seen, in all three cases, the spacings of the first several fringes, which are primarily dictated by  $\mu(0, z_2)$ , are larger than the free-space wavelength. This increased spacing was discussed earlier for the coherent case, and is due to the behavior of the Gouy phase. Accordingly, if the fringe spacings were due solely to  $\mu(0, z_2)$ , we would expect, in coherent case, that they would be identical except when the region between the corresponding intensity maxima contains a phase discontinuity of the Gouy phase. That this is not the case is due to the fact that the spectral density  $S(z_2)$  modulates the spectral degree of coherence [in Eq. (4.56)]

and displaces additional maxima in the neighborhood of the discontinuities. By contrast, for the partially coherent cases, a greater number of fringes are inherently affected near the phase jumps of the generalized Gouy phase. This is because the transition at the jumps is more gradual (i.e. not a true discontinuity). Furthermore, as the field becomes less coherent, the size of the jumps (i.e. the modulation depth) decreases and the transition near the jumps becomes smoother. Therefore, the fringe spacing is highly irregular in all three cases, with the maximum fringe displacement (#8) occurring for the coherent case ( $\sigma/a = 50$ ) and the maximum fringe variation (greater number of affected fringes) and smallest fringe displacement occurring for the least coherent case. The maximum fringe displacements, given by the 8<sup>th</sup> fringe in each case, are 0.5944, 0.5579, and 0.4647, from least coherent to most coherent.

Table 4.1: Fringe spacings for three values of the transverse coherence length  $\sigma$ . In all cases the aperture radius  $a = 1$  cm, the focal length  $f = 2$  cm, and the free-space wavelength is  $\lambda = 0.6328$   $\mu\text{m}$ .

#	$\sigma/a = 0.5$	$\sigma/a = 1$	$\sigma/a = 50$
1	0.6675	0.6702	0.6730
2	0.6671	0.6699	0.6730
3	0.6662	0.6695	0.6730
4	0.6642	0.6683	0.6729
5	0.6602	0.6657	0.6724
6	0.6509	0.6582	0.6702
7	0.6284	0.6311	0.6560
8	0.5944	0.5579	0.4647
9	0.6044	0.5926	0.5975
10	0.6368	0.6465	0.6652
11	0.6519	0.6601	0.6704

In Figs. 4.10 and 4.11, we have plotted the interferograms corresponding to the first and third cases in Table 4.1 ( $\sigma/a = 0.5$  and  $\sigma/a = 50$ ).

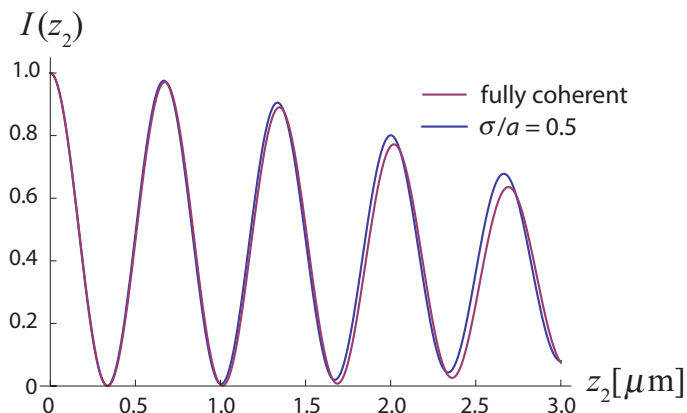


Figure 4.10: Interferogram for a fully coherent field ( $\sigma/a = 50$ ) (red curve), and for a partially coherent field ( $\sigma/a = 0.5$ ) (blue curve). In both cases  $a = 1$  cm,  $f = 2$  cm, and  $\lambda = 0.6328$   $\mu\text{m}$ .

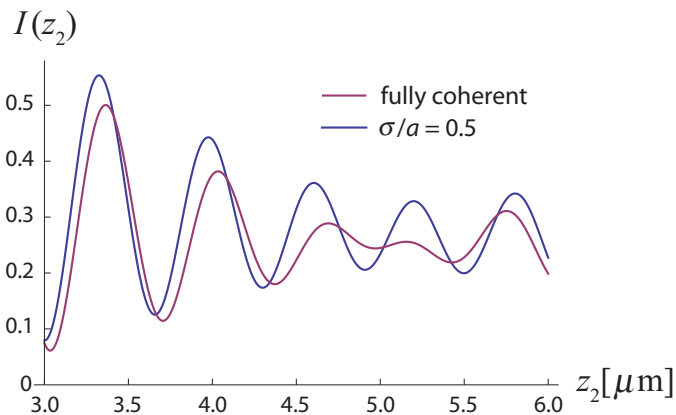


Figure 4.11: Same as Figure 4.10, but for larger values of the axial position  $z_2$ .

It is seen from Fig. 4.10 that the fringe spacing of the fully coherent field (red curve) is initially somewhat larger than that of the partially coherent field (blue curve). However, Fig. 4.11 shows that for larger values of  $z_2$  the fringes of the fully coherent field move closer together and the

maxima of the fringe pattern go from trailing the partially coherent case to leading it. This transition occurs around  $z_2 = 4.5 \mu\text{m}$ , which is precisely the point where the slope of the generalized Gouy phase changes from being negative to being positive (see the top panel of Fig. 4.3). Near  $z_2 = 6.0 \mu\text{m}$  the sign of the slope changes again and fringe spacing of the partially coherent field again becomes smaller than that of the fully coherent field. The slope of the classical Gouy phase (as shown in Fig. 4.12) is, apart from the discontinuities at the axial phase singularities, always negative. Therefore such an effect does not occur for coherent fields.

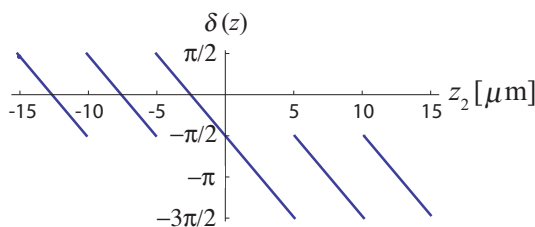


Figure 4.12: The generalized Gouy phase  $\delta_\mu(0, z_2)$  of a fully coherent field. In this example  $a = 1 \text{ cm}$ ,  $f = 2 \text{ cm}$ , and  $\lambda = 0.6328 \mu\text{m}$ .

## 4.7 Conclusions

We have defined a generalized Gouy phase for partially coherent fields. In contrast to its traditional counterpart, this phase pertains to the spectral degree of coherence, a two-point correlation function, rather than to the phase of a deterministic wave field that depends only on a single point. It was shown that the classical phase anomaly is a special case of the generalized Gouy phase. The generalized Gouy phase was examined numerically and analytically for the broad class of Gaussian-correlated fields. It was demonstrated that our findings have important implications for metrology with partially coherent fields.

## Chapter 5

# Manifestation of the Gouy phase in strongly focused, radially polarized beams

This Chapter is based on

- X. Pang and T.D. Visser,  
“Manifestation of the Gouy phase in strongly focused, radially polarized beams,”  
*Optics Express* vol. 21, pp. 8331-8341 (2013).

### **Abstract**

The Gouy phase, sometimes called the focal phase anomaly, is the curious effect that in the vicinity of its focus a diffracted field, compared to a non-diffracted, converging spherical wave of the same frequency, undergoes a rapid phase change by an amount of  $\pi$ . We theoretically investigate the phase behavior and the polarization ellipse of a strongly focused, radially polarized beam. We find that the significant variation of the state of polarization in the focal region, is a manifestation of the different Gouy phases that the two electric field components undergo.

## 5.1 Introduction

The phase anomaly is a measure of how the phase of a monochromatic, focused wave field differs from that of a non-diffracted, converging spherical wave of the same frequency. Since its first description by L.G. Gouy in the 1890s [GOUY, 1890; GOUY, 1891], his namesake phase has been observed under a wide variety of circumstances. Recently investigated systems range from vortex beams [BAUMANN *et al.*, 2009; PHILIP *et al.*, 2012] to fields of surface plasmon polaritons [ZHU *et al.*, 2007]. Surprisingly many different explanations for the physical origin of this remarkable effect have been suggested (see [VISSER AND WOLF, 2010] and the references therein). Because of its crucial role in many applications such as mode conversion [BEIJERSBERGEN *et al.*, 1993], coherence tomography [LAMOUCHE *et al.*, 2004], the tuning of the resonance frequency of laser cavities [KLAASSEN *et al.*, 2004], and interference microscopy (Chapter 4 of this thesis), the Gouy phase continues to attract attention.

When a beam of light is focused by a high-aperture system, the usual scalar formalism no longer suffices, and an analysis of the Gouy phase must then take the vector nature of the field into account. This has recently been done for strongly focused, linearly polarized beams (see Chapter 2 of this thesis). It was found that the Gouy phases of the three Cartesian components of the electric field exhibit quite different behaviors. Another example which requires a vectorial description is the focusing of radially polarized beams [YOUNGORTH AND BROWN, 2000; MARTÍNEZ-HERRERO AND MEJÍAS, 2012]. Because of their intriguing properties, such as a relatively small focal spot size [DORN *et al.*, 2003], these beams are widely used in, for example, the probing of the dipole moment of individual molecules [NOVOTNY *et al.*, 2001], high-resolution microscopy [SHEPPARD AND CHOUDHURY, 2004], trapping of strongly scattering particles [ZHAN, 2004b; NIEMINEN *et al.*, 2008] and in dark-field imaging [BISS *et al.*, 2006]. A review is presented in [BROWN, 2011].

A first indication of the complicated phase behavior of focused, radially polarized beams was the observation that their wave spacing near focus is highly irregular [VISSER AND FOLEY, 2005]. This was followed by a study of the Gouy phase of the longitudinal component of the electric field vector at the focal plane [CHEN *et al.*, 2007]. In the present chapter, the Gouy phase of the total electric field vector, consisting of a radial

and longitudinal longitudinal component, is examined in the entire focal region. It is found that the strong changes in the shape and orientation of the polarization ellipse near focus is a consequence of the different Gouy phases that these two components undergo.

## 5.2 Focused, radially polarized fields

Consider an aplanatic focusing system  $L$  of focal length  $f$  with a semi-aperture angle  $\alpha$ . The geometrical focus is indicated by  $O$  and is taken to

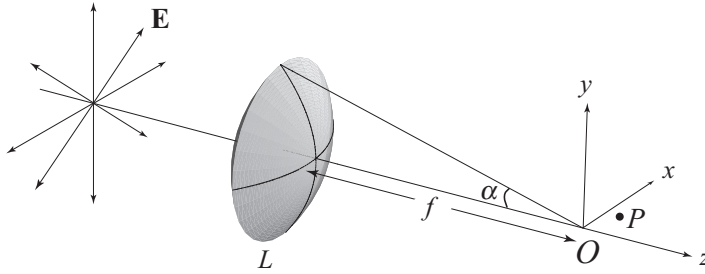


Figure 5.1: A high-numerical-aperture focusing system with an incident beam that is radially polarized.

be the origin of a Cartesian coordinate system (see Fig. 5.1). A monochromatic, radially polarized beam with angular frequency  $\omega$  is incident upon the system. The electric and magnetic fields at time  $t$  at position  $\mathbf{r}$  are given by the expressions

$$\mathbf{E}(\mathbf{r}, t) = \text{Re} [\mathbf{e}(\mathbf{r}) \exp(-i\omega t)], \quad (5.1)$$

$$\mathbf{H}(\mathbf{r}, t) = \text{Re} [\mathbf{h}(\mathbf{r}) \exp(-i\omega t)], \quad (5.2)$$

respectively, where  $\text{Re}$  denotes the real part. Such a field may be generated, for example, by the superposition of two, mutually orthogonally polarized, Hermite-Gaussian beams. If we assume that the entrance plane of the focusing system coincides with the waist plane of the beam, then the longitudinal component  $e_z$  and the radial component  $e_\rho$  of the electric field at a point  $P = (\rho, z)$  in the focal region are given by the equations [VISSER

AND FOLEY, 2005]<sup>1</sup>

$$e_z(\rho, z) = -ikf \int_0^\alpha l(\theta) \sin^2 \theta \cos^{1/2} \theta \times e^{ikz \cos \theta} J_0(k\rho \sin \theta) d\theta, \quad (5.3)$$

$$e_\rho(\rho, z) = -kf \int_0^\alpha l(\theta) \sin \theta \cos^{3/2} \theta \times e^{ikz \cos \theta} J_1(k\rho \sin \theta) d\theta, \quad (5.4)$$

where  $J_i$  is the Bessel function of the first kind of order  $i$  and  $k = \omega/c$ , with  $c$  the speed of light in vacuum, is the wavenumber associated with frequency  $\omega$ . Furthermore,  $l(\theta)$  denotes the angular amplitude function

$$l(\theta) = f \sin \theta \exp[-f^2 \sin^2 \theta / \omega_0^2], \quad (5.5)$$

where  $\omega_0$  is the spot size of the beam in the waist plane. Note that since the incident electric field has no azimuthal component and the configuration is invariant with respect to rotations around the  $z$ -axis, there is no azimuthal component of the electric field in the focal region. The position of an observation point  $P$  may be indicated by the dimensionless Lommel variables  $u$  and  $v$  [RICHARDS AND WOLF, 1959], namely

$$u = kz \sin^2 \alpha, \quad (5.6)$$

$$v = k\rho \sin \alpha. \quad (5.7)$$

Eqs. (5.3) and (5.4) can then be rewritten as

$$e_z(u, v) = -ikf^2 \int_0^\alpha \sin^3 \theta \cos^{1/2} \theta e^{-\beta^2 \sin^2 \theta} \times e^{iu \cos \theta / \sin^2 \alpha} J_0\left(\frac{v \sin \theta}{\sin \alpha}\right) d\theta, \quad (5.8)$$

$$e_\rho(u, v) = -kf^2 \int_0^\alpha \sin^2 \theta \cos^{3/2} \theta e^{-\beta^2 \sin^2 \theta} \times e^{iu \cos \theta / \sin^2 \alpha} J_1\left(\frac{v \sin \theta}{\sin \alpha}\right) d\theta, \quad (5.9)$$

---

<sup>1</sup>This was first derived in [YOUNGORTH AND BROWN, 2000], but we adopt the notation of [VISSER AND FOLEY, 2005].

where

$$\beta = f/\omega_0, \quad (5.10)$$

which denotes the ratio of the focal length of the system and the spot size of the beam in the waist plane.

It follows from Eqs. (5.8) and (5.9) that the field obeys the following symmetry relations:

$$e_z(-u, v) = -e_z^*(u, v), \quad (5.11)$$

$$e_\rho(-u, v) = e_\rho^*(u, v). \quad (5.12)$$

### 5.3 Two Gouy phases

The Gouy phase  $\delta$  is defined as the difference between the actual phase of the field and that of a (non-diffracted) spherical wave converging to the focus in the half-space  $z < 0$  and diverging from it in the half-space  $z > 0$  ([BORN AND WOLF, 1999, Sec. 8.8, Eq. (48)]). For each individual component of the electric field we therefore define a Gouy phase as

$$\delta_z(u, v) = \arg[e_z(u, v)] - \text{sign}(u)kR, \quad (5.13)$$

$$\delta_\rho(u, v) = \arg[e_\rho(u, v)] - \text{sign}(u)kR, \quad (5.14)$$

where  $R$  is the distance from the observation point to the geometrical focus, i.e.

$$kR = k\sqrt{z^2 + \rho^2} = \frac{1}{\sin \alpha} \sqrt{\frac{u^2}{\sin^2 \alpha} + v^2}, \quad (5.15)$$

and  $\text{sign}(x)$  denotes the sign function

$$\text{sign}(x) = \begin{cases} -1 & \text{if } x < 0, \\ 1 & \text{if } x > 0. \end{cases} \quad (5.16)$$

For the longitudinal field component  $e_z$ , one finds from Eqs. (5.8), (5.11) and (5.13) that the Gouy phase at two points that are symmetrically located with respect to the focus satisfies the relation

$$\delta_z(-u, v) + \delta_z(u, v) = -\pi \pmod{2\pi}. \quad (5.17)$$

At the focus we have

$$\delta_z(0, 0) = -\pi/2 \pmod{2\pi}. \quad (5.18)$$

For the radial field component  $e_\rho$ , it follows from Eqs. (5.9), (5.12) and (5.14) that the Gouy phase satisfies the symmetry relations

$$\delta_\rho(-u, v) + \delta_\rho(u, v) = 0 \pmod{2\pi}. \quad (5.19)$$

Even though  $e_\rho = 0$  when  $v = 0$ , it is useful to study the behavior of  $\delta_\rho$  along a tilted ray through focus; for such a ray  $v \propto |u|$ . Using the fact that for small arguments  $J_n(x) \sim x^n$  [ABRAMOWITZ AND STEGUN, 1965, p. 360] we find from Eq. (5.9) that along such a ray  $e_\rho \sim -|u|$ . Hence

$$\lim_{u \downarrow 0} \delta_\rho(u, v) = \lim_{u \uparrow 0} \delta_\rho(u, v) = \pi \pmod{2\pi}. \quad (5.20)$$

It is seen from Eqs. (5.8) and (5.9) that the electric field components are characterized by two parameters, namely the semi-aperture angle  $\alpha$ , and the beam-size parameter  $\beta$ . These two parameters have a different effect on the Gouy phase behavior as we will now demonstrate.

On the central axis of the system ( $v = 0$ ) only the longitudinal field component  $e_z$  is non-zero. The Gouy phase pertaining to this component,  $\delta_z$ , is shown in Fig. 5.2 for various values of the semi-aperture angle  $\alpha$ . It is seen that the phase change of  $e_z$  decreases as  $\alpha$  increases. Unlike the  $\pi$  phase jump of the longitudinal component in linearly polarized fields (see Chap. 2 of this thesis), the Gouy phase here is continuous at focus. Note that the longitudinal coordinate  $u$  is dependent on the value of the semi-aperture angle  $\alpha$  [See Eq. (5.6)]. In Fig. 5.3 the Gouy phase  $\delta_z$  is depicted for selected values of the beam-size parameter  $\beta$ . For a decreasing beam waist-size ( $\omega_0$ ) the Gouy phase decreases as well. In these two figures, the negative or positive slope of the Gouy phase means that the wave-front spacings can be smaller or bigger than  $\lambda$ . This has been discussed by [VISSER AND FOLEY, 2005].

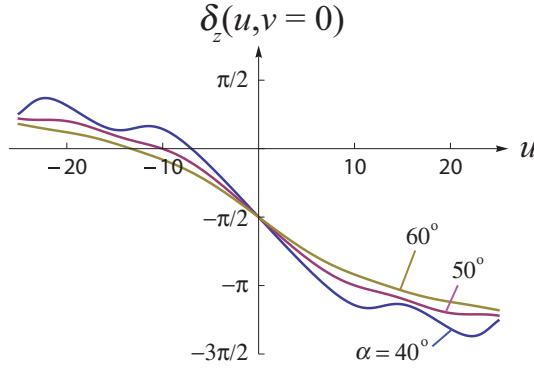


Figure 5.2: The Gouy phase  $\delta_z$  along the optical axis ( $v = 0$ ) of the electric field component  $e_z$  for selected values of the semi-aperture angle  $\alpha$  (blue curve:  $\alpha = 40^\circ$ , red curve:  $\alpha = 50^\circ$ , olive curve:  $\alpha = 60^\circ$ ). The beam-size parameter  $\beta = 3$ .

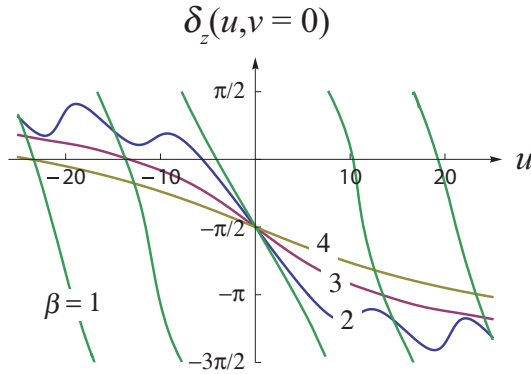


Figure 5.3: The Gouy phase  $\delta_z$  along the optical axis ( $v = 0$ ) of the electric field component  $e_z$  for selected values of the beam-size parameter  $\beta = f/\omega_0$  (green curve:  $\beta = 1$ , blue curve:  $\beta = 2$ , red curve:  $\beta = 3$ , olive curve:  $\beta = 4$ ). The semi-aperture angle  $\alpha = 60^\circ$ .

When  $v \neq 0$ , it follows from Eqs. (5.8) and (5.9) that both the lon-

gitudinal component  $e_z$  and the radial component  $e_\rho$  contribute to the field. The two Gouy phases  $\delta_z$  and  $\delta_\rho$  along an oblique ray through focus, which makes an angle  $\theta = 35^\circ$  with the  $z$ -axis, are shown in Fig. 5.4. It is clear that their respective behaviors are quite different. For example, when  $-10 < u < -5$  the oscillations of  $\delta_z$  and  $\delta_\rho$  are out of phase. The implications of this effect for the state of polarization will be discussed in the next section.

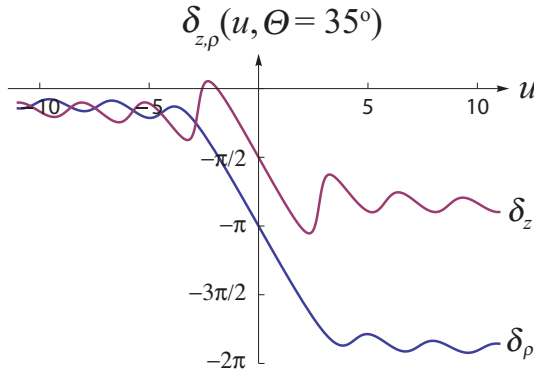


Figure 5.4: The Gouy phase of the longitudinal component  $e_z$  (red curve) and that of the radial component  $e_\rho$  (blue curve) along an oblique ray through focus under an angle  $\theta = 35^\circ$ . Here  $\alpha = 40^\circ$  and  $\beta = 1$ .

## 5.4 The Gouy phase and the state of polarization

It is convenient to characterize the state of polarization of a two-dimensional field by the four Stokes parameters ([BORN AND WOLF, 1999], Sec. 1.4). For a beam propagating in the  $z$ -direction, these parameters are defined in terms of  $e_x$  and  $e_y$ . For a focused, radially polarized fields the two non-zero components of the electric field are  $e_z$  and  $e_\rho$ . It is natural, therefore, to define the Stokes parameters in this case in terms of these components rather than  $e_x$  and  $e_y$  [SCHOONOVER AND VISSER, 2006; MARTÍNEZ-HERRERO

AND MEJÍAS, 2010]. We thus define

$$S_0 = |e_z|^2 + |e_\rho|^2, \quad (5.21)$$

$$S_1 = |e_z|^2 - |e_\rho|^2, \quad (5.22)$$

$$S_2 = 2|e_z||e_\rho| \cos \delta, \quad (5.23)$$

$$S_3 = 2|e_z||e_\rho| \sin \delta, \quad (5.24)$$

where  $\delta = \arg[e_z] - \arg[e_\rho] = \delta_z - \delta_\rho$ . The normalized forms  $s_1 = S_1/S_0$ ,  $s_2 = S_2/S_0$ ,  $s_3 = S_3/S_0$ , can be represented as a point on the Poincaré sphere [GBUR, 2011, p. 316], as shown in Fig. 5.5. On the northern hemisphere ( $s_3 > 0$ ), the polarization is right-handed (clockwise), whereas on the southern hemisphere it is left-handed (counter-clockwise). On both poles ( $s_3 = \pm 1$ ), the polarization is circular and on the equator ( $s_3 = 0$ ), it is linear.

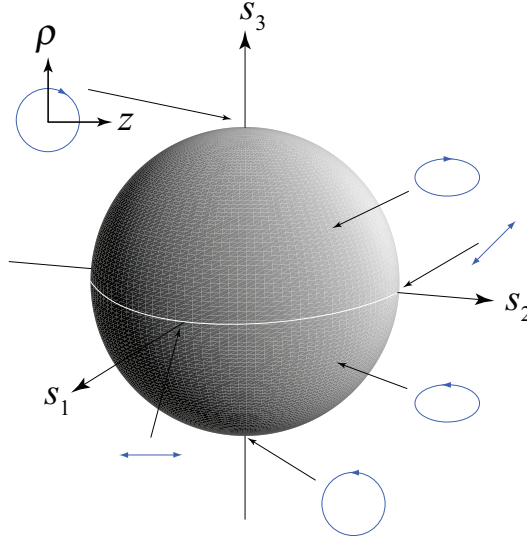


Figure 5.5: The Poincaré sphere with Cartesian axes  $(s_1, s_2, s_3)$  adapted for focused, radially polarized fields.

Along a ray through focus, which makes an angle  $\theta$  with the  $z$ -axis,

we have

$$v = |u| \tan \theta / \sin \alpha. \quad (5.25)$$

From Eqs. (5.11) and (5.12) it immediately follows that

$$|e_z(-u, v)| = |e_z(u, v)|, \quad (5.26)$$

$$|e_\rho(-u, v)| = |e_\rho(u, v)|. \quad (5.27)$$

These two relations are illustrated in Fig. 5.6. They also imply that the first Stokes parameter  $S_0$  is an even function in  $u$ . Using Eqs. (5.17) and (5.19), it is seen that

$$[\delta_z(u, v) - \delta_\rho(u, v)] + [\delta_z(-u, v) - \delta_\rho(-u, v)] = \pi \pmod{2\pi}, \quad (5.28)$$

for the quantity  $\delta$ , which is defined below Eq. (5.24), this implies that  $\cos[\delta(-u, v)] = -\cos[\delta(u, v)]$  and  $\sin[\delta(-u, v)] = \sin[\delta(u, v)]$ . Thus we find the following symmetry relations for the normalized Stokes parameters along a ray through focus:

$$s_1(-u, v) = s_1(u, v), \quad (5.29)$$

$$s_2(-u, v) = -s_2(u, v), \quad (5.30)$$

$$s_3(-u, v) = s_3(u, v). \quad (5.31)$$

An example is presented in Fig. 5.7. It is seen that  $S_0$ ,  $S_1$  and  $S_3$  are even, whereas  $S_2$  is odd.

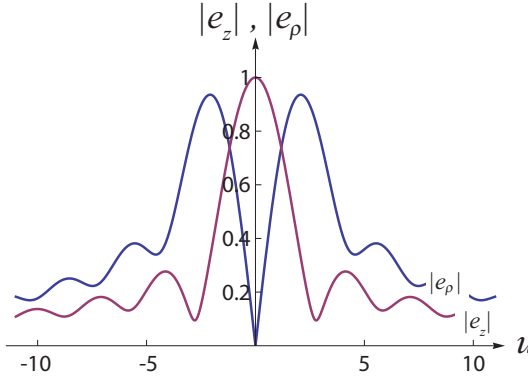


Figure 5.6: The normalized moduli of the longitudinal component  $e_z$  and that of the radial component  $e_\rho$  of the electric field along an oblique ray under an angle  $\theta = 35^\circ$  with the  $z$ -axis. Here we have chosen  $\alpha = 40^\circ$  and  $\beta = 1$ .

The polarization ellipse may be characterized by two angular parameters (see Fig. 5.8). One is the orientation angle,  $\psi$  ( $0 \leq \psi < \pi$ ), which is the angle between the  $z$ -axis and the major axis of the polarization ellipse. The other is the ellipticity angle,  $\chi$  ( $-\pi/4 \leq \chi < \pi/4$ ).  $|\tan \chi|$  represents the ratio of the axes of the ellipse. The values  $\pm\pi/4$  correspond to circular polarization; whereas the value 0 indicates linear polarization. The sign of  $\chi$  distinguishes the two senses of handedness, i.e., it is right-handed when  $\chi > 0$ , and left-handed when  $\chi < 0$ , see [BORN AND WOLF, 1999, Sec. 1.4]. The two angular parameters can be expressed in terms of the normalized Stokes parameters, as

$$\psi = \frac{1}{2} \arctan \left( \frac{s_2}{s_1} \right), \quad (5.32)$$

$$\chi = \frac{1}{2} \arcsin(s_3). \quad (5.33)$$

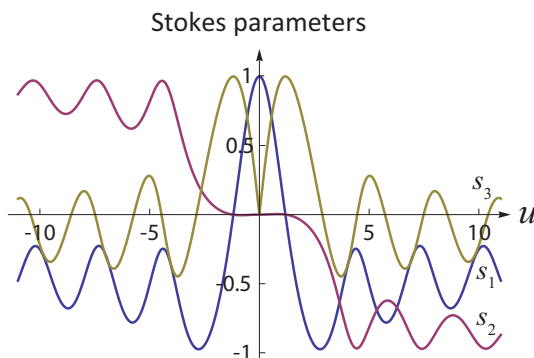


Figure 5.7: The Stokes parameters along an oblique ray through focus which makes an angle  $\theta = 35^\circ$  with the  $z$ -axis ( $s_1$ : blue curve,  $s_2$ : red curve,  $s_3$ : olive curve). Here  $\alpha = 40^\circ$  and  $\beta = 1$ .

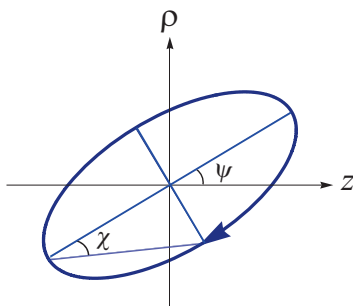


Figure 5.8: Defining the angles  $\psi$  and  $\chi$  of a polarization ellipse.

From the symmetry relations of  $s_1$ ,  $s_2$  and  $s_3$ , it is seen that

$$\psi(-u, v) = \pi - \psi(u, v), \quad (5.34)$$

$$\chi(-u, v) = \chi(u, v). \quad (5.35)$$

Two kinds of polarization singularities can occur. When the polarization ellipse is circular, the orientation angle  $\psi$  is undefined. This happens at

so-called  $C$ -points. When the polarization is linear, the handedness is undefined. This occurs at so-called  $L$ -points. When a system parameter, such as the semi-aperture angle  $\alpha$ , is varied in a continuous manner, these polarization singularities can be created or annihilated. This has been described in [SCHOONOVER AND VISSER, 2006; DIEHL *et al.*, 2006].

The curves of the orientation angle  $\psi$  and the ellipticity angle  $\chi$  along an oblique ray under angle  $\theta = 35^\circ$  are displayed in Figs. 5.9 and 5.10. In Fig. 5.9 it is seen that the orientation angle of the ellipse oscillates somewhat along the ray. Also, a  $C$ -point is seen near  $u = \pm 1.2$ , where the orientation angle  $\psi$  is singular. To the left of the  $C$ -point at  $u = -1.2$ , the polarization ellipse is slightly larger in the  $\rho$ -direction than it is in the  $z$ -direction. This situation is reversed to the right of that  $C$ -point. This coincides with a  $\pi/2$  jump of the angle  $\psi$ . In Fig. 5.10, these  $C$ -points occur when the ellipticity angle  $\chi$  takes on the value  $\pi/4$ . When  $\chi$  equals 0, an  $L$ -point occurs, which happens near points such as  $u = \pm 2.9$ .

In Fig. 5.11 the polarization ellipse is shown for different positions along an oblique ray. The ellipses at  $(u, v)$  and  $(u, -v)$  have the same ellipticity and handedness, whereas their orientations are mirror-symmetric. The changes in the polarization ellipse are closely related to the two Gouy phases, as we will now discuss. When  $u = -4$ , it is seen from Fig. 5.4 that  $\delta = \delta_z - \delta_\rho < 0$ , according to Eq. (5.24) the polarization is then counter-clockwise which corresponds to a point on the southern half of the Poincaré sphere. Near the point  $u = -2.87$ ,  $\delta_z = \delta_\rho$ , and hence the field is linearly polarized with its handedness undefined, corresponding to a point on the equator. In the vicinity of the focus, the Gouy phase difference,  $\delta_z - \delta_\rho$ , is approximately  $\pi/2$  (see Fig. 5.4) and when  $u = -1.2$  the moduli of the two components attain the same magnitude (see Fig. 5.6), therefore the field there is circularly polarized which corresponds to a point on the North pole. The field is linearly polarized at focus due to the zero amplitude of the field component  $e_\rho$ . We also find that from  $u = -4$  to  $u = -1.2$  the handedness of the polarization changes from counter-clockwise, to undefined, to clockwise.

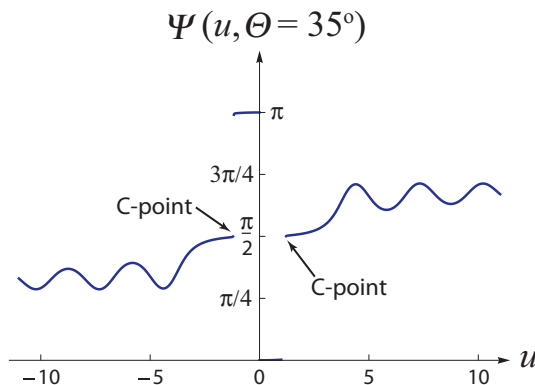


Figure 5.9: The orientation angle  $\psi$  of the polarization ellipse along an oblique ray through focus under an angle  $\theta = 35^\circ$ . Here we have chosen  $\alpha = 40^\circ$  and  $\beta = 1$ .

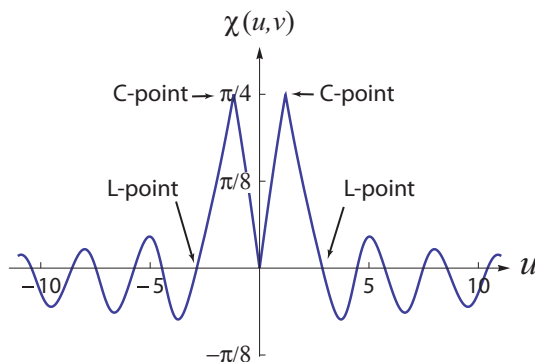


Figure 5.10: The ellipticity angle  $\chi$  of the polarization ellipse along an oblique ray through focus under an angle  $\theta = 35^\circ$ . Here we have chosen  $\alpha = 40^\circ$  and  $\beta = 1$ .

It is seen from Figs. 5.12, 5.13, and 5.14 that along different oblique rays through focus, the polarization ellipse goes through different shapes and states of handedness. This behavior mirrors the different Gouy phases

along these rays. In Fig. 5.12 (with  $\theta = 10^\circ$ ) the handedness is clockwise at all observation points. This means that the Stokes parameter  $s_3 > 0$ , i.e.  $\delta_z - \delta_\rho > 0$ . From Eq. (5.24) we see that this implies that the relative change of the two Gouy phases is limited along this ray. This is also the case for  $\theta = 20^\circ$ , as can be seen from Fig. 5.13. In that case, however, the ellipticity is considerably larger. If the obliquity angle  $\theta$  is further increased to  $30^\circ$  (see Fig. 5.14), the polarization ellipses becomes even narrower. In addition, the handedness evolves from counter-clockwise to clockwise, reflecting the fact that  $\delta_z - \delta_\rho$  changes sign along the ray. Finally, the change in the orientation angle of the ellipses is seen to decrease significantly when the angle  $\theta$  is increased.

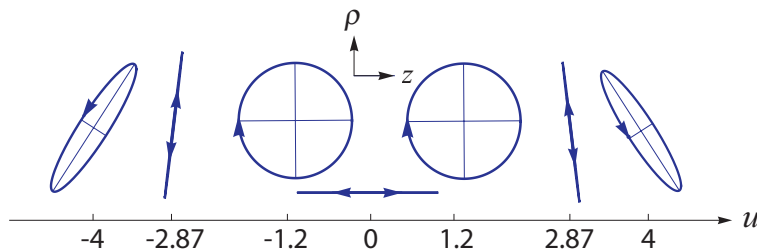


Figure 5.11: Polarization ellipse of the field at selected points along an oblique ray through focus. The ray is under an angle  $\theta = 35^\circ$ . Also,  $\alpha = 40^\circ$  and  $\beta = 1$ .

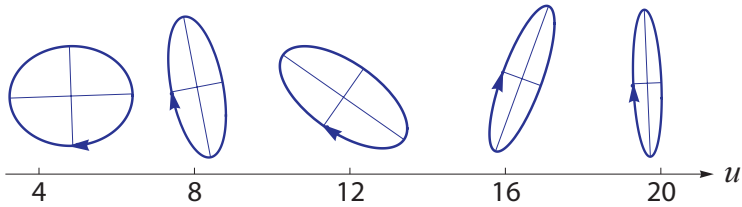


Figure 5.12: Polarization ellipse of the field at selected points along an oblique ray through focus. The ray is under an angle  $\theta = 10^\circ$ . Also,  $\alpha = 40^\circ$  and  $\beta = 1$ .

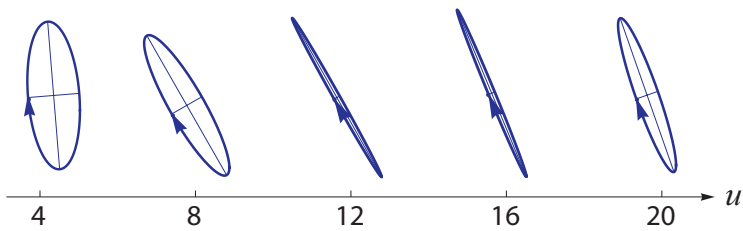


Figure 5.13: Polarization ellipse of the field at selected points along an oblique ray through focus. The ray is under an angle  $\theta = 20^\circ$ . Also,  $\alpha = 40^\circ$  and  $\beta = 1$ .

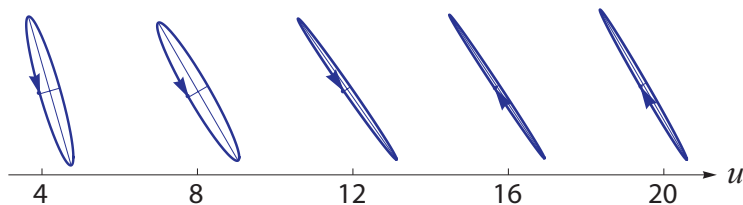


Figure 5.14: Polarization ellipse of the field at selected points along an oblique ray through focus. The ray is under an angle  $\theta = 30^\circ$ . Also,  $\alpha = 40^\circ$  and  $\beta = 1$ .

## 5.5 Conclusions

We have analyzed the phase behavior of strongly focused, radially polarized fields. We found that the Gouy phase of the two components of the electric field are quite different, and have different symmetries. Our results show that the semi-aperture angle  $\alpha$  and the beam-size parameter  $\beta$  can both influence the Gouy phase. If we follow the polarization ellipse along a tilted ray through focus, it is seen to “tumble”, i.e., it changes its orientation, its shape and handedness. This behavior is due to the different Gouy phases that the two components of the electric field undergo.



## Chapter 6

# Wavefront spacing and the Gouy phase in the presence of primary spherical aberration

This Chapter is based on

- X. Pang, D.G. Fischer and T.D. Visser,  
“Wavefront spacing and the Gouy phase in the presence of primary spherical aberration,”  
to be submitted.

### **Abstract**

We study the Gouy phase of a scalar wavefield that is focused by a lens suffering from primary spherical aberration. It is found that the Gouy phase has different behaviors at the two sides of the intensity maximum. This results in a systematic increase of the successive wavefront spacings around the diffraction focus. Since all lenses have some amount of spherical aberration, this observation has implications for optical calibration and metrology.

## 6.1 Introduction

Because of its importance in interference microscopy and optical metrology, the wavefront spacing of focused fields has been the subject of many studies. Linfoot and Wolf [LINFOOT AND WOLF, 1956] derived that the effective wavelength of a scalar field near focus is given by the expression  $\lambda_{\text{eff}} = \lambda/(1 - a^2/4f^2)$ , where  $\lambda$  is the free-space wavelength,  $a$  is the aperture radius and  $f$  denotes the focal length. More recently, the analysis of strongly focused, linearly [FOLEY AND WOLF, 2005] and radially polarized beams [VISSER AND FOLEY, 2005] predicted a wavefront spacing that is highly irregular. Experimental observations of fringe spacings have been discussed in e.g. [CREATH, 1989; SHEPPARD AND LARKIN, 1995; WIEGAND *et al.*, 1998].

A measure of how an actual diffracted focused field differs from an ideal spherical wave is provided by the Gouy phase (sometimes called the “phase anomaly”). This is the sudden  $\pi$  phase shift that a focused field undergoes, compared to a non-diffracted spherical wave of the same frequency [GOUY, 1890; GOUY, 1891]. Its physical origin has been discussed in [VISSER AND WOLF, 2010]. Recently, it has been theoretically investigated in a variety of configurations, such as high-numerical aperture systems (Chapter 2 and Chapter 5 of this thesis), non-diffracting beams [MARTELLI *et al.*, 2010] (Chapter 3) and partially coherent focused fields (Chapter 4). Experimental observations were reported in, e.g. [RUFFIN *et al.*, 1999; MCGOWAN *et al.*, 2000; CHOW *et al.*, 2004; HAMAZAKI *et al.*, 2006; ZHU *et al.*, 2007; KANDPAL *et al.*, 2007]. A precise knowledge of the Gouy phase is crucial in a wide variety of metrological applications. Examples are measurements of acceleration [ROBERTSSON, 2007], distance [CODDINGTON *et al.*, 2009], refractive indices [KUŽEL *et al.*, 2010] and volumes [ANDREAS *et al.*, 2011].

In an actual focusing system aberrations are always present, especially primary spherical aberration, perhaps the most common of the classical Seidel aberrations [BORN AND WOLF, 1999]. It is of interest, therefore, to examine the restrictions that a small amount of spherical aberration puts on the accuracy levels that can be achieved in optical metrology and calibration. In this Letter we analyze the influence of primary spherical aberration on the Gouy phase and the wavefront spacing. We derive expressions for the phase behavior in terms of imaginary error functions

that can easily be calculated. Our main result is that the Gouy phase at the two sides of the diffraction focus (the point of maximum intensity) is markedly different. This results in a systematic increase of the wavefront spacing around the diffraction focus. We show by numerical examples that even a small amount of spherical aberration ( $< \lambda$ ) introduces a change in the wavefront spacing that is significantly larger than is usually assumed.

## 6.2 A focused field with spherical aberration

Let us then consider an aberrated, converging, monochromatic wavefield of frequency  $\omega$  that emerges from a circular aperture with radius  $a$  (see Fig. 6.1). The geometrical focus  $O$  is taken to be the origin of the coordinate system, and  $f$  is the radius of a Gaussian reference sphere  $S$ .

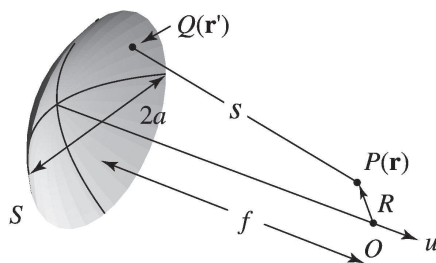


Figure 6.1: Illustrating the notation.

dinate system, and  $f$  is the radius of a Gaussian reference sphere  $S$ . The field in the focal region is given by the expression [BORN AND WOLF, 1999, Sec. 9.1.1]

$$U(P) = -\frac{i}{\lambda} \frac{\mathcal{A} e^{-ikf}}{f} \iint_S \frac{e^{ik[\Phi+s]}}{s} dS, \quad (6.1)$$

where  $k = 2\pi/\lambda$  represents the wavenumber,  $\mathcal{A}$  is an amplitude,  $\Phi$  denotes the aberration function (see Fig. 6.2), and  $s$  is the distance from a point of integration  $Q$  on  $S$  to the observation point  $P$ . For a wavefront with spherical aberration [BORN AND WOLF, 1999, Sec. 9.3, Eq. (7)]

$$\Phi(\rho) = A_0 \rho^4, \quad (6.2)$$

with  $A_0$  the wave aberration at the edge of the exit pupil, and  $0 \leq \rho \leq 1$  a scaled transverse distance. We notice that the focused field is rotationally

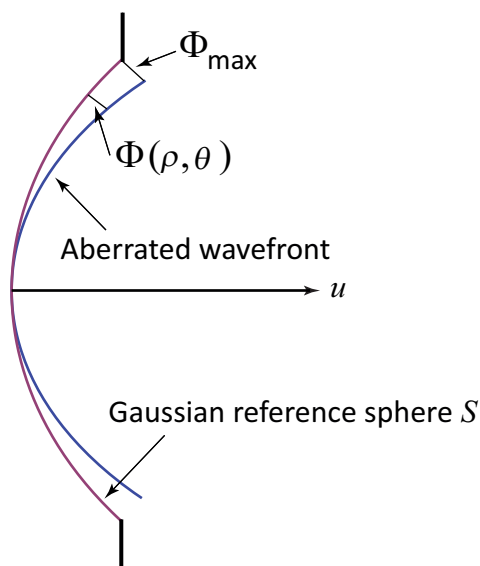


Figure 6.2: An aberrated wavefront, the Gaussian reference sphere  $S$  and the aberration function  $\Phi(\rho, \theta)$ .

symmetric about the optical axis. The position of an observation point  $P$  is indicated by the dimensionless Lommel variables  $u$  and  $v$ , i.e.

$$u = kz \left( \frac{a}{f} \right)^2, \quad (6.3)$$

$$v = k(x^2 + y^2)^{1/2} \frac{a}{f}. \quad (6.4)$$

After approximating the factor  $1/s$  in Eq. (6.1) by  $1/f$ , and applying the usual Debye approximation  $s - f \approx -\mathbf{q} \cdot \mathbf{R}$ , where  $\mathbf{q}$  denotes a unit vector in the direction  $OQ$  [BORN AND WOLF, 1999, Sec. 8.8.1], [STAMNES, 1986, sec. 12.1.2], we find that

$$U(u, v; A_0) = C \int_0^1 J_0(\rho v) e^{i(-u\rho^2/2 + kA_0\rho^4)} \rho \, d\rho, \quad (6.5)$$

where  $C = -ikA(a/f)^2 e^{i(f/a)^2 u}$  and  $J_0$  denotes the Bessel function of the first kind of order 0. It follows from Eq. (6.5) that

$$U^*(u, v; A_0) = -U(-u, v; -A_0), \quad (6.6)$$

which means that the axial intensity distribution obeys the symmetry relation

$$|U(u, 0; A_0)|^2 = |U(-u, 0; -A_0)|^2, \quad (6.7)$$

and that the phase of the field,  $\arg[U(u, v; A_0)]$ , satisfies the formula

$$\arg[U(u, v; A_0)] + \arg[U(-u, v; -A_0)] = -\pi. \quad (\text{mod } 2\pi) \quad (6.8)$$

Equation (6.8) is a generalization of the expression

$$\arg[U(u, v)] + \arg[U(-u, v)] = -\pi, \quad (6.9)$$

for a focused field without spherical aberration [BORN AND WOLF, 1999, Sec. 8.8.4 ].

For axial points ( $v = 0$ ), Eq. (6.5) can be written (omitting the  $v$ -dependence from now on) as

$$U(u; A_0) = -C \frac{(-1)^{3/4} \sqrt{\pi}}{4\sqrt{kA_0}} e^{-iu^2/16kA_0} \left\{ \operatorname{erfi} \left[ \frac{(-1)^{1/4}(4kA_0 - u)}{4\sqrt{kA_0}} \right] + \operatorname{erfi} \left[ \frac{(-1)^{1/4}u}{4\sqrt{kA_0}} \right] \right\}, \quad (6.10)$$

where  $\operatorname{erfi}$  denotes the imaginary error function. It is seen from Eq. (6.10) that the axial intensity distribution is symmetric about the position  $u = 2kA_0$  [BORN AND WOLF, 1999, Sec. 9.3]. When  $|A_0| \lesssim \lambda$ , this point is also the intensity maximum (“the diffraction focus”). For large values of  $A_0$ , there may be two peaks, as is illustrated in Fig. 6.3. It is also seen that the distribution becomes wider with increasing  $A_0$ .

### 6.3 The Gouy phase

The Gouy phase is defined as the difference between the actual phase of the field and that of a non-diffracted spherical wave that converges to

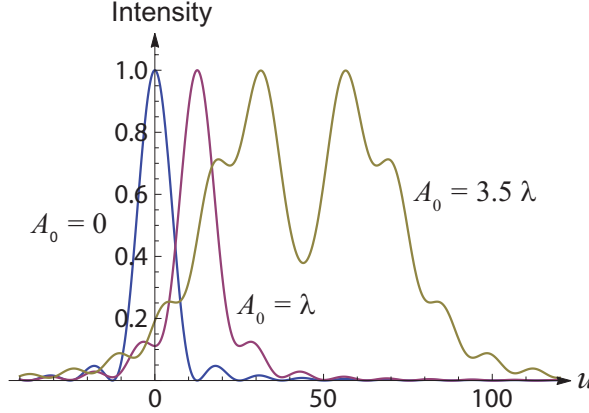


Figure 6.3: The axial intensity distribution for different values of the spherical aberration parameter,  $A_0 = 0$  (blue curve),  $A_0 = \lambda$  (red curve) and  $A_0 = 3.5\lambda$  (olive curve). Here, and in all the following examples,  $a/f$  is taken to be  $1/2$ .

the geometrical focus in the half-space  $z < 0$  and diverges from it in the half-space  $z > 0$  [BORN AND WOLF, 1999, Sec. 8.8.4], i.e.

$$\delta(u; A_0) = \arg[U(u; A_0)] - \text{sign}(u)kR, \quad (6.11)$$

with  $R$  the distance from the observation point to the geometrical focus, i.e.

$$kR = k|z| = \left(\frac{f}{a}\right)^2 |u|, \quad (6.12)$$

and  $\text{sign}(x)$  denotes the sign function

$$\text{sign}(x) = \begin{cases} -1 & \text{if } x < 0, \\ 1 & \text{if } x > 0. \end{cases} \quad (6.13)$$

From Eqs. (6.8) and (6.11), we find that the Gouy phase satisfies the relation

$$\delta(u; A_0) + \delta(-u; -A_0) = -\pi \pmod{2\pi}. \quad (6.14)$$

The dependence of the Gouy phase on the amount of spherical aberration is shown in Fig. 6.4. It is seen that the oscillations of the Gouy phase

in front of the diffraction focus decrease when the parameter  $A_0$  increases. Notice that the three curves are parallel at the respective diffraction foci ( $u = 1.3, 3.1, 12.6$ ). This is explained by noting that it follows from Eq. (6.10) that  $\partial \arg[U(2kA_0; A_0)]/\partial u = (f/a)^2 - 1/4$ , which is independent of the value the aberration parameter (see Appendix).

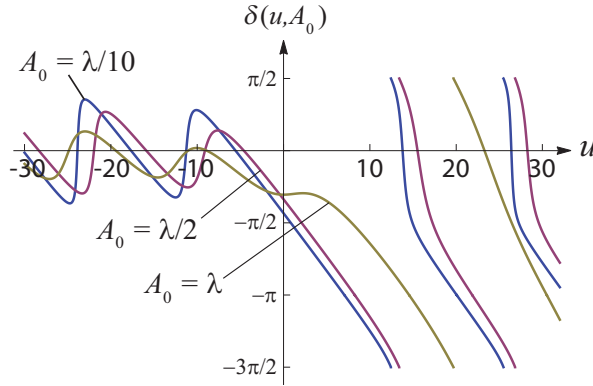


Figure 6.4: Gouy phase of the field along the axis for different values of the aberration parameter  $A_0$ .

The field at geometrical focus can be calculated from Eq. (6.10), which gives

$$U(0; A_0) = ik\mathcal{A} \left(\frac{a}{f}\right)^2 \frac{(-1)^{3/4} \sqrt{\pi}}{4\sqrt{kA_0}} \operatorname{erfi}[(-1)^{1/4} \sqrt{kA_0}]. \quad (6.15)$$

This expression implies that the phase, and equivalently, the Gouy phase, at  $(u, v) = (0, 0)$  depends on the aberration parameter  $A_0$ , but not on the value of  $f/a$ . This is illustrated in Fig. 6.5. Notice that the symmetry relation Eq. (6.8) is also satisfied.

However, for practical purposes, the diffraction focus (the position of maximum intensity, when  $|A_0| \lesssim \lambda$ ) is more important than the geometrical focus. It is therefore of interest to examine the Gouy phase at  $u = 2kA_0$ . The field there can be written as

$$U(2kA_0; A_0) = ik\mathcal{A} \left(\frac{a}{f}\right)^2 \frac{(-1)^{3/4} \sqrt{\pi}}{2\sqrt{kA_0}} e^{i2kA_0(f/a)^2} \times e^{-ikA_0/4} \operatorname{erfi}(\sqrt{ikA_0}/2), \quad (6.16)$$

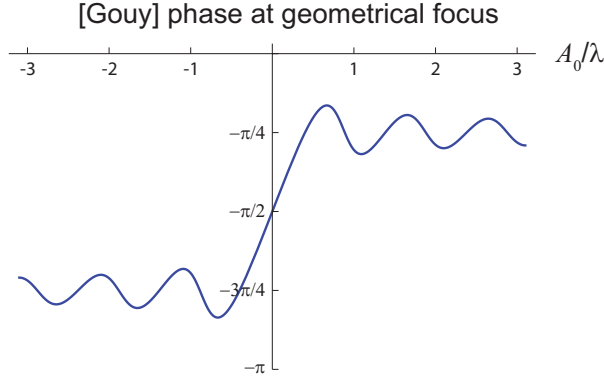


Figure 6.5: The phase, and equivalently, the Gouy phase at the geometrical focus  $(u, v) = (0, 0)$  for different values of the spherical aberration parameter  $A_0$ .

which shows that the phase of the field there depends on  $A_0$ , and also on  $a/f$ . However the Gouy phase is only dependent on  $A_0$  and is shown in Fig. 6.6. Notice that the Gouy phase at the diffraction focus can attain any value.

As mentioned above, all these results are derived while making use of the Debye approximation. However, if one pursues a high level of accuracy, as in metrology, this may introduce a slight error in the calculated wavefront spacings [SHEPPARD, 2000]. We therefore evaluate Eq. (6.1) for on-axis points, without making use of the Debye approximation. This yields the expression

$$U(u; A_0) = -ik\mathcal{A} \left(\frac{a}{f}\right)^2 e^{-ikf} \int_0^1 e^{ik(s+A_0\rho^4)} \rho \, d\rho, \quad (6.17)$$

with

$$s = f \left[ 1 + \left(\frac{uf}{ka^2}\right)^2 + \frac{2u}{ka^2} \sqrt{f^2 - a^2\rho^2} \right]^{1/2}. \quad (6.18)$$

The Gouy phase and the intensity distribution of the field along axis calculated from Eq. (6.17) are shown in Figs. 6.7 and 6.8 for two opposite values of the aberration parameter  $A_0$ . These two figures illustrate the

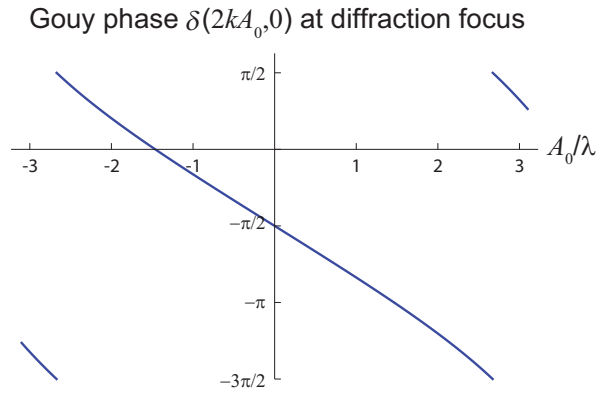


Figure 6.6: The Gouy phase of the field at point  $(2kA_0, 0)$ .

approximate symmetry relation (6.14). But more importantly, they show a highly antisymmetric behavior of the Gouy phase with respect to the diffraction focus. From this observation we may expect that the wavefront spacing before and after the diffraction focus will be different.

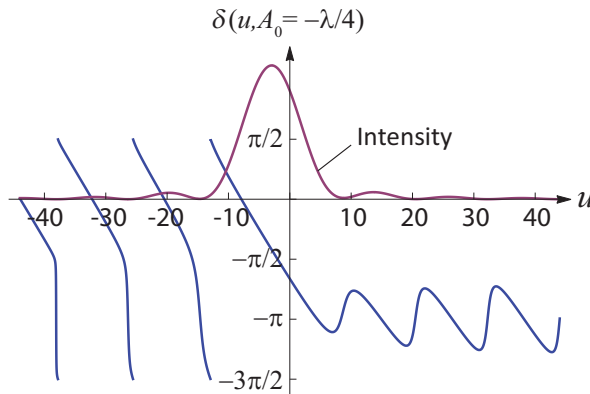


Figure 6.7: The Gouy phase and the intensity distribution of the field along the axis for the case  $A_0 = -\lambda/4$ .

We define the wavefront spacings as the distance between the successive roots of the expression  $\text{Re}[U(u; A_0)] = 0$ . The axial wavefront spacings for three cases ( $A_0 = 0$ ,  $A_0 = \lambda/4$  and  $A_0 = -\lambda/4$ ) are listed in Table 6.1.

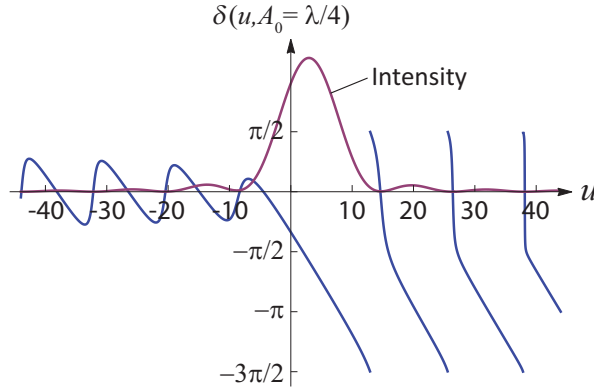


Figure 6.8: The Gouy phase and the intensity distribution of the field along the axis for the case  $A_0 = \lambda/4$ .

The spacings are labeled by the index  $N$ , with  $N = 1$  indicating the distance between the first zero for which  $u > 2kA_0$ , and the nearest zero at a smaller value of  $u$ . From the Table several trends can be deduced:

- For the case of an aberration-free lens ( $A_0 = 0$ ) the wavefront spacings are somewhat irregular, but consistently larger than the effective wavelength  $\lambda_{\text{eff}} = \lambda/(1 - a^2/4f^2) = 1.0667\lambda$  derived in [LINFOOT AND WOLF, 1956] on the basis of the Debye approximation.
- For a small amount of spherical aberration ( $A_0 = \lambda/4$ ), the wavefront spacings increase with increasing  $N$ . This means that the spacings to the right of the diffraction focus ( $N \geq 1$ ) are systematically larger than those to the left of the diffraction focus ( $N \leq -1$ ). The difference between the smallest and the largest spacing ( $N = -4$  and  $N = 4$ ) is more than 1%. This is considerably larger than the typically aspired metrological accuracy levels.
- When the aberration parameter is slightly increased (not shown) the systematic increase in wavefront spacing with increasing  $N$  gets larger.
- For negative values of the aberration parameter ( $A_0 = -\lambda/4$ ) the wavefront spacings decrease with increasing  $N$ . This is in agreement

with the symmetry expressed by Eq. (6.6), and Figs. 6.7 and 6.8.

Table 6.1: Wavefront spacings [in free-space wavelengths  $\lambda$ ] near the diffraction focus for different amounts of spherical aberration, for the case  $a/f = 1/2$ .

$N$	$A_0 = 0$	$A_0 = \lambda/4$	$A_0 = -\lambda/4$
-4	1.06683	1.06087	1.08080
-3	1.06871	1.06530	1.07540
-2	1.06948	1.06767	1.07304
-1	1.06982	1.06918	1.07162
1	1.06995	1.07034	1.07050
2	1.06991	1.07144	1.06935
3	1.06971	1.07279	1.06789
4	1.06923	1.07495	1.06567

## 6.4 Conclusions

In summary, we have derived expressions for the Gouy phase of a focused field in the presence of primary spherical aberration. Its behavior around the diffraction focus is found to be highly asymmetric. This coincides with a wavefront spacing that is systematically larger on one side of the intensity maximum than on the other side. The distance between successive wavefronts is found to increase with increasing spherical aberration, and is typically larger than predicted by previous analyses that relied on the Debye approximation. Since even for an amount of spherical aberration  $\sim \lambda/4$  the difference in fringe spacing can exceed 1%, these results may put restrictions on the accuracy that can be achieved in optical metrology and calibration.

## Appendix - The axial wavefront spacing near a diffraction focus

In this part, we will derive the axial wavefront spacing near a diffraction focus. Firstly, we can write Eq. (6.10) into two functions as

$$U(u; A_0) = U_1(u; A_0) \times U_2(u; A_0), \quad (19)$$

where

$$U_1(u; A_0) = -C \frac{(-1)^{3/4} \sqrt{\pi}}{4\sqrt{kA_0}} e^{-iu^2/16kA_0}, \quad (20)$$

$$U_2(u; A_0) = \operatorname{erfi} \left[ \frac{(-1)^{1/4} (4kA_0 - u)}{4\sqrt{kA_0}} \right] + \operatorname{erfi} \left[ \frac{(-1)^{1/4} u}{4\sqrt{kA_0}} \right]. \quad (21)$$

Since  $d \operatorname{erfi}(x)/dx = 2e^{x^2}/\sqrt{\pi}$ , we find that

$$\frac{\partial U_2}{\partial u} \Big|_{u=2kA_0} = 0, \quad (22)$$

together with  $U_2(2kA_0, 0; A_0) \neq 0$ , hence we can obtain the conclusion that

$$\frac{\partial \arg[U_2]}{\partial u} \Big|_{u=2kA_0} = 0. \quad (23)$$

While, for the function  $U_1$ , one can find that

$$\frac{\partial \arg[U_1]}{\partial u} = \left( \frac{f}{a} \right)^2 - \frac{u}{8kA_0}, \quad (24)$$

and at the diffraction focus it becomes

$$\frac{\partial \arg[U_1]}{\partial u} \Big|_{u=2kA_0} = \left( \frac{f}{a} \right)^2 - \frac{1}{4}. \quad (25)$$

Also Eq. (19) indicates that

$$\arg[U] = \arg[U_1] + \arg[U_2], \quad (26)$$

adding Eqs. (23), (25) the slope of the phase near the diffraction focus is

$$\frac{\partial \arg[U]}{\partial u} \Big|_{u=2kA_0} = \left(\frac{f}{a}\right)^2 - \frac{1}{4}. \quad (27)$$

If we adopt the variable  $z$  rather than  $u$ , the slope of the phase,  $\partial \arg[U]/\partial z$  equals the wavenumber  $k$  for a non-diffracted wave. From Eq. (6.3), the slope of the phase  $\partial \arg[U]/\partial u$  should be  $(f/a)^2$  in a non-diffracted field. So Eq. (27) shows that near the diffraction focus the phase changes more slowly than it does in a non-diffracted field. It also indicates that the axial wavefront spacing,  $\lambda_{eff}$ , around the diffraction focus is larger than  $\lambda$ , i.e.

$$\lambda_{eff} = \lambda(f/a)^2 / [(f/a)^2 - 1/4] = \lambda / (1 - a^2/4f^2), \quad (28)$$

which is exactly the same result that was found for an aberration-free field by [LINFOOT AND WOLF, 1956].



# Bibliography

- M. ABRAMOWITZ AND I.A. STEGUN, *Handbook of Mathematical Functions with Formulas, Graphs, and Mathematical Tables*, Dover, New York (1965).
- L. ALLEN, M.W. BEIJERSBERGEN, R.J.C. SPREEUW, AND J.P. WOERDMAN, “Orbital angular momentum of light and the transformation of Laguerre-Gaussian laser modes”, *Phys. Rev. A* 45, pp. 8185–8189 (1992).
- B. ANDREAS, L. FERROGLIO, K. FUJII, N. KURAMOTO, AND G. MANA, “Phase corrections in the optical interferometer for Si sphere volume measurements at NMIJ”, *Metrologia* 48, pp. S104–s111 (2011).
- G.B. ARFKEN AND H.J. WEBER, *Mathematical Methods for Physicists*, fourth edition, Academic Press, San Diego (1995).
- J. ARLT AND M.J. PADGETT, “Generation of a beam with a dark focus surrounded by regions of higher intensity: the optical bottle beam”, *Opt. Lett.* 25, pp. 191–193 (2000).
- M.A. BANDRES, “Accelerating parabolic beams”, *Opt. Lett.* 33, pp. 1678–1680 (2008).
- V.J. BARGE, Z. HU, AND R.J. GORDON, “Contribution of the Gouy phase to two-pathway coherent control of the photoionization and photodissociation of vinyl chloride”, *J. Chem. Phys.* 129, 244301 (2008).
- V.J. BARGE, Z. HU, J. WILLING, AND R.J. GORDON, “Role of the Gouy phase in the coherent phase control of the photoionization

- and photodissociation of vinyl chloride”, *Phys. Rev. Lett.* 88, 263001 (2006).
- S.M. BAUMANN, D.M. KALB, AND E.J. GALVEZ, “Propagation dynamics of optical vortices due to Gouy phase”, *Opt. Express* 17, pp. 9818–9827 (2009).
- M.W. BEIJERSBERGEN, L. ALLEN, H.E.L.O. VAN DER VEEN, AND J.P. WOERDMAN, “Astigmatic laser mode converters and transfer of orbital angular momentum”, *Opt. Commun.* 96, pp. 123–132 (1993).
- M.V. BERRY, “Wave dislocation reactions in non-paraxial Gaussian beams”, *J. Mod. Optics* 45, pp. 1845–1858 (1998).
- M.V. BERRY AND N.L. BALAZS, “Nonspreading wave packets”, *Am. J. Phys.* 47, pp. 264–267 (1979).
- M.V. BERRY AND M.R. DENNIS, “Polarization singularities in isotropic random vector waves”, *Proc. R. Soc. Lond. A* 475, pp. 141–155 (2001).
- D.P. BISS, K.S. YOUNGWORTH, AND T.G. BROWN, “Dark-field imaging with cylindrical-vector beams”, *Appl. Opt.* 45, pp. 470–479 (2006).
- A. BOIVIN, J. DOW, AND E. WOLF, “Energy flow in the neighborhood of the focus of a coherent beam”, *J. Opt. Soc. Am.* 57, pp. 1171–1175 (1967).
- A. BOIVIN AND E. WOLF, “Electromagnetic field in the neighborhood of the focus of a coherent beam”, *Phys. Rev.* 138, pp. B1561–B1565 (1965).
- M. BORN AND E. WOLF, *Principles of Optics: Electromagnetic Theory of Propagation, Interference and Diffraction of Light*, Seventh (expanded) edition, Cambridge University Press, Cambridge (1999).
- R.W. BOYD, “Intuitive explanation of the phase anomaly of focused light beams”, *J. Opt. Soc. Am.* 70, pp. 877–880 (1980).
- R.W. BOYD, *Nonlinear Optics*, Academic Press, San Diego (1992).

- J. BROKY, G.A. SIVILOGLOU, A. DOGARIU, AND D.N. CHRISTODOULIDES, “Self-healing properties of optical Airy beams”, *Opt. Express* 16, pp. 12880–12891 (2008).
- T.G. BROWN, “Unconventional polarization states: Beam propagation, focusing, and imaging”, In: E. Wolf, editor, *Progress in Optics*, volume 56, pp. 81–129, Elsevier, Amsterdam (2011).
- H. CHEN, Q. ZHAN, Y. ZHANG, AND Y.-P. LI, “The Gouy phase shift of the highly focused radially polarized beam”, *Phys. Lett. A* 371, pp. 259–261 (2007).
- J.H. CHOW, G. DE VINE, M.B. GRAY, AND D.E. MCCLELLAND, “Measurement of Gouy phase evolution by use of spatial mode interference”, *Opt. Lett.* 29, pp. 2339–2341 (2004).
- I. CODDINGTON, W.C. SWANN, L. NENADOVIC, AND N.R. NEWBURY, “Rapid and precise absolute distance measurements at long range”, *Nat. Photonics* 3, pp. 351–356 (2009).
- K. CREATH, “Calibration of numerical aperture effects in interferometric microscope objectives”, *Appl. Optics* 28, pp. 3333–3338 (1989).
- M.R. DENNIS, K. O’HOLLERAN, AND M.J. PADGETT, “Singular optics: Optical vortices and polarization singularities”, In: E. Wolf, editor, *Progress in Optics*, volume 53, pp. 293–364, Elsevier, Amsterdam (2009).
- D.W. DIEHL, R.W. SCHOONOVER, AND T.D. VISSER, “The structure of focused, radially polarized fields”, *Opt. Express* 14, pp. 3030–3038 (2006).
- D.W. DIEHL AND T.D. VISSER, “Phase singularities of the longitudinal field components in the focal region of a high-aperture optical system”, *J. Opt. Soc. Am. A* 21, pp. 2103–2108 (2004).
- R. DORN, S. QUABIS, AND G. LEUCHS, “Sharper focus for a radially polarized light beam”, *Phys. Rev. Lett.* 91, 233901 (2003).
- J. DURBIN, “Exact solution for nondiffracting beams. I. The scalar theory”, *J. Opt. Soc. Am. A* 4, pp. 651–654 (1987).

- J. DURBIN, J. MICELI, AND J.H. EBERLY, “Diffraction-free beams”, *Phys. Rev. Lett.* 58, pp. 1499–1501 (1987).
- G.W. FARNELL, “Measured phase distribution in the image space of a microwave lens”, *Canadian J. Phys.* 36, pp. 935–943 (1958).
- J.F. FEDERICI, R.L. WAMPLE, D. RODRIGUEZ, AND S. MUKHERJEE, “Application of terahertz Gouy phase shift from curved surfaces for estimation of crop yield”, *Opt. Express* 14, pp. 8382–8392 (2006).
- S. FENG AND H.G. WINFUL, “Physical origin of the Gouy phase shift”, *Opt. Lett.* 26, pp. 485–487 (2001).
- T. FEURER, N.S. STOYANOV, D.W. WARD, AND K.A. NELSON, “Direct visualization of the Gouy phase by focusing phonon polaritons”, *Phys. Rev. Lett.* 88, 257402 (2002).
- D.G. FISCHER AND T.D. VISSER, “Spatial correlation properties of focused partially coherent light”, *J. Opt. Soc. Am. A* 21, pp. 2097–2102 (2004).
- J.T. FOLEY AND E. WOLF, “Wave-front spacing in the focal region of high-numerical-aperture systems”, *Opt. Lett.* 30, pp. 1312–1314 (2005).
- G. GBUR AND T.D. VISSER, “Coherence vortices in partially coherent beams”, *Opt. Commun.* 222, pp. 117–125 (2003).
- G. GBUR AND T.D. VISSER, “The structure of partially coherent fields”, In: E. Wolf, editor, *Progress in Optics*, volume 55, pp. 285–341, Elsevier, Amsterdam (2010).
- G.J. GBUR, *Mathematical Methods for Optical Physics and Engineering*, Cambridge University Press, Cambridge (2011).
- R.J. GORDON AND V.J. BARGE, “Effect of the Gouy phase on the coherent phase control of chemical reactions”, *J. Chem. Phys.* 127, 204302 (2007).

- L.G. GOUY, “Sur une propriété nouvelle des ondes lumineuses”, *Comptes Rendus hebdomadaires des Séances de l’Académie des Sciences* 110, pp. 1251–1253 (1890).
- L.G. GOUY, “Sur la propagation anormale des ondes”, *Annales des Chimie et de Physique* 6<sup>e</sup> séries 24, pp. 145–213 (1891).
- Y.L. GU AND G. GBUR, “Scintillation of Airy beam arrays in atmospheric turbulence”, *Opt. Lett.* 35, pp. 3456–3458 (2010).
- G. GUZZINATI, P. SCHATTSCHNEIDER, K.Y. BLOKH, F. NORI, AND J. VERBEECK, “Observation of the Larmor and Gouy Rotations with Electron Vortex Beams”, *Phys. Rev. Lett.* 110, 093601 (2013).
- J. HAMAZAKI, Y. MINETA, K. OKA, AND R. MORITA, “Direct observation of Gouy phase shift in a propagating optical vortex”, *Opt. Express* 14, pp. 8382–8392 (2006).
- G.M. HANNAPPEL, D.J. STEVENSON, D. DAY, M. GU, AND K. DHO-LAKIA, “Optical redistribution of microparticles and cells between microwells”, *Lab Chip* 9, pp. 1334–1336 (2009).
- P. HARIHARAN AND P.A. ROBINSON, “The Gouy phase shift as a geometrical quantum effect”, *J. Mod. Optics* 43, pp. 219–221 (1996).
- N.C.R. HOLME, B.C. DALY, AND T.B. NORRIS, “Gouy phase shift of single-cycle picosecond acoustic pulses”, *Appl. Phys. Lett.* 83, pp. 392–394 (2003).
- J. HWANG AND W.E. MOERNER, “Interferometry of a single nanoparticle using the Gouy phase of a focused laser beam”, *Opt. Commun.* 280, pp. 487–491 (2007).
- Y. KAGANOVSKY AND E. HEYMAN, “Wave analysis of Airy beams”, *Opt. Express* 18, pp. 8440–8452 (2010).
- N.G. VAN KAMPEN, “An asymptotic treatment of diffraction problems”, *Physica* XIV, pp. 575–589 (1949).

- H.C. KANDPAL, S. RAMAN, AND R. MEHROTRA, “Observation of Gouy phase anomaly with an interferometer”, *Opt. Lasers Eng.* 45, pp. 249–251 (2007).
- G.P. KARMAN, M.W. BEIJERSBERGEN, A. VAN DUIJL, AND J.P. WOERDMAN, “Creation and annihilation of phase singularities in a focal field”, *Opt. Lett.* 22, pp. 1503–1505 (1997).
- G.S. KINO AND T.R. KORLE, *Confocal Scanning Optical Microscopy and Related Imaging Systems*, Academic Press, San Diego (1996).
- T. KLAASSEN, A. HOOGEBOOM, M.P. VAN EXTER, AND J.P. WOERDMAN, “Gouy phase of nonparaxial eigenmodes in a folded resonator”, *J. Opt. Soc. Am. A* 21, pp. 1689–1693 (2004).
- AL.A. KOLOMENSKII, S.N. JEREBTISOV, AND H.A. SCHUESSLER, “Focal transformation and the Gouy phase shift of converging one-cycle surface acoustic waves excited by femtosecond laser pulses”, *Opt. Lett.* 30, pp. 2019–2021 (2005).
- P. KUŽEL, H. NĚMEC, F. KADLEC, AND C. KADLEC, “Gouy shift correction for highly accurate refractive index retrieval in time-domain terahertz spectroscopy”, *Opt. Express* 18, pp. 15338–15348 (2010).
- G. LAMOUCHE, M.L. DUFOUR, B. GAUTHIER, AND J. P. MONCHALIN, “Gouy phase anomaly in optical coherence tomography”, *Opt. Commun.* 239, pp. 297–301 (2004).
- F. LINDNER, G.G. PAULUS, H. WALTHER, A. BALTUŠKA, E. GOULIELMAKIS, M. LEZIUS, AND F. KRAUSZ, “Gouy phase shift for few-cycle laser pulses”, *Phys. Rev. Lett.* 92, 113001 (2004).
- F. LINDNER, W. STREMME, M. SCHÄTZEL, F. GRASBON, G. PAULUS, H. WALTHER, R. HARTMANN, AND L. STRÜDER, “High-order harmonic generation at a repetition rate of 100 khz”, *Phys. Rev. A* 68, 013814 (2003).
- E.H. LINFOOT AND E. WOLF, “Phase distribution near focus in an aberration-free diffraction image”, *Proc. Phys. Soc. B* 69, pp. 823–832 (1956).

- L. MANDEL AND E. WOLF, *Optical Coherence and Quantum Optics*, Cambridge University Press, Cambridge (1995).
- P. MARTELLI, M. TACCA, A. GATTO, G. MONETA, AND M. MARTINELLI, “Gouy phase shift in nondiffracting Bessel beams”, *Opt. Express* 18, pp. 7108–7120 (2010).
- R. MARTÍNEZ-HERRERO AND P.M. MEJÍAS, “Stokes-parameters representation in terms of the radial and azimuthal field components: A proposal”, *Opt. Laser Technol.* 42, pp. 1099–1102 (2010).
- R. MARTÍNEZ-HERRERO AND P.M. MEJÍAS, “Propagation and parametric characterization of the polarization structure of paraxial radially and azimuthally polarized beams”, *Opt. Laser Technol.* 44, pp. 482–485 (2012).
- R.W. MCGOWAN, R.A. CHEVILLE, AND D. GRISCHKOWSKYA, “Direct observation of the Gouy phase shift in THz impulse ranging”, *Appl. Phys. Lett.* 76, pp. 670–672 (2000).
- L. MERTZ, “A new demonstration of the anomalous phase change of light at a focus”, *J. Opt. Soc. Am.* 49, pp. AD 10–iv (1959).
- J.E. MORRIS, M. MAZILU, J. BAUMGARTL, T. CIZMAR, AND K. DHO-LAKIA, “Propagation characteristics of Airy beams: dependence upon spatial coherence and wavelength”, *Opt. Express* 17, pp. 13236–13245 (2009).
- T.A. NIEMINEN, N.R. HECKENBERG, AND H. RUBINSZTEIN-DUNLOP, “Forces in optical tweezers with radially and azimuthally polarized trapping beams”, *Opt. Lett.* 33, pp. 122–124 (2008).
- L. NOVOTNY, M.R. BEVERSLUIS, K.S. YOUNGWORTH, AND T.G. BROWN, “Longitudinal field modes probed by single molecules”, *Phys. Rev. Lett.* 86, pp. 5251–5254 (2001).
- J.F. NYE, “Unfolding of higher-order wave dislocations”, *J. Opt. Soc. Am. A* 15, pp. 1132–1138 (1998).
- J.F. NYE, *Natural Focusing and Fine Structure of Light*, Institute of Physics, Bristol (1999).

- J.F. NYE AND M.V. BERRY, “Dislocations in wave trains”, *Proc. R. Soc. Lond. A* 336, pp. 165–190 (1974).
- G.M. PHILIP, V. KUMAR, G. MILIONE, AND N.K. VISWANATHAN, “Manifestation of the Gouy phase in vector-vortex beams”, *Opt. Lett.* 37, pp. 2667–2669 (2012).
- P. POLYNKIN, M. KOLESIK, J.V. MOLONEY, G.A. SIVILOGLOU, AND D.N. CHRISTODOULIDES, “Curved plasma channel generation using ultraintense Airy beams”, *Science* 324, pp. 229–232 (2009).
- B. RICHARDS AND E. WOLF, “The Airy pattern in systems of high angular aperture”, *Proc. Phys. Soc. B* 69, pp. 854–856 (1956).
- B. RICHARDS AND E. WOLF, “Electromagnetic diffraction in optical systems. II. Structure of the image field in an aplanatic system”, *Proc. R. Soc. A.* 253, 1274, pp. 358–379 (1959).
- L. ROBERTSSON, “On the diffraction correction in absolute gravimetry”, *Metrologia* 44, pp. 35–39 (2007).
- J.P. ROLLAND, T. SCHMID, J. TAMKIN JR., K. LEE, K.P. THOMPSON, AND E. WOLF, “Gouy phase anomaly in astigmatic beams”, International Optical Design Conference 2010, OSA Technical Digest (CD), page IWC2, Jackson Hole, WY (2010).
- A.B. RUFFIN, J.V. RUDD, J.F. WHITAKER, S. FENG, AND H.G. WINFUL, “Direct observation of the Gouy phase shift with single-cycle terahertz pulses”, *Phys. Rev. Lett.* 83, pp. 3410–3413 (1999).
- K. FUERSCHBACH S. VO, K.P. THOMPSON, M.A. ALONSO, AND J.P. ROLLAND, “Airy beams: a geometric optics perspective”, *J. Opt. Soc. Am. A* 27, pp. 2574–2582 (2010).
- R.W. SCHOONOVER AND T.D. VISSER, “Polarization singularities of focused, radially polarized fields”, *Opt. Express* 14, pp. 5733–5745 (2006).
- H.F. SCHOUTEN, T.D. VISSER, G. GBUR, D. LENSTRA, AND H. BLOK, “Creation and annihilation of phase singularities near a sub-wavelength slit”, *Opt. Express* 11, pp. 371–380 (2003).

- T. SETÄLA, J. TERVO, AND A.T. FRIBERG, “Contrasts of stokes parameters in young’s interference experiment and electromagnetic degree of coherence”, *Opt. Lett.* 31, pp. 2669–2671 (2006).
- C.J.R. SHEPPARD, “Validity of the Debye approximation”, *Opt. Lett.* 25, pp. 1660–1662 (2000).
- C.J.R. SHEPPARD AND A. CHOUDHURY, “Annular pupils, radial polarization, and superresolution”, *Appl. Opt.* 43, pp. 4322–4327 (2004).
- C.J.R. SHEPPARD AND K.G. LARKIN, “Effect of numerical aperture on interference fringe spacing”, *Appl. Opt.* 34, pp. 4731–4734 (1995).
- A.E. SIEGMAN, *Lasers*, University Science Books, Mill Hill (1986), in this work Gouy’s name is consistently misspelled as “Guoy”.
- R. SIMON AND N. MUKUNDA, “Bargmann invariant and the geometry of the G uyoy effect”, *Phys. Rev. Lett.* 70, pp. 880–883 (1993).
- G.A. SIVILOGLOU, J. BROKY, A. DOGARIU, AND D.N. CHRISTODOULIDES, “Observation of accelerating Airy beams”, *Phys. Rev. Lett.* 99, 213901 (2007).
- G.A. SIVILOGLOU AND D.N. CHRISTODOULIDES, “Accelerating finite energy Airy beams”, *Opt. Lett.* 32, pp. 979–981 (2007).
- M.S. SOSKIN AND M.V. VASNETSOV, “Singular optics”, In: E. Wolf, editor, *Progress in Optics*, volume 42, pp. 219–276, Elsevier, Amsterdam (2001).
- J.J. STAMNES, *Waves in Focal Regions*, Adam Hilger, Bristol (1986).
- O. STEUERNAGEL, E. YAO, K. O’HOLLERAN, AND M. PADGETT, “Observation of Gouy-phase-induced transversal intensity changes in focused beams”, *J. Mod. Optics* 52, pp. 2713–2721 (2005).
- D. SUBBARAO, “Topological phase in Gaussian beam optics”, *Opt. Lett.* 20, pp. 2162–2164 (1995).
- J. TURUNEN AND A.T. FRIBERG, “Propagation-invariant optical fields”, In: E. Wolf, editor, *Progress in Optics*, volume 54, pp. 1–88, Elsevier, Amsterdam (2010).

- T.D. VISSER AND J.T. FOLEY, “On the wavefront spacing of focused, radially polarized beams”, *J. Opt. Soc. Am. A* 22, pp. 2527–2531 (2005).
- T.D. VISSER AND E. WOLF, “The origin of the Gouy phase anomaly and its generalization to astigmatic wavefields”, *Opt. Commun.* 283, pp. 3371–3375 (2010).
- J. WALKER, *The Analytical Theory of Light*, Cambridge University Press, Cambridge (1904).
- G. WIEGAND, K.R. NEUMAIER, AND E. SACKMANN, “Microinterferometry: Three-Dimensional Reconstruction of Surface Microtopography for Thin-Film and Wetting Studies by Reflection Interference Contrast Microscopy (RICM)”, *Appl. Opt.* 37, pp. 6892–6905 (1998).
- E. WOLF, “A macroscopic theory of interference and diffraction of light from finite sources. ii. fields with a spectral range of arbitrary width”, *Proc. R. Soc. Lond. A* 230, pp. 246–265 (1955).
- E. WOLF, “Electromagnetic diffraction in optical systems I. An integral representation of the image field”, *Proc. R. Soc. Lond. A* 253, pp. 358–379 (1959).
- E. WOLF, “Young’s interference fringes with narrow-band light”, *Opt. Lett.* 8, pp. 250–252 (1983).
- E. WOLF, “Correlation-induced changes in the degree of polarization, the degree of coherence, and the spectrum of random electromagnetic beams on propagation”, *Opt. Lett.* 28, pp. 1078–1080 (2003a).
- E. WOLF, “Unified theory of coherence and polarization of random electromagnetic beams”, *Phys. Lett. A* 312, pp. 263–267 (2003b).
- E. WOLF, *Introduction to the Theory of Coherence and Polarization of Light*, Cambridge University Press, Cambridge (2007).
- K.S. YOUNGWORTH AND T.G. BROWN, “Focusing of high numerical aperture cylindrical-vector beams”, *Opt. Express* 7, pp. 77–87 (2000).

- 
- Q. ZHAN, “Second-order tilted wave interpretation of the Gouy phase shift under high numerical aperture uniform illumination”, *Opt. Commun.* 242, pp. 351–360 (2004a).
- Q. ZHAN, “Trapping metallic Rayleigh particles with radial polarization”, *Opt. Express* 12, pp. 3377–3382 (2004b).
- W. ZHU, A. AGRAWAL, AND A. NAHATA, “Direct measurement of the Gouy phase shift for surface plasmon-polaritons”, *Opt. Express* 15, pp. 9995–10001 (2007).



# List of publications

- **X. Pang**, T.D. Visser and E. Wolf, “Phase anomaly and phase singularities of the field in the focal region of high-numerical aperture systems,” *Optics Communications*, vol. 284, pp. 5517-5522 (2011).
- **X. Pang**, G. Gbur and T.D. Visser, “The Gouy phase of Airy beams,” *Optics Letters*, vol. 36, pp. 2492-2494 (2011).
- **X. Pang**, D.G. Fischer and T.D. Visser, “Generalized Gouy phase for focused, partially coherent light and its implications for optical metrology,” *J. Opt. Soc. Am. A.*, vol. 29, pp. 989-993 (2012).
- **X. Pang** and T.D. Visser, “Manifestation of the Gouy phase in strongly focused, radially polarized beams,” *Optics Express*, vol. 21, pp. 8331-8341 (2013).
- **X. Pang**, D.G. Fischer and T.D. Visser, “Wavefront spacing and the Gouy phase in the presence of primary spherical aberration,” to be submitted



# Samenvatting

De Nederlandse titel van dit proefschrift luidt: *Gedaantes van Gouy: de fase anomalie in optische golfvelden*. De verschillende hoofdstukken zijn gebaseerd op reeds verschenen artikelen. Alleen het laatste hoofdstuk moet nog worden ingediend. Hoofdstuk 1 bevat, naast een inleiding over geometrische- en golf-optica, een korte beschrijving van concepten die in latere delen worden gebruikt. Allereerst bespreken we het centrale thema van dit proefschrift, de Gouy fase. Dat is het opmerkelijke verschijnsel dat de fase van een gefocusseerd veld, vergeleken met die van een bolgolf van dezelfde frequentie, een plotselinge verandering ter grootte van  $\pi$  ondergaat. Verschillende verklaringen voor de fysische oorzaak hiervan worden besproken. Daarna worden enkele begrippen uit de singuliere optica en de coherentietheorie kort toegelicht. In Hoofdstuk 2 wordt het focuseren van een elektromagnetische bundel met lineaire polarisatie behandeld. Het elektrische vectorveld verkrijgt drie componenten. We laten zowel analytisch als numeriek zien dat deze drie verschillende Gouy fases hebben. Ook de fasesingulariteiten van deze veldcomponenten worden besproken. Hoofdstuk 3 gaat over de recent ontdekte Airy-bundels. Deze lichtbundels hebben de unieke eigenschap dat ze een gekromd traject volgen. Voor het ideale geval van een oneindig brede bundel kunnen we exacte vergelijkingen voor het fasegedrag afleiden. Met numerieke simulaties laten we zien dat deze formules uitstekende benaderingen zijn voor Airy-bundels zoals die in het laboratorium worden gemaakt. In Hoofdstuk 4 staan partieel coherente velden centraal. Zulke velden hebben een stochastische fase, en hun Gouy fase valt dus niet te definiëren. Het statistische gedrag wordt beschreven door correlatiefuncties met een fase die wel goed gedefinieerd is. We laten zien dat bij het focuseren van partieel coherente

velden deze functies een zogenaamde gegeneraliseerde Gouy fase vertonen, waarvan de klassieke fase anomalie een speciaal geval blijkt te zijn. Deze gegeneraliseerde fase verklaart het onregelmatige patroon dat in sommige interferentie opstellingen wordt geobserveerd. Het onderwerp van Hoofdstuk 5 is radieel gepolariseerde lichtbundels. Vanwege hun toepassing in optical trapping is het van belang om het polarisatiegedrag te kennen. Het blijkt, als we de reis van het licht door het focus volgen, dat de elektrische polarisatie-ellips "tuimelt." We laten zien dat dit een gevolg is van de verschillende Gouy fases die de twee componenten van het elektrische veld ondervinden. In Hoofdstuk 6, tenslotte, analyseren we de invloed van primaire sferische aberratie op het fasegedrag van gefocusseerde scalaire velden. Het blijkt dat een minimale hoeveelheid aberratie van minder dan een golflengte, zoals die in ieder praktisch systeem aanwezig is, een belangrijke afwijking van  $\sim 1\%$  in de effectieve golflengte oplevert. Dit resultaat heeft implicaties voor optische metrologie en kalibratie.

# Biography

Xiaoyan Pang was born in Yanshi, China, on 2 December 1983. She received her Bachelor's degree in Electronics and Information Engineering from Northwestern Polytechnical University, China in June 2007. She obtained a Master degree in Electromagnetic Field and Microwave Technology from the same University. During her Master's study, her research topic was on the design of a multi-polarization antenna. Since 2009, she has been working on her Ph.D. research which is about physical optics with Prof. T.D. Visser in the Netherlands. Her work is funded by the China Scholarship Council.



# Acknowledgments

Foremost, I would like to express my sincere gratitude to my supervisor Prof. T.D. Visser for giving me the opportunity to pursue my Ph.D. and for his supervision. As a researcher, he is always curious, creative and critical. While working with him, every research is like a ‘treasure hunt’ and the most important thing is to find clues-ask the right questions, which I will be reminding myself all the time. Prof. T.D. Visser, thank you for your tolerance, encouragement and care during my Ph.D. study and I will never forget these days when you were driving me to hospital for my eye disease.

Besides my supervisor, I have had the honor of collaborating with Prof. E. Wolf, Prof. G. Gbur and Dr. D.G. Fischer. Their suggestions and work have contributed a lot to the papers that we wrote together. I would really like to thank them for that. In addition, I would like to show my appreciation to my reading committee for their valuable comments.

The China Scholarship Council (CSC) allowed me to go to the Netherlands, and I am always grateful for that.

My wonderful office mate Shreyas, you are so positive and dare to do challenges and create your own life. I would like to express my appreciation to you for all your help, especially at the police station when my wallet was stolen. Also thank you very much for the spirited discussions. I believe that you will win more splendor in your life.

I would like to thank my friends Wenbo, Song, Qing, Liran, Liyuan, Huaizhou, Xinyue for their help in my Ph.D. life. I also would like to thank the ‘family’ group: Xuexue and Yao for their company. A special thanks to Jianing for his support during my tough time. I wish you success with your career. I would like to thank Zili and Mrs Wang on 14th floor

for many pleasant chats. Thanks to the warm lady Anna Hoek for all her care. I also want to thank the beautiful lady, Anjar for her encouragement.

Finally, I would like to give my deepest gratitude to my parents for all their love, support and unwavering belief in me. I would like to thank my sister, Xiaodong for your unconditional love and you are really a wonder in my life.

Xiaoyan

September 2013